Hyperlipidemia-induced MicroRNA-155-5p improves β-cell Function by targeting *Mafb*

Mengyu Zhu

München 2017

Aus dem Institut für Prophylaxe und Epidemiologie der Kreislaufkrankheiten
des Klinikums der Ludwig-Maximilians-Universität München
Direktor: Univ.-Prof. Dr. med. Christian Weber

Hyperlipidemia-induced MicroRNA-155-5p improves β-cell Function by targeting *Mafb*

Dissertation
zum Erwerb des Doktorgrades der Humanbiologie
an der Medizinischen Fakultät
der Ludwig-Maximilians-Universität
München

vorgelegt von

Mengyu Zhu

aus
Tianjin, VR China

2017

Mit Genehmigung der Medizinischen Fakultät
der Universität München

Berichterstatter:	Prof. Dr. med. Andreas Schober
Mitberichterstatter:	Prof. Dr. med. Jochen Seißler
	Prof. Dr. Andreas G. Ladurner
	Prof. Dr. med. Julia Mayerle

Mitbetreuung durch den
promovierten Mitarbeiter:

Dekan: Prof. Dr. med. dent. Reinhard Hickel

Tag der mündlichen Prüfung: 10.08.2017

Hyperlipidemia-induced MicroRNA-155-5p improves β-cell Function by targeting *Mafb*

TABLE OF CONTENT

ABBREVIATION

Ab	Antibody
AcGFP1	Aequrea coerulescences green fluorescent protein
Actb	Beta-actin
Adipoq	Adiponectin
Ago	Argonaute
AMP	Adenosine monophosphate
Apoe	Apolipoprotein E
Arg1	Arginase 1
Arx	Aristaless related homeobox
Auh	AU RNA binding protein/enoyl-coenzyme A hydratase
BIC	B-cell Integration Cluster
BSA	Bovine serum albumin
CB	Citrate buffer
CCD	Charge-coupled device
CD	Cluster of differentiation
Cdk	Cyclin-dependent kinases
Cdkn	Cyclin-dependent kinase inhibitor
CNS	Central nervous system
Cy3	Cyanine 3
C. elegans	Caenorhabditis elegans
d	Day(s)
DAPI	4', 6-diamidino-2-phenylindole
DDC	Cholesterol enriched-diabetogenic diet
DGCR8	DiGeorge syndrome critical region 8
DM	Diabetes mellitus
DMEM	Dulbecco's modified eagle medium
DMSO	Dimethyl sulfoxide
DNase	Seoxyribonuclease
EDTA	Ethylenediaminetetraacetic acid
ELISA	Enzyme-linked immunosorbant assay
ERK	Extracellular signal-regulated kinase
EvG	Elastic van Gieson
eWAT	Epididymal white adipose tissue
FBG	Fasting blood glucose
FBS	Fetal bovine serum
FITC	Fluorescein isothiocyanate
Foxa1	Forkhead box A1
Gapdh	Glyceraldehyde 3-phosphate dehydrogenase
Gcg	Glucagon
GIP	Glucose-dependent insulinotropic polypeptide
GLP-1	Glucagon-like peptide-1
GLuc	Gaussia luciferase
Glut	Glucose transporter

GRA	Granulocyte(s)
h	Hour(s)
HBSS	Hank's balanced salt solution
HCl	Hydrochloric acid
HDL	High-density lipoproteins
HFD	High fat diet
HPLC	High-performance liquid chromatography
Hprt1	Hypoxanthine guanine phosphoribosyl transferase
Hsa	Homo sapiens
H&E	Hematoxylin and eosin ()
IGT	Impaired glucose tolerance
IL-6	Interleukin-6
Ins	Insulin
IPA	Ingenuity Pathway Analysis software
IPGTT	Intraperitoneal glucose tolerance test
Isl1	ISL LIM homeobox 1
JAK	Janus kinase
LAL	Limulus amebocyte lysate
LAS	Leica application suite
LBP	Lipopolysaccharide binding protein
LDL	Low-density lipoproteins
Ldlr	Low-density lipoprotein receptor
LED	Light-emitting diode
Lep	Leptin
LPS	Lipopolysaccharide
LNA	Locked nucleic acid
LYM	Lymphocyte(s)
Mafb	V-maf musculoaponeurotic fibrosarcoma oncogene family, protein B
Med12l	Mediator complex subunit 12-like
MetS	Metabolic syndrome
min	Minute(s)
miRISC	MiRNA-induced silencing complex
miRNA	MicroRNA
miR/*Mir*	MicroRNA
Mmu	Mus musculus
mRNA	Messenger RNA
MO	Monocyte(s)
moxLDL	Mildly oxidized low-density lipoprotein
Mrc1	Mannose receptor, C type 1
ND	Normal diet
Neurod1	Neurogenic differentiation 1
NF-κB	Nuclear factor-κB
NGT	Normal glucose tolerance
nLDL	Native low-density lipoprotein
Nos2	Nitric oxide synthase 2
nt	Nucleotides

oxLDL	Oxidized low-density lipoprotein
Pax6	Paired box 6
PC	Proprotein convertase 1
Pcsk	Proprotein convertase subtilisin/kexin type
PBS	Phosphate buffered saline
Pdx1	Pancreatic and duodenal homeobox 1
PFA	Paraformaldehyde
pH	Potential of hydrogen
PTEN	Phosphatase and tensin homolog
qPCR	Quantitative real-time polymerase chain reaction
RCF	Relative centrifugal force
RIPA	Radioimmunoprecipitation assay buffer
RIN	RNAintegrity number
RNase	Ribonuclease
RPMI	Roswell Park Memorial Institute
RT	Room temperature
s	Second(s)
SA-PE	Streptavidin-phycoerythrin conjugate
SEAP	Secreted Alkaline Phosphatase
Sema5a	Semaphorin 5A
SHIP1	SH2-containing inositol-5'-phosphatase
SMA	α- smooth muscle actin
sno	Small nucleolar RNA
Sst	Somatostatin
STAT	Signal transducer and activator of transcription
Stmn2	Stathmin-like 2
T1DM	Type 1 diabetes
T2DM	Type 2 diabetes
TLR	Toll-like receptor
TNB	Tris-NaCl blocking
TNT	Tris-NaCl Tween
Tnf	Tumor necrosis factor
TSB	Target site blocker
VLDL	Very low-density lipoproteins
UP	Ultrapure
UTR	Untranslated region
WBC	White blood cell(s)
wk	Week(s)
w/v	Weight per volume
w/w	Weight per weight

1 INTRODUCTION

1.1 Diabetes mellitus (DM)

1.1.1 Prevalence of the diabetes

Diabetes mellitus (DM) is one of the largest global health emergencies of the 21st century,[1] [2] whose prevalence is increasing at an alarming rate throughout the world. Globally, as of 2015, an estimated 422 million adults (or 8.5% of the population) were living with diabetes, compared to 108 million (4.7%) in 1980. It is estimated by the International Diabetes Federation that the number will rise to 642 million by the year 2040.[1] The World Health Organization estimates that hyperglycemia is the third highest global risk factor for premature mortality, after high blood pressure and tobacco use.[3] Indeed, DM caused 1.5 million deaths in 2012. Higher-than-optimal blood glucose caused an additional 2.2 million deaths by increasing the risks of cardiovascular and other diseases.[1,2]

1.1.2 Type 1 and type 2 DM

DM, commonly referred to as diabetes, is a group of metabolic disorders characterized by chronic hyperglycemia with impairment in the metabolism of carbohydrates, lipids and proteins resulting from defects in insulin secretion, insulin action, or both.[4] DM is one of the oldest known diseases, which was first described in an Egyptian manuscript around 1500 B.C.[5] In 1935, two types of DM (type 1 and type 2) were differentiated.[5] Type 1 DM (T1DM), which was previously referred to as insulin-dependent DM (IDDM) or juvenile diabetes, is characterized by destruction or damaging of the β-cells in the islets of Langerhans caused by an autoimmune process, leading to absolute insulin deficiency and hyperglycemia.[4] The cause of T1DM is not known and it is not preventable with current knowledge.[6,7] In contrast, type 2 DM (T2DM), that was formerly known as non-insulin dependent DM (NIDM) or adult-onset diabetes, is characterized by high levels of blood glucose due to insulin resistance and deficiency.[8] T2DM is the most prevalent form of DM and accounts for 90% all cases of DM.[1,2] It is

a major cause of mortality and morbidity, mainly through the increased risk of atherosclerotic vascular diseases which is responsible for up to 80% of these deaths.[1,9]

1.1.3 β-cell dysfunction during progression of T2DM

T2DM is primarily caused by over-nutrition and physical inactivity in individuals that have underlying genetic and acquired predispositions to both insulin resistance and β-cell dysfunction.[10] The co-occurence of metabolic risk factors such as abdominal obesity or central obesity (defined by the absolute waist circumference >102 cm in men and >88 cm in women), insulin resistance, dyslipidemia, and hypertension which has been embraced as the metabolic syndrome (MetS), is highly prevalent worldwide and frequently develops T2DM and cardiovascular diseases.[11-15] Nutrient and energy overload triggers a chronic inflammatory response in adipose tissue characterized by increased cytokine expression (e.g., tumor necrosis factor alpha, TNF-α) and increased infiltration of immune cells (e.g., macrophages) that decreases insulin sensitivity.[16] In response to a chronic fuel surfeit and obesity-associated insulin resistance, pancreatic β-cells increase circulating insulin levels through expansion of β-cell mass and enhancement of β-cell functions, and thereby maintaining normal glucose levels.[10] Impaired compensation of β-cell to insulin resistance results in progressive decline in β-cell function and gradual loss of β-cell mass due to apoptosis and dedifferentiation.[17-20] As a consequence, subjects progress from normal glucose tolerance (NGT) to impaired glucose tolerance (IGT) and finally develop to T2DM[10,21] (**Figure 1**).

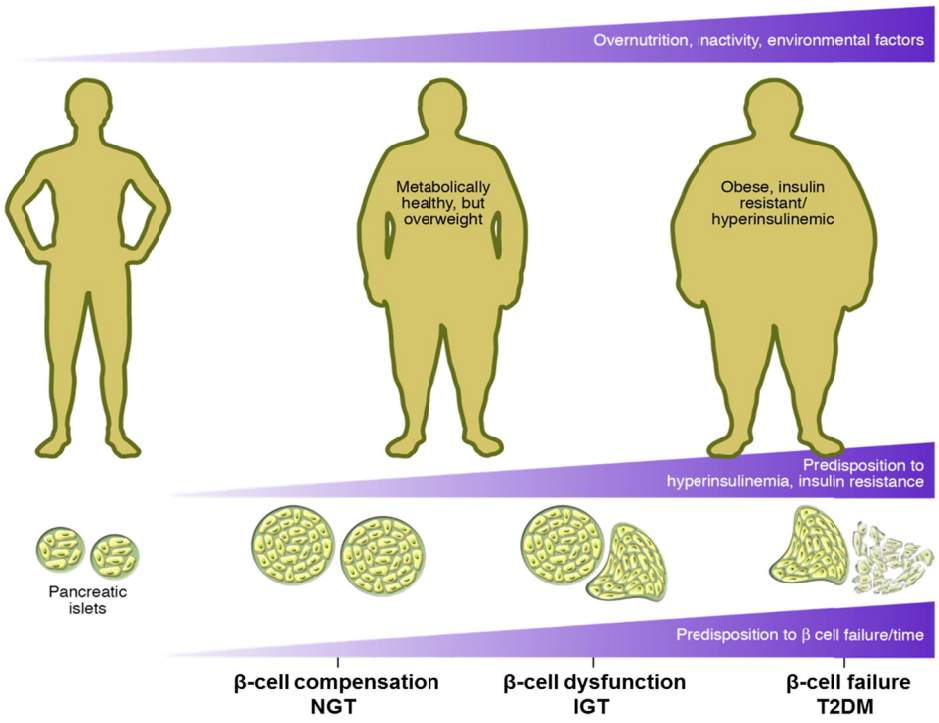

Figure 1. Development of T2DM. Insulin resistance is usually associated with obesity and precedes the development of hyperglycemia. In the early stage, pancreatic β-cells compensate for insulin resistance by hypersecretion of insulin, and thereby maintain normal glucose levels. Over time, β-cell compensation fails due to a decline in β-cell function. As a consequence, normal glucose tolerance (NGT) progresses to impaired glucose tolerance (IGT) and finally to overt T2DM. Figure modified from Goodpaster and Wolf.[22]

1.1.4 Glucagon-like peptide-1 (GLP-1)

Impaired nutrient-induced secretion of glucagon-like peptide-1 (GLP-1) contributes to progressive β-cell failure in T2DM and obesity.[23-25] GLP-1 is a potent incretin hormone derived from the glucagon (GCG) gene, which encodes a large proglucagon precursor containing the four distinct peptides glucagon, GLP-1, GLP-2 and glicentin.[26,27] The maturation and relative amounts of these peptides are regulated by tissue-specific post-translational modification through prohormone convertases (PC). PC2 (encoded by the Pcsk2 gene) produces primarily glucagon from proglucagon in pancreatic α-cells, whereas PC1/3 (encoded by the Pcsk1 gene) generates GLP-1 in intestinal epithelial enteroendocrine L-cells[28,29] and to a lesser extent in neuronal cells of central nervous system (CNS)[30-33] (**Figure 2**). Notably, accumulated evidence demonstrates that

bioactive GLP-1 and PC1/3 may also be co-expressed in rodent and human α-cells, which plays a protective role in hyperglycemia and β-cell dysfunction.[34-40]

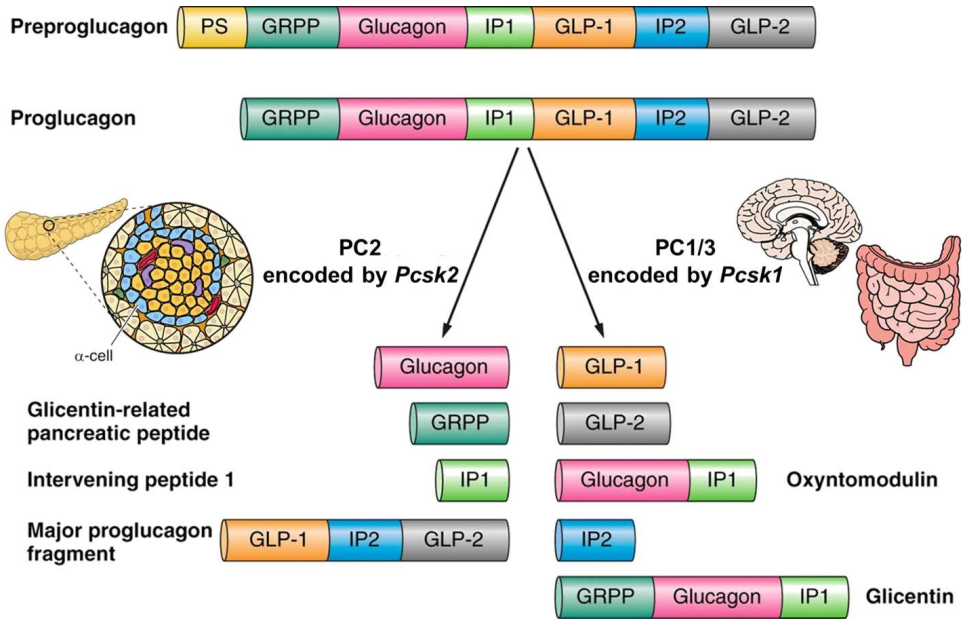

Figure 2 Posttranslational processing of proglucagon. Proglucagon is differentially processed based on the relative activities of the PC1/3 and PC2. In the intestinal L-cell and specific CNS neurons, PC1 activity is greater than that of PC2 and results in the cleavage of proglucagon to GLP-1, GLP-2, oxyntomodulin, glicentin, and IP2. In pancreatic α-cells, PC2 processes proglucagon to glucagon, glicentin-related pancreatic polypeptide (GRPP), intervening peptide 1 (IP1), and a proglucagon fragment. Recent evidence indicates that biologically active GLP-1 may also be produced in α-cells by PC 1/3 following injury. Figure modified from Sandoval and D'Alessio.[41]

The constant basal secretion of GLP-1 from endocrine cells usually ranges from 5 to 10 pmol/l and is rapidly increased after oral nutrient ingestion.[32,41-46] Notably, the cytokine interleukin-6 (IL-6) is an important stimulus of GLP-1 secretion. Administration of IL-6 or elevated IL-6 concentrations in response to exercise stimulate GLP-1 secretion from intestinal L-cells and pancreatic α-cells.[47] Moreover, IL-6 increased GLP-1 production in α-cells by upregulating proglucagon and PC1/3 expression[47,48] (**Figure 3**).

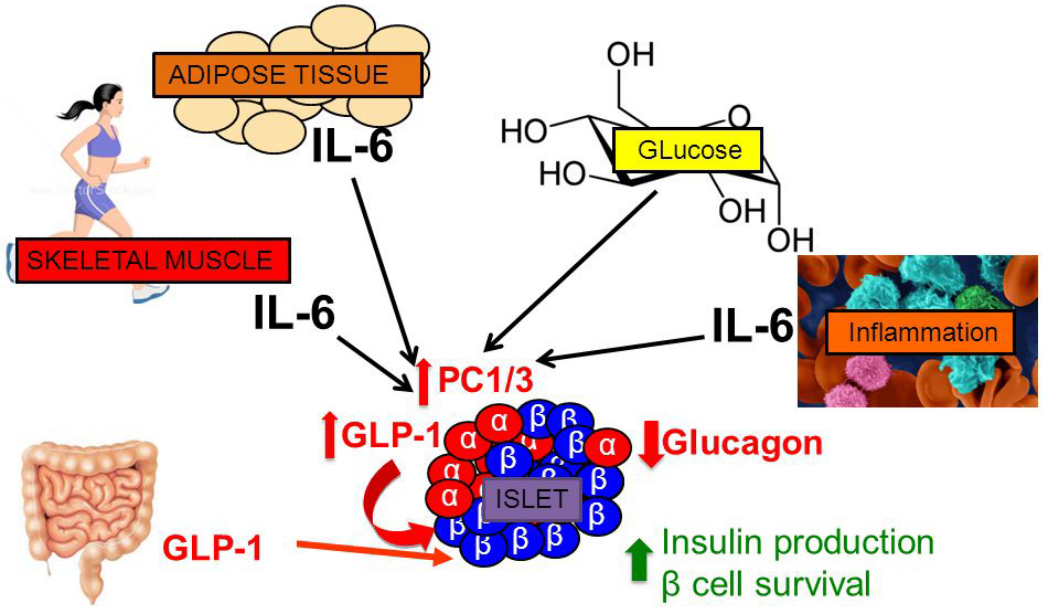

Figure 3. IL-6 serves as a trigger of GLP-1 production. Elevated IL-6 levels in response to exercise as well as acute and chronic IL-6 administration can stimulate GLP-1 production in pancreatic α-cells by upregulating proglucagon and PC1/3 expression, leading to improved glucose homeostasis. Figure modified from Donath and Burcelin.[49]

Upon its release, GLP-1 affects multiple target organs throughout the body by binding to the G protein-coupled GLP-1 receptor (GLP-1R).[50,51] In addition to triggering glucose-dependent insulin secretion, GLP-1 suppresses glucagon secretion, increases insulin synthesis, promotes β-cell growth and neogenesis, and inhibits β-cell apoptosis.[41,45,50-53] *Glp1r* knockout in β-cell results in β-cell dysfunction, impaired intraperitoneal glucose tolerance in response to parenteral GLP-1 administration.[54] Selective restoration of the GLP-1R in the murine pancreas promoted β-cell mass expansion and improved glucose tolerance.[55] Peripheral actions of GLP-1 include alteration of gastrointestinal motility and retardation of gastric emptying.[41,50] In the CNS, GLP-1 induces satiety and body weight loss.[56,57] CNS-specific inactivation of GLP-1R in nestin-Cre $Glp1r^{-/-}$ mice blunted the weight loss-inducing effects of GLP-1.[58] Although glucose tolerance and the glucose-lowering effects of GLP-1 are not affected in mice lacking neuronal GLP1R, GLP-1R agonists have no effect on food intake and body weight, or causing a conditioned taste aversion in those mice.[59] Moreover, beneficial effects of GLP-1 independent of glucose homeostasis have been described in heart[60-63], adipose tissue[64,65], skeleton[66], subpopulations of immune

cells[67,68], and other target organs,[69,70] through direct actions on tissues expressing GLP-1R and indirect effects mediated by neuronal and endocrine pathways.[46]

1.2 Lipopolysaccharide (LPS) in glucose homeostasis and obesity

The effect of a high fat diet (HFD) on obesity and diabetes is mediated by chronically elevated circulating LPS levels, which triggers low-grade inflammation and leads to adipose tissue inflammation, obesity, and insulin resistance.[71-74] However, low dose LPS also promotes glucose-stimulated insulin secretion by up-regulating IL-6 mediated GLP-1 production and thus lower blood glucose levels (**Figure 5**),[48,75] indicating a protective effect of LPS on glucose homeostasis.

1.2.1 Structure and biological functions of LPS

LPS, also termed endotoxin, is the major outer membrane component of gram-negative bacteria contributing greatly to the structural stability and integrity of the bacteria, and protecting the membrane from certain kinds of environmental stresses.[76,77] LPS is a macromolecular glycolipid typically composed of a hydrophobic domain known as lipid A that is responsible for the major bioactivity of endotoxin, a non-repeating "core" oligosaccharide, and a distal hydrophilic polysaccharide composed of O-antigen.[76,78] The common structural pattern of LPS in diverse bacterial species is recognized by a cascade of accessory proteins and LPS receptors, such as the LPS binding protein (LBP)[79,80], cluster of differentiation 14 (CD14)[81] and the Toll-like receptor 4 (TLR4)–MD-2 complex[82,83]. LPS is initially extracted and disaggregated by LPB from bacterial membranes. LBP functions as a catalytic transfer protein in plasma that delivers LPS to CD14, which can be found either in soluble form (sCD14) or linked to the surface of innate immune cells by a glycosyl-phosphatidylinositol (GPI) anchor (mCD14). CD14 then transfers LPS to a heterodimeric complex of MD2 bound to TLR4, which leads to activation of multiple signaling pathways, such as nuclear factor-κB (NF-κB) and IRF3, and the subsequent production of pro-inflammatory cytokines. (**Figure 4**) [84-86]

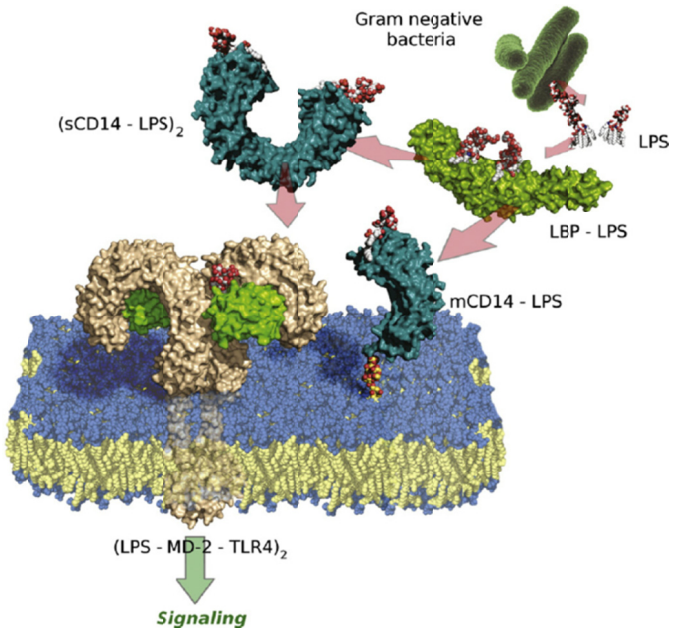

Figure 4. A schematic overview of the immune recognition of LPS. LPS is extracted from bacterial membranes by LBP in serum. LBP then transfers LPS to CD14, which can be found either in soluble form (sCD14) or linked to the cell surface by a glycosyl-phosphatidylinositol anchor (mCD14). CD14 splits LPS into monomeric molecules and presents them to the TLR4–MD-2 complex. Aggregation of the TLR4–MD-2 complex after binding LPS triggers an intracellular signaling cascade. Figure modified from Peri and Piazza.[87]

1.2.2 LPS and hyperlipidemia

Although LPS concentrations are very high in the gut lumen, where trillions of commensal bacteria reside,[88] circulating LPS levels in the blood of healthy humans and animals are normally low (between 1 and 200 pg/ml).[89-91] However, a HFD increases the intestinal permeability by altering distribution and localization of tight-junction proteins and promotes the leakage of intestinal LPS into the circulation.[73,92-94] In plasma, LPS binds primarily to ApoB-containing lipoproteins, such as low-density lipoproteins (LDL) and very low-density lipoproteins (VLDL), which form a LPS-lipoprotein complex via LBP[95,96] (**Figure 5**). Notably, in hyperlipidemic patients, elevated lipoprotein levels rapidly induce high levels of LBP in the circulation, which facilitates the LPS-lipoprotein complex formation and enhances LPS-LDL/VLDL interaction.[95,96] Accordingly, a large clinical study has found that patients with familial hypercholesterolemia (a genetic disorder characterized by extreme LDL cholesterol

levels due to LDL-receptor mutations) have a reduced risk for T2DM and obesity.[97] However, the mechanism by which hyperlipidemia affects pancreatic β-cell function and glucose homeostasis is not clear.

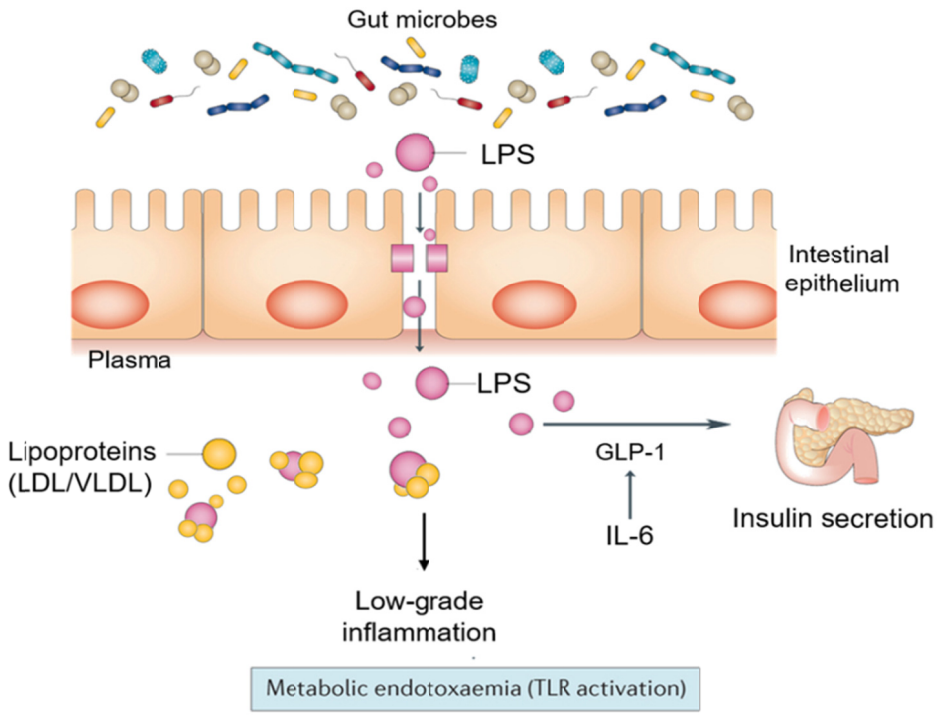

Figure 5 Effect of LPS on metabolism and glucose homeostasis. In response to a high fat diet, LPS leaks into the blood due to increased intestinal permeability. In plasma, lipoproteins, such as LDL and VLDL primarily bind to circulating LPS via LBP. Moreover, low-dose LPS induces GLP-1-mediated insulin secretion and reduces blood glucose levels. However, chronically elevated circulating LPS levels (termed metabolic endotoxemia) trigger adipose tissue inflammation, obesity, and insulin resistance via the TLR4 pathway. Figure modified from Cani, Plovier *et al.*[74]

1.3 MicroRNA-155-5p (miR-155-5p)

A class of small non-coding RNAs termed microRNAs (miRNAs), was first discovered in *Caenorhabditis elegans (C. elegans)* in 1993.[98] In the past few decades, hundreds of miRNAs were subsequently found in all known plant and animal species, and have been recognized as key regulators in various physiological and pathological processes.[99] Mature miRNAs are approximately 20-25 nucleotides (nt) in length and regulate gene expression by binding to complementary sites within the 3-untranslated regions (3'-

UTRs) of target messenger RNAs (mRNAs).[100] In contrast to plants, where miRNAs are perfect complementary to their mRNA targets, partial sequence complementarity including Watson-Crick base pairings of the nt 2 – 7 of the miRNA with the target mRNA is characteristic in mammals.[101]

1.3.1 Biogenesis of miR-155-5p

Hyperlipidemia and LPS promote inflammatory gene expression in macrophages by up-regulating miR-155-5p,[102-105] whose mature sequence is highly conserved throughout evolution. miR-155-5p is encoded by the *MIR155* host gene (*MIR155HG*, # NR_001458),[106] which is located on chromosome 21 in humans within an exon of the conserved region of the non-coding *B-cell integration cluster* (BIC) RNA.[107,108] The *MIR155HG* is initially transcribed by the RNA Polymerase (RNase) II into an approximately 1500-nt long primary miRNA transcript (known as pri-miR-155) with a poly(A)-tail and 5'-cap.[109] Pri-miR-155 is cleaved in the nucleus by the nuclear microprocessor complex, consisting of the RNase III type endonuclease Drosha and its cofactor DiGeorge syndrome critical region 8 (DGCR8),[110,111] to produce a 65-nt long precursor miRNA (pre-miR-155, **Figure 6**) hairpin with a 2-nt overhang at the 3'-end[110,112]. The 2-nt overhang is recognized by the nuclear export factor exportin 5, which translocates the pre-miR-155 into the cytoplasm through a nuclear pore complex in a guanosine-5'-triphosphate-dependent manner.[113]

In the cytoplasm, the pre-miR-155 hairpin is cleaved by the RNase III enzyme Dicer into a double-stranded miRNA duplex with a length of 22-nt.[114,115] Following Dicer cleavage, the miRNA duplex is loaded into Argonaute (Ago) proteins in an ATP-dependent manner, generating the precursor RNA-induced silencing complex (pre-RISC).[116] During duplex unwinding, the two strands of the miRNA duplex are separated and the "guide strand" or "mature miRNA" (miR-155-5p or miR-155) remains within the Ago protein, which leads to the formation of the mature RISC.[114] The other strand of the previous miRNA duplex, termed "passenger miRNA" (miR-155-3p or miR-155*), is released and mostly degraded[114] (**Figure 6**). Recent studies suggest that both strands of the pre-miR-155 hairpin can give rise to mature miRNAs[117,118] and pre-miR-155 products are denoted with the suffix -5p (miR-155-5p, from the 5′ strand) and -3p (miR-

155-3p, from the 3′ strand) following their name.[119] However, the expression level of miR-155-5p is generally higher than that of miR-155-3p.

The miR-155-5p bound to Ago proteins recognize their target mRNAs by base pairing between the miRNA seed sequence (nt 2 – 8 in the 5' end of the miR-155-5p) and the complementary nucleotides predominantly in the 3'-UTR of the target mRNA.[120] The miR-155-5p-target interaction can promote mRNA degradation by exonucleases or induce translational repression without affecting the mRNA stability by blocking translational initiation or elongation.[114]

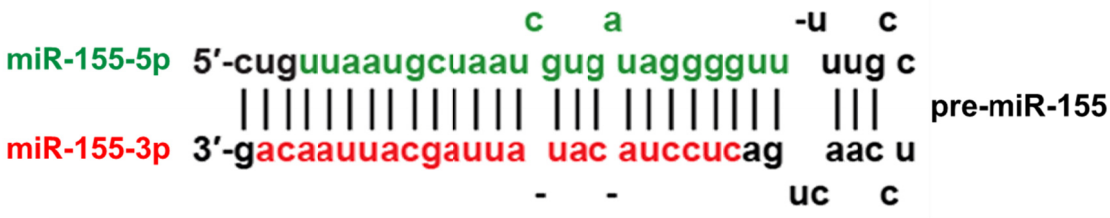

Figure 6. The sequence of the pre-mir-155 stem loop. The mature miR-155-5p sequence is shown in green and mature miR-155-3p sequence is shown in red.

1.3.2 miR-155-5p mediates the effects of LPS

In macrophages, many LPS effects are mediated through miR-155-5p, which is preferentially up-regulated upon TLR4 activation.[102,103,121] In addition to LPS, modified LDL and hyperlipidemia also induce miR-155-5p in a TLR4-dependent manner.[104,122] The functional role of miR-155 in macrophages, however, seems to be stimulus and context-dependent. miR-155-5p targets SH2-containing inositol-5'-phosphatase (SHIP1), an important negative regulator of the PI3K/Akt pathway and TLR4 signalling, and suppressor of cytokine signalling (SOCS1) in macrophages indicating a pro-inflammatory effect,[102,123] whereas anti-inflammatory effects of miR-155-5p have also been reported[124]. Silencing of oxidized LDL (oxLDL)-induced miR-155-5p in macrophages enhanced lipid uptake, activated the NF-κB pathway, increased the expression of scavenger receptors, and promoted the secretion of several pro-inflammatory cytokines.[125] In atherosclerosis, miR-155-5p increases advanced atherosclerosis by impairing efferocytosis and promoting inflammatory activation, but reduces early lesion formation through inhibition of macrophage

proliferation.[103,104,122,126-129] In adipocytes, inflammatory cytokines, such as TNF-α promotes to adipocyte dysfunction by up-regulating miR-155-5p expression,[130] which may contribute to HFD-induced obesity progression in female mice[131] by limiting brown adipose tissue differentiation.[132] By contrast, miR-155-5p levels in adipose tissue are downregulated in patients with T2DM and negatively correlated with adipocyte size and macrophage infiltration in human adipose tissue, indicating a beneficial role of miR-155-5p.[133]

Hence, the role of miR-155-5p in obesity and obesity-related metabolic and cardiovascular diseases is incompletely understood. Whether miR-155-5p mediates the effect of endotoxemia on glucose homeostasis, pancreatic β-cell function and lipid metabolism is not clear.

1.4 Aims of the study

Obesity and adipocyte hypertrophy are accompanied by inflammatory macrophage recruitment, which contributes to insulin resistance through secretion of inflammatory cytokines and frequently results in metabolic dysfunction and T2DM.[134] The effect of a HFD on obesity and insulin resistance is mediated by increased circulating LPS levels.[72,73] miR-155-5p is preferentially expressed in macrophages upon activation with LPS and other TLR ligands, which promotes pro-inflammatory signaling and the polarization into a M1 phenotype.[102,104,122] To investigate the role of miR-155-5p in HFD-induced metabolic and cardiovascular diseases, obesity associated-adipose tissue inflammation, hyperglycemia, dyslipidemia and atherosclerosis was studied in *Mir155*$^{-/-}$ *Ldlr*$^{-/-}$ and *Mir155*$^{+/+}$*Ldlr*$^{-/-}$ mice after a 24-wks cholesterol enriched-diabetogenic diet (DDC) feeding period.

In the circulation, LPS binds to ApoB-containing lipoproteins, such as LDL and VLDL, and thereby prevent LPS from binding to cells and retard its clearance.[96,135] Notably, patients with mutations in the *Ldlr* gene (known as familial hypercholesterolemia) have a reduced risk for T2DM,[97] probably due to increased LPS binding capacity of lipoproteins during hyperlipidemia.[96] Moreover, LPS directly affects the glucose homeostasis by inducing GLP-1 mediated insulin secretion,[48,75]

however, the molecular mechanism is not clear. Therefore, we hypothesized that miR-155-5p mediates the effect of hyperlipidemia-associated endotoxemia on glucose homeostasis. To test this hypothesis, the role of miR-155-5p in pancreatic islets function under hyperlipidemic condition was studied in *Ldlr*$^{-/-}$ mice with or without DDC feeding by intraperitoneal glucose tolerance test (IPGTT), immunostaining staining, Luminex assay and quantitative real-time polymerase chain reaction (qPCR). Next, I sought to determine the regulation of miR-155-5p expression in islets by hyperlipidemia and LPS. Moreover, to investigate the mechanism by which miR-155-5p affects glucose homeostasis, microarray analysis was performed is islets and potential targets were studied by luciferase assay, immunoprecipitation, and gain-and-loss-of-function experiments both *in vivo* and *in vitro*. Finally, to investigate the role of a specific miR-155-5p-target interaction in hyperlipidemia-regulated β-cell function, target site blockers (TSB) were used to inhibit the interaction between miR-155-5p and v-maf musculoaponeurotic fibrosarcoma oncogene family, protein B (MafB).

2 MATERIALS AND METHODS

All solutions were prepared with ultrapure (UP, Type 1) water (Milli-Q Integral 3/5/10/15 Systems, Merck Millipore, Darmstadt, Germany). The reagents were purchased from Thermo Fisher Scientific (Waltham, MA, USA), Sigma-Aldrich (St. Louis, Missouri, USA), Carl Roth (Karlsruhe, Germany), Merck (Darmstadt, Germany), and Fluka (Buchs, Switzerland) unless stated otherwise in the text.

2.1 General equipment

Balances	Precisa 92SM-202A analytical balance, Sartorius CPA64 analytical balance (both from Sartorius Mechatronics, Göttingen, Germany; weighing accuracy of 0.1 mg), and Precision balance EMB 6000-1, (KERN & SOHN GmbH, Balingen, Germany; weighing accuracy of 0.1 g)
Centrifuges	Heraeus Pico 17, Heraeus Megafuge 1.0R (both from Thermo Fisher Scientific, Waltham, MA, USA), Eppendorf 5430R, Eppendorf 5415C, Eppendorf 5415D (all from Eppendorf AG, Hamburg, Germany)
Cryogenic freezer	Panasonic MDF-C2156VAN-PE ultra-low temperature freezer (-150 °C; Panasonic, Osaka, Japan) and NewBrunswick Premium U570 comfort (-80 °C; Eppendorf AG)
Microscopes	Leica DM6000B, Leica LMD7000 (both from Leica Microsystem, Wetzlar, Germany), Olympus IX50 (Olympus optical Co., Tokyo, Japan) and Zeiss 47 30 11-9901 (Carl Zeiss, Oberkochen, Germany)

Imaging software	Leica Application Suite (LAS) AF version 3.2.0.9652 and X LAS X version 1.9.0.13747 (Leica Microsystem)
Tissue homogenizer	TissueLyser LT (Qiagen, Hilden, Germany)
Tissue processor	Leica ASP200 S fully enclosed tissue processor (Leica Biosystems Nussloch GmbH, Nussloch, Germany)
Embedding station	Leica EG 1160 embedding center (Leica Biosystems)
Microtome	Leica RM 2235 (Leica Biosystems)
Cryostat	Leica CM 3050S (Leica Biosystems)
Hematology analyzer	ScilVet ABC (scil animal care company GmbH, Viernheim, Germany)
PCR thermal cyclers	Master Cycler Nexus (Eppendorf AG), Applied Biosystems 2720 and 7900HT Fast Real-Time PCR System (Applied Biosystems, Darmstadt, Germany)
Gel documentation	Intas UV transillumination AF100 312nm/16x20cm (INTAS Science Imaging Instruments GmbH, Göttingen, Germany)
Fragment analyser	Fragment analyser (Agilent Technologies, Santa Clara, CA, USA)
CO_2 Incubator	Galaxy S 170-200 (RS Biotech, Irvine, UK)
Laminar flow hood	Herasafe and Maxisafe 2020 Class II Biological Safety Cabinets (both from Thermo Fisher Scientific)
Flow cytometers	BD FACS Canto II (Becton, Dickinson and Company, NJ, USA) and Attune Acoustic Focusing Cytometer (Thermo Fisher Scientific)

Sephadex column	Sephadex Column for Lipid Analytics Fraction collector (SHIMADZU, Tokyo, Japan)
Plate reader	Infinite F200 PRO (Tecan Trading AG, Männedorf, Switzerland)
pH-meter	WTW Labor-pH-Meters pH 526 (Xylem Analytics Germany Sales GmbH & Co. KG, Weilheim, Germany)
Spectrophotometer	Nanodrop 1000 (PeqLab, Erlangen, Germany)
Syringes	BD Discardit II (Becton, Dickinson and Company), Omnican F (B. Braun AG, Melsungen, Germany)
Thermoblocks	Thermostat Plus and Thermomixer comfort (both from Eppendorf AG)
Vortex mixer	Vortex-Genie 2 (Scientific Industries, Inc., Bohemia, NY, USA)
Autoclave	Systec VX-95 (Systec GmbH, Wettenberg, Germany)
Oven	Memmert U40 (Memmert GmbH + Co. KG, Schwabach, Germany)
Water bath	Memmert WB14 (Memmert GmbH + Co. KG)

2.2 Chemicals

β-Mercaptoethanol (Sigma-Aldrich, Steinheim, Germany)

Dimethyl sulfoxide (DMSO, Carl Roth, Karlsruhe, Germany)

Lipofectamin 2000 (Thermo Fisher Scientific Inc., Waltham, MA, USA)

Antifade Mounting Medium with 4', 6-diamidino-2-phenylindole (DAPI) (Vector laboratories, INC., Burlingame, CA, USA)

Paraformaldehyde (PFA) (Carl Roth)

Paxgene tissue container (Qiagen, Hilden, Germany)

Eosin Y-solution 0.5% alcoholic (Merck Millipore, Darmstadt, Germany)

Hematoxylin Solution, Mayer's (Sigma-Aldrich)

Avidin/Biotin blocking solution (Vector laboratories)

Phosphate buffered saline (PBS) powder (Biochrom AG, Berlin, Germany)

PBS solution (for cell culture, Potential of hydrogen (pH) 7.4, Thermo Fisher Scientific)

Hank's balanced salt solution (HBSS, 10X, no calcium, no magnesium, no phenol red, Thermo Fisher Scientific)

HBSS (10X, calcium, magnesium, no phenol red, Thermo Fisher Scientific)

RNaseZap® decontamination solution (Thermo Fisher Scientific Inc)

RNAlater® Ambion, (Thermo Fisher Scientific)

Triton X-100 (Sigma-Aldrich)

Tween® 20 (Merck Millipore)

Vitro Clud® embedding medium (R. Langenbrinck, Emmendingen, Germany)

2.3 Antibodies

2.3.1 Primary antibodies

Antigen	Clone	Host	Catalog	Company
MafB	polyclonal	rabbit	IHC-00351	Bethyl Laboratories, TX, USA
Insulin	polyclonal	guinea pig	ab7842	Abcam, Cambridge, UK

Glucagon	monoclonal (EP3070)	rabbit	ab92517	Abcam
Ki67	polyclonal	rabbit	ab15580	Abcam
IL-6	polyclonal	rabbit	ab6672	Abcam
IL-6	monoclonal (20F3)	rat	MM600C	Thermo Fisher Scientific
α- smooth muscle actin (SMA)	monoclonal (1A4)	mouse	MO851	Dako, Glostrup, Denmark
Mac2	monoclonal (M3/38)	rat	CL8942AP	Cedarlane, Burlington, Canada
cluster of differentiation (CD)3	monoclonal (CD3-12)	rat	MCA1477	AbD Serotec, Kidlington, UK
Caspase3	polyclonal	rabbit	9661S	Cell Signaling Technology, MA, USA
OxLDL	monoclonal (E06)	mouse	330002S	Avanti Polar Lipids, AL, USA
IgG	N/A	guinea pig	sc-2711	Santa Cruz Biotechnology, CA, USA
IgG	N/A	rat	sc-2026	Santa Cruz
IgG	N/A	mouse	sc-2025	Santa Cruz
IgG	polyclonal	rabbit	ab27472	Abcam

2.3.2 Secondary antibodies

Antigen	**Conjugation**	**Host**	**Catalog #**	**Company**
guinea pig IgG	fluorescein isothiocyanate (FITC)	goat	106-095-003	Jackson ImmunoResearch, Suffolk, UK
rabbit IgG	FITC	donkey	711-095-152	Jackson ImmunoResearch
rabbit IgG	Cy3	goat	111-165-144	Jackson ImmunoResearch
rat IgG	FITC	donkey	712-095-153	Jackson ImmunoResearch
rat IgG	Cyanine 3 (Cy3)	donkey	712-165-153	Jackson ImmunoResearch
mouse IgG	Cy3	donkey	715-165-151	Jackson ImmunoResearch

2.4 Buffers and solutions

UP water (Type I) was generated by Milli-Q Integral 3/5/10/15 Systems and was used to prepare all the buffers and solutions.

Cell lysis buffer (Total protein extraction): 1 tablet of cOmplete, ethylenediaminetetraacetic acid (EDTA)-free protease inhibitor cocktail tablet (Roche Diagnostics GmbH) in 10 mL of radioimmunoprecipitation assay buffer (RIPA) buffer (Sigma-Aldrich).

Citrate buffer: 630 mL UP water, 12.6 mL solution A (2.101 g citric acid in 100 mL UP water), 57.4 mL solution B (14.70 g sodium citrate in 500 mL UP water), 320 μL Tween 20, pH 6.0.

Tris-EDTA antigen retrieval buffer: 1.21 g Tris (10mM, Carl Roth), 0.37 g EDTA (1mM, Sigma-Aldrich), 0.5 mL Tween 20 (0.05%) in 1000 mL UP water, pH 9.0.

EVG staining solutions:

Solution A: 10 g of hematoxylin was dissolved in 100 mL of 96% ethanol.

Solution B: 29% Iron (III)-Chloride solution (145 g of Iron (III)-Chloride was dissolved in 500 mL of UP water), and 7.5 mL of 37% Hydrochloric acid (HCl) was added to 950 mL of UP water.

4% Paraformaldehyde (PFA):

16 g of PFA was added to 184 mL of Millipore water and dissolved by adding 5 mL of 10 M NaOH during heating at 100 °C. The pH was decreased to 7.4 – 8.0 by adding 25% HCl. Subsequently, an equal volume of 2×PBS was added and the solution was filtered through a filter paper (thickness 0.20 mm, Ø 270mm, Macherey-Nagel GmbH & Co. KG, Düren, Germany), pH was adjusted to 7.4 – 8.0.

Immunofluorescence staining:

1% Bovine serum albumin (BSA)-blocking solution: 5.4 mL PBS, 600 µL 10% BSA (SERVA Electrophoresis GmbH, Heidelberg, Germany), 3 drops 2.5% normal horse serum (Vector laboratories, INC., Burlingame, CA, USA).

Antibody solution: 6 mL PBS, 90 µL 1% BSA-blocking solution.

Anesthesia formulary: Take 40 µL of xylazine (5 mg/kg, Serumwerk, Bernburg, Germany) and 160 µL of ketamine hydrochloride (80 mg/kg, Pfizer, Berlin, Germany) with a 1 mL syringe. Fill the syringe with 800 µL of 0.9% weight per volume (w/v) NaCl up to 1mL and mix it properly.

Sodium nitroprusside dehydrate solution: 156 mg of sodium nitroprusside dihydrate in 50 mL PBS.

20× Saline-sodium citrate (SSC) buffer: 3 M NaCl, 0.3 M Na citrate (pH 7.0).

Tris-NaCl blocking (TNB) buffer: 7.88 g Tris-HCl was dissolved in 500 mL water and pH adjusted to 7.5 using NaOH. NaCl (4.383g) and 2.5g blocking reagent were added and the solution heated up to 55°C for about 30 min.

Tris-NaCl Tween (TNT) buffer: 250 µL of Tween 20 to Tris-NaCl solution.

2.5 Mouse husbandry

Animals were housed in cages with microisolator filter tops and maintained on a 12-h light/dark cycle in a temperature-controlled room of the animal laboratory facility of the university, the Zentrale Versuchstierhaltung (ZVH), Klinikum Universität München (KUM). Mice had free access to water and mouse chow. All animal experimental procedures were reviewed and approved by the government of upper Bavaria (Regierung von Oberbayern) in accordance with German animal protection laws.

2.6 Mouse strains

MicroRNA-155 knock out (*Mir155*$^{-/-}$) and low-density lipoprotein receptor knock out (*Ldlr*$^{-/-}$) mice on a C57BL/6J background (both from Jackson Laboratory, Bar Harbor,

ME, USA) were crossed to obtain *Mir155*$^{-/-}$*Ldlr*$^{-/-}$ mice. *Mir155*$^{+/+}$*Ldlr*$^{+/+}$ (*Mir155*$^{+/+}$) and *Mir155*$^{+/+}$ *Ldlr*$^{-/-}$ mice served as control of *Mir155*$^{-/-}$ *Ldlr*$^{+/+}$ and *Mir155*$^{-/-}$*Ldlr*$^{-/-}$ mice in this study, respectively.

2.7 Animal models

2.7.1 Diabetogenic diet-induced MetS model

Male *Mir155*$^{-/-}$*Ldlr*$^{-/-}$ and *Mir155*$^{+/+}$*Ldlr*$^{-/-}$ mice (8 – 10 wk old) were fed a diabetogenic diet supplemented with cholesterol (DDC; 35.5% pork lard as fat, 20.1% crude protein, 36.3% carbohydrates with 0.15% weight per weight (w/w) total cholesterol; catalog # S0580-E005, ssniff Spezialdiäten GmbH, Soest, Germany) or a normal diet (ND; 3.3% fat, 19.0% crude protein, Catalog # V1534-3, ssniff Spezialdiäten GmbH) for 24 wk. Body weight was measured every 2 wk using a calibrated digital scale (Kern & Sohn GmbH; weighing accuracy of 0.1 g). Fasting blood glucose (FBG) levels were measured every 4 wk in blood samples obtained from the tail vein after a 5 – 6 h fasting period using a glucometer (Roche Diagnostics GmbH, Basel, Switzerland, **see also section 2.9.1**).

2.7.2 Tissue harvesting

After a fasting period of 5 – 6 h, mice were anesthetized by intraperitoneal injection of ketamine hydrochloride (80 mg/kg) and xylazine (5 mg/kg). Blood was collected from the orbital vein to determine blood cell count and metabolic parameters. The abdominal and chest cavities were then surgically opened. A catheter was inserted into the left ventricle through an incision in the apex. Ice-cold PBS (10 – 15 mL, Thermo Fisher Scientific) was perfused using a sterile syringe (10 mL, Becton, Dickinson and Company) through the left ventricle and drained via an incision in the right atrium.

After perfusion with PBS, aortic roots and pancreas were harvested and placed in PAXgene Tissue Fix solution (Qiagen, Hilden, Germany) for 2 – 4 h at room temperature (RT). Subsequently, tissues were removed from the PAXgene Tissue Fix solution and transferred to the PAXgene Tissue Stabilizer solution. In contrast to paraformaldehyde, PAXgene Tissue Fix is a fixation system that does not cause

destructive nucleic acid crosslinking and degradation, and preserves the morphology. It includes the two components: PAXgene Tissue Fix, which rapidly penetrates and fixes the tissue, and PAXgene Tissue Stabilizer in which nucleic acids and the morphology of the tissue are stable for up to 7 d at RT and for longer periods at 2 – 8 °C or -20 °C. Stabilized samples were embedded in paraffin (**see also section 2.11.1**) for histological studies.

Before the PBS perfusion, epididymal white adipose tissue (eWAT) was excised from reproductive fat pads, and the weight of the fat pads was measured using an analytical balance (Sartorius mechatronics; weighing accuracy of 0.1 mg). The same region of the fat pad was excised in all animals to minimize cell size variation due to differences in anatomical location [136]. The eWAT samples were either fixed using PAXgene Tissue Fix containers for histological studies or immediately stored in RNAlater stabilization solution (Ambion, Thermo Fisher Scientific Inc., Waltham, MA, USA) for RNA isolation (**see also section 2.15**). All instruments used during organ dissection were first treated with RNaseZap® (Ambion, Austin, TX, USA) to remove ribonuclease (RNase).

Pancreas tissue from *Mir155*$^{-/-}$*Ldlr*$^{-/-}$ and *Mir155*$^{+/+}$*Ldlr*$^{-/-}$ mice (10 – 12 wk old) was either fixed with PAXgene followed by paraffin embedding (**see also section 2.11.1**) or embedded in Tissue-Tek O.C.T. Compound (Sakura Finetek, Staufen, Germany), snap frozen on dry ice and stored at -80 °C (**see also section 2.11.3**).

2.8 Blood profile

2.8.1 Serum and plasma preparation

After anesthetizing the animals, approximately 400 – 500 μL of whole blood was collected from the orbital veins in serum-separating tubes (brown tops, SST, Sarstedt, Nümbrecht, Germany) and allowed to clot at RT for 2 h. Subsequently, the tubes were centrifuged at 2000 relative centrifugal force (RCF) for 20 min in a refrigerated centrifuge (4 °C, Eppendorf 5430R, Eppendorf AG). The serum in the supernatant was collected.

For plasma preparation, 200 – 400 μL of whole blood was collected into commercially available anticoagulant-treated tubes (EDTA tubes, red tops, SST) and stored on ice. Cells were removed from plasma by centrifugation for 20 min at 6000 – 8000 RCF using a refrigerated centrifuge. Following centrifugation, the supernatant (plasma) was immediately transferred into a polypropylene tube. The plasma samples were processed within 30 min after collection and maintained at 2 – 8 °C throughout the procedure.

The serum and plasma samples were aliquoted (50 – 100 μL per tube) to avoid freeze-thaw cycles, and stored at -80 °C (NewBrunswick Premium U570 comfortm, Eppendorf AG).

2.8.2 Complete blood cell count

Approximately 20 – 30 μL of whole blood from the orbital veins was collected in EDTA tubes (SST). The complete blood cell count was performed within 1 h after the collection using an animal hematology analyzer (ScilVet ABC, scil animal care company GmbH)

2.8.3 Measurement of cholesterol and triglyceride

Cholesterol concentrations were measured by a fluorometric cholesterol assay kit (Cayman Chemical, Ann Arbor, MI, USA) in plasma and in very low-density lipoprotein (VLDL), low-density lipoprotein (LDL) and high-density lipoprotein (HDL) fractions separated by high-performance liquid chromatography (HPLC) using Sephadex column (SHIMADZU, Tokyo, Japan). Fluorescence intensity was measured using excitation wavelengths at 550 nm and emission wavelengths at 590 nm by a microplate reader (Infinite F200 PRO, Tecan Trading AG, Männedorf, Switzerland).

Plasma triglycerides concentrations were analyzed using the enzymatic colorimetric method (Triglycerides-GPO-PAP kit, Cobas, Roche Diagnostics GmbH)[137]. The plasma samples were diluted with 0.9% w/v NaCl in a proportion of 1:20. The absorbance was measured at 510 nm by a microplate reader (Infinite F200 PRO, Tecan Trading AG).

2.9 Glucose tests

2.9.1 FBG level

FBG levels were determined after a 5 – 6 h fasting period in blood samples obtained from the tail vein using the ACCU-CHEK Inform II test strip and a glucometer (sample size: 0.6 μL; test time: 5 seconds (s); range: 10 – 600 mg/dL). Glucose concentrations were measured at least in duplicate. The ACCU-CHEK Inform II control solutions were used for calibration (all from Roche Diagnostics GmbH).

2.9.2 Intraperitoneal glucose tolerance test (IPGTT)

Mice (10 – 12 wk old) were fasted overnight for approximately 16 h and subsequently injected intraperitoneally with glucose (2 mg/g body weight, cat. no. A2494001, Thermo Fisher Scientific). Venous blood was obtained from the tail vein before (0 min) and 15, 30, 60, 90 and 120 min after the glucose injection. Glucose levels were measured by a glucometer (ACCU-CHEK Inform II, Roche Diagnostics GmbH). For each time point, glucose concentrations of each mouse were measured at least in duplicate.

2.10 Isolation of pancreatic islets

Murine pancreatic islets were isolated by collagenase digestion and density gradient centrifugation using sodium diatrizoate (Histopaque 1119 and Histopaque 1077, Sigma-Aldrich) as previously described[138,139]. In all experiments, islets from 2 – 3 mice were pooled for each biological replicate. The individual steps of the procedure are described in the following sections in detail.

2.10.1 Preparation of solutions

Collagenase P solution: Collagenase P (Roche Diagnostics GmbH) was diluted in 1× HBSS buffer (Thermo Fisher Scientific) at concentration of 1 mg/mL. The solution was used within 4 h.

Stop solution: Add $CaCl_2$ (1 mM, 73.5 mg) into 500 mL 1× HBSS. The solution was used within 24 h.

Murine islet medium: Add L-glutamine (20 mM), gentamicin (0.1%) and fetal bovine serum (FBS; 10%) into Roswell Park Memorial Institute (RPMI) 1640 medium (all from Thermo Fisher Scientific). The solution was used within 4 h.

Histopaque 1100 solution: Combine 120 mL of Histopaque 1.119 g/mL with 100 mL of Histopaque 1077 (1.077 g/mL) to produce a Histopaque 1100 solution (1.100 g/mL).

2.10.2 Pancreas perfusion and removal

Mice were anesthetized by intraperitoneal injection of ketamine hydrochloride (80 mg/kg) and xylazine (5 mg/kg). Blood was drawn from the left ventricle of the heart, and the abdominal cavity was opened to expose the liver and intestines. Collagenase P solution (5 mL) was slowly injected into the common bile duct after occlusion of the ampulla in the duodenum (**Figure 7**).

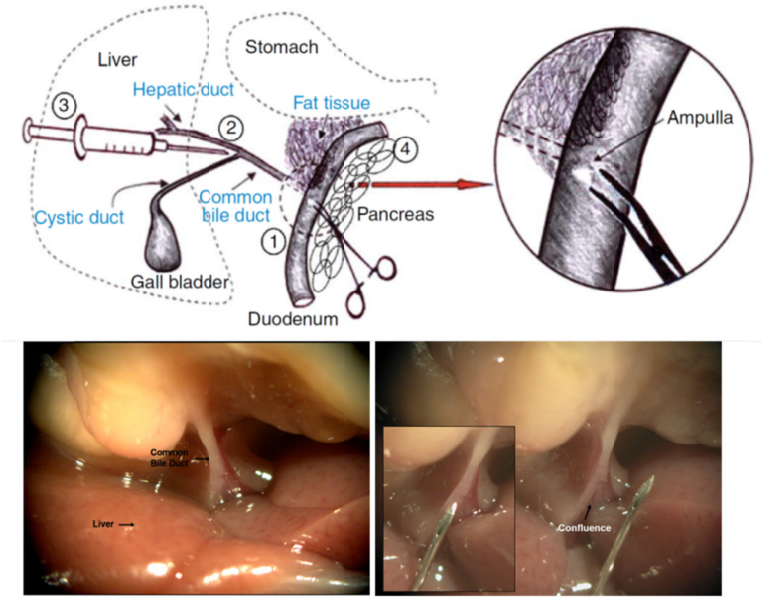

Figure 7. **Procedure of mouse pancreas perfusion and removal.**[139] (1) Find and clamp the ampulla with curved homeostatic forceps. (2) Insert the needle into the common bile duct through the joint site of the hepatic duct and the cystic duct. (3) The solution was injected slowly (4) Harvest the pancreas and avoid fat tissue.

2.10.3 Pancreas digestion and islets purification

The pancreas was excised and digested in 5 mL of the collagenase P solution at 37 °C for 20 min. After incubation, tubes were shaken by hand to disrupt the pancreas until the suspension turns homogeneous. Once the tissue suspension is dissolved to very fine particles, the digestion was terminated by putting the tube on ice, adding 25 mL of stop solution, centrifuging at 300 RCF for 1 min and discarding the supernatant. After a brief washing step, islets were purified by gradient separation. The cell pellet was resuspended by adding 10 mL of Histopaque 1100, overlaid with 10 mL of 1× HBSS and centrifuged at 900 RCF for 20 min. The entire 20 mL of supernatant was then passed through an inverted 70 μm cell strainer (Thermo Fisher Scientific). The islets were collected into a 10 cm Petri culture dish (Corning Inc., NY, USA) by pipetting 10 mL murine islet medium through the strainer.

2.10.4 Islets isolation

Islets were handpicked using a pipette (10 – 100 μL, Eppendorf AG) and counted under an inverted microscope (Olympus optical Co.). After isolation, the islets were either immediately processed for RNA isolation using NucleoSpin microRNA Kit (Macherey-Nagel GmbH & Co. KG, Düren, Germany) (**see also section 2.15**) or lysed in 50 μL of cell lysis buffer (RIPA buffer, Sigma-Aldrich) containing protease inhibitors (cOmplete, EDTA-free protease inhibitor cocktail tablet, Roche Diagnostics GmbH) for protein extraction.

2.11 Histology and Immunostaining

2.11.1 Histology of aortic roots, eWAT and pancreata

Aortic roots, eWAT and pancreata from *Mir155*$^{-/-}$*Ldlr*$^{-/-}$ and *Mir155*$^{+/+}$*Ldlr*$^{-/-}$ mice fed a DDC for 24 wk, and pancreata from *Mir155*$^{-/-}$*Ldlr*$^{-/-}$ and *Mir155*$^{+/+}$*Ldlr*$^{-/-}$ mice (10 – 12 wk old) fed a ND were fixed with PAXgene, dehydrated using tissue processor (Leica ASP200 S) and embedded in paraffin (**Table 1**).

Table 1. Procedure of dehydration.

Step	Reagent	Time (min)	Temperature (ºC)
1	70% Ethanol	60	20
2	80% Ethanol	60	20
3	96% Ethanol	30	20
4	96% Ethanol	30	20
5	100% Ethanol	30	20
6	100% Ethanol	30	20
7	Xylene	30	45
8	Xylene	30	45
9	Paraffin	30	62
10	Paraffin	30	62
11	Paraffin	overnight	62

The paraffin blocks hardened at 0 °C (Leica EG 1160 embedding center, Leica Biosystems) before sectioning using a microtome. Serial sections from aortic roots (5 μm thickness), pancreas (7 μm thickness) and eWAT (7 μm thickness) were collected on glass slides (Superfrost plus glass slides, Thermo Fisher Scientific). The aortic root sections were collected when the first valve was visible. After sectioning, the slides were incubated in a 37 ºC incubator for 5 – 6 h or at RT overnight to reduce detachment of the tissue during staining. Deparaffinization and rehydration of the sections was performed before staining (**Table 2**).

Table 2. Procedure of deparaffinization and rehydration.

Step	Reagent	Time (min)
1	Xylene	10
2	Xylene	10
3	100% Ethanol	5
4	100% Ethanol	5
5	96% Ethanol	5
6	70% Ethanol	5
7	PBS	5 – 10

To measure lesion size, serial sections from aortic roots were selected once all 3 aortic valves appear (every 10 sections, 4 – 5 sections in total per mouse) and stained

with Elastic van Gieson (EvG) stain using an Elastica nach van GIESON kit (12739, Baacklab, Armin Baack, Schwerin, Germany) (**Table 3**). Pancreas (every 10 sections, 4 sections per mouse) and eWAT (every 10 sections, 2 – 3 sections per mouse) sections were stained with hematoxylin and eosin (H&E) (**Table 4**).

Table 3. Procedure of EvG stain.

Step	Reagent	Time	Remark
1	Resorcerin-Fuchsin	15 min	staining of elastic fibers
2	Running tap water	1 min	Wash step
3	Solution A+B	20 min	staining of nuclei*
4	Tap water	10 s	Wash step
5	1 % HCl-alcohol	5 – 10 s	1% HCl in 70% alcohol,
6	UP water	5 s	Wash step
7	Van GIESON Pikrofuchsin solution	1 min	staining of collagen
8	UP water	5 s	Wash step
9	96% ethanol	2 min	Dehydration step
10	96% ethanol	2 min	Dehydration step
11	Isopropanol	2 min	Dehydration step
12	Xylene	5 min	Dehydration step
13	Xylene	5 min	Dehydration step
14	Vitro Clud® mounting solution	N/A	Mounting step

Table 4. Procedure of H&E stain.

Step	Reagent	Time	Remark
1	Hematoxylin	3 – 5 min	Filter before each use
2	Running tap water	10 min	Wash step
3	1 % HCl-alcohol	5 – 10 s	1% HCl in 70% alcohol
4	Tap water	3 min	Wash step
5	Eosin	30 s	Staining of collagen
6	96% ethanol	2 min	Discard after each use
7	96% ethanol	2 min	Dehydration step
8	96% ethanol	2 min	Dehydration step
9	96% ethanol	2 min	Dehydration step
10	Xylene	5 min	Dehydration step

11	Xylene	5 min	Dehydration step
12	Vitro Clud® mounting solution	N/A	Mounting step

2.11.2 Double α-SMA and Mac2 immunostaining

To study the lesion composition, immunostaining was performed in PAXgene-fixed and paraffin-embedded aortic roots sections (5 μm thickness) using antibodies against α-SMA and macrophage-specific Mac2 (**Table 5, see also section 2.3.1**). Briefly, 2 – 3 sections per mouse (50 – 100 μm distances between sections) were selected and deparaffinized (**Table 2**). Antigen retrieval was performed by cooking the sections in citrate buffer (**see section 2.4**) for 20 min. The tissues were then blocked with 1% BSA-blocking solution for 30 min at RT and then incubated over night with the anti-Mac2 antibody at 4°C. The sections were then washed 3 times with PBS and incubated with the specific secondary antibody for 30 min. The sections were then washed and incubated with anti-α-SMA antibody for 4 h at 37ºC, followed by incubation with the secondary antibody. Cell nuclei were counterstained with DAPI (Vectashield, Vector Laboratories, Peterborough, UK). Non-specific primary antibodies were used as negative controls (Santa Cruz Biotechnology, Santa Cruz, CA, USA).

To quantify macrophage infiltration in eWAT, Mac2 staining was performed on PAXgene-fixed and paraffin-embedded eWAT sections (7 μm thickness, 2 – 3 sections per mouse) from *Mir155*$^{+/+}$*Ldlr*$^{-/-}$ and *Mir155*$^{-/-}$*Ldlr*$^{-/-}$ mice fed a DDC for 24 wk, as described above.

Table 5. Immunostaining protocols.

Antigen	**Antigen retrieval**	**Blocking**	**1st primary Ab**	**1st secondary Ab**	**2nd primary Ab**	**2nd secondary Ab**
Mac2/α-SMA	CB, 2×10 min (100ºC)	1% BSA-blocking solution , 30 min	Mac2, 1:200, 4 ºC, overnight	anti-rat IgG FITC-conjugated, 1:100, 30 min	α-SMA, 1:200, 37 ºC, 4 h	anti-mouse IgG cy3-conjugated, 1:300, 30 min

CB = Citrate buffer; Ab = antibody details are provided in sections 2.3;

2.11.3 Immunofluorescence staining in pancreas

Pancreas tissues from *Mir155*$^{-/-}$*Ldlr*$^{-/-}$ and *Mir155*$^{+/+}$*Ldlr*$^{-/-}$ mice (10 – 12 wk old) were embedded in Tissue-Tek O.C.T. Compound (Sakura Finetek) and stored at -80 °C. The frozen blocks were warmed up to -20 °C in a pre-cooled cryostat (Leica CM 3050S, Leica Biosystems) before sectioning. Serial pancreatic sections (10 μm thickness) were collected on glass slides (Superfrost plus glass slides, Thermo Fisher Scientific) and air-dried at RT for 30 – 60 min before being stored at -80 °C. For fixation, the frozen sections were quickly thawed at 37 °C for 1 min using a dry block incubator (Thermostat Plus, Eppendorf AG) and air-dried for 30 – 40 min at RT. The sections were then fixed with either pre-cold acetone or PFA (2 – 4%) (**Table 6**) and permeabilized with Triton X-100 (0.1% in PBS for 5 – 8 min) or Tween 20 (0.2% in PBS for 10 – 20 min).

Table 6. Fixation of pancreatic cryosections.

Reagent and step	Time (min)	Temperature
Acetone fixation		
Pre-cold acetone	10	-20 °C
Air-dry	20 – 30	RT
PBS rehydration	10	4 °C or RT
PFA fixation		
2 – 4 % pre-cold PFA	10	4 °C
PBS rehydration	10	4 °C or RT

Single immunostaining was performed on pancreatic cryosections by sequential incubation with primary antibodies against insulin, glucagon, IL-6, MafB, Ki67, cleaved caspase-3, Mac2 or CD3, and fluorescently conjugated secondary antibodies (**Table 7**).

Table 7. Immunostaining protocols.

Step	Insulin	Glucagon	IL-6	MafB	Ki67	Caspase 3
1	Acetone	Acetone	4% PFA	Acetone	Acetone	Acetone
2	N/A	0.1% Triton X-100, 5 min	N/A	0.1% Triton X-100, 5 min	0.1% Triton X-100, 5 min	0.1% Triton X-100, 5 min
3	1% BSA, 30	1% BSA, 30	1% BSA, 30		1% BSA,	1% BSA, 30

	min	min	min		30 min	min
3	Anti-insulin Ab, 1:200, 4ºC, overnight	Anti-glucagon Ab, 1:1500, 37 ºC, 3 h	1:400, 4 ºC, overnight	Anti-MafB Ab, 1:200, 4ºC, overnight	Anti-Ki67 Ab, 1:1500, 37ºC, 2 h	1:200, 4 ºC, overnight
4	Anti-guinea pig IgG FITC-conjugated, 1:100, 30 min	Anti-rabbit IgG Cy3-conjugated, 1:300, 30 min	anti-rabbit IgG, FITC-conjugated, 1:100, 30 min	Anti-rabbit IgG Cy3-conjugated, 1:300, 30 min	anti-rabbit IgG Cy3-conjugated, 1:300, 30 min	anti-rabbit IgG Cy3-conjugated, 1:300, 30 min
5			Anti-CD3 Ab, 1:100, 37 ºC, 4 h			
6			Anti-rat IgG Cy3-conjugated, 1:300, 30 min			

Ab details are given in **sections 2.3.1 and 2.3.2**

Double immunostaining of insulin and glucagon, insulin and MafB, or Mac2 and CD3 was performed by sequential incubation of the sections with the primary and secondary antibodies for each antigen (**Table 8**).

Table 8. Double immunostaining protocols.

Step	**Insulin/glucagon**	**Insulin/MafB**	**Mac2/CD3**
1	Acetone	Acetone	Acetone
2	N/A	0.1% Triton X-100, 5 min	N/A
3	Anti-insulin Ab, 1:200, 4 ºC, overnight	Anti-insulin Ab, 1:200, 4 ºC, overnight	Anti-Mac2 Ab, 1:200, 4 ºC, overnight
4	Anti-guinea pig IgG FITC-conjugated, 1:100, 30 min	Anti-guinea pig IgG FITC-conjugated, 1:100, 30 min	Anti-rat IgG FITC-conjugated, 1:100, 30 min
5	Anti-glucagon Ab, 1:1500, 37ºC, 3 h	Anti-MafB Ab, 1:200, 4ºC, overnight	Anti-CD3 Ab, 1:100, 37ºC, 4 h
6	Anti-rabbit IgG Cy3-conjugated, 1:300, 30 min	Anti-rabbit IgG Cy3-conjugated, 1:300, 30 min	Anti-rat IgG Cy3-conjugated, 1:300, 30 min

Ab details are given in **sections 2.3.1 and 2.3.2**

In addition, a biotinylated murine monoclonal antibody (mouse monoclonal E06) followed by a Dylight 549-labeled streptavidin (Kirkegaard & Perry Laboratories, Gaithersburg, MD, USA) was used for oxLDL immunostaining. Cell nuclei were counterstained with DAPI. Non-specific primary antibodies were used as negative controls (Santa Cruz Biotechnology).

2.11.4 Image acquisition and planimetry

Digital images were acquired using Leica-DM6000 B microscope (Leica microsystems) connected to a charge-coupled device (CCD) camera (DFC295, Leica microsystems) and the LAS AF software (version 3.2.0.9652). The size of the positively stained area ($Mac2^+$, SMA^+) per aortic lesion area (2 – 3 sections per mouse) and the positive cell number ($Mac2^+$) per total adipocytes in each section (4 – 5 sections per mouse) were determined using image analysis software (ImageJ 1.43n, NIH, USA). In pancreatic islets, the percentage of positive cells ($Insulin^+$, $Glucaon^+$, $MafB^+$) was calculated by dividing the number of positive cells in one islet by the total number of cells in this islet and multiplying this ratio by 100. At least 10 islets were analyzed per each section, and 2 – 3 sections were used for each individual. The background of the negative control staining defined the threshold for the positive staining.

2.12 *In situ* reverse transcriptase PCR

To determine the expression and localization of miR-155-5p in murine pancreatic islets, *in situ* reverse transcriptase PCRs were performed on pancreatic sections from *Mir155*$^{+/+}$*Ldlr*$^{-/-}$ mice fed a ND. The method includes an overnight deoxyribonuclease (DNase) digestion, followed by *in situ* miRNA extension and amplification (reverse transcription and PCR with designed Taq-*in situ*-primers), short low stringency washes and probe visualization. Taq-*in situ*-reverse transcription primer containing the complementary sequence of the miRNA at its 3′ terminus was designed to increase the length of mature miRNAs. Then, the extended miRNA was amplified using pre-designed miRNA specific taq-*in situ*-forward and -reverse primers. The digoxigenin-dUTPs served as reporter nucleotides that were incorporated into the synthesized DNA and detected by anti-digoxigenin antibodies (**Figure 8**).[126,140]

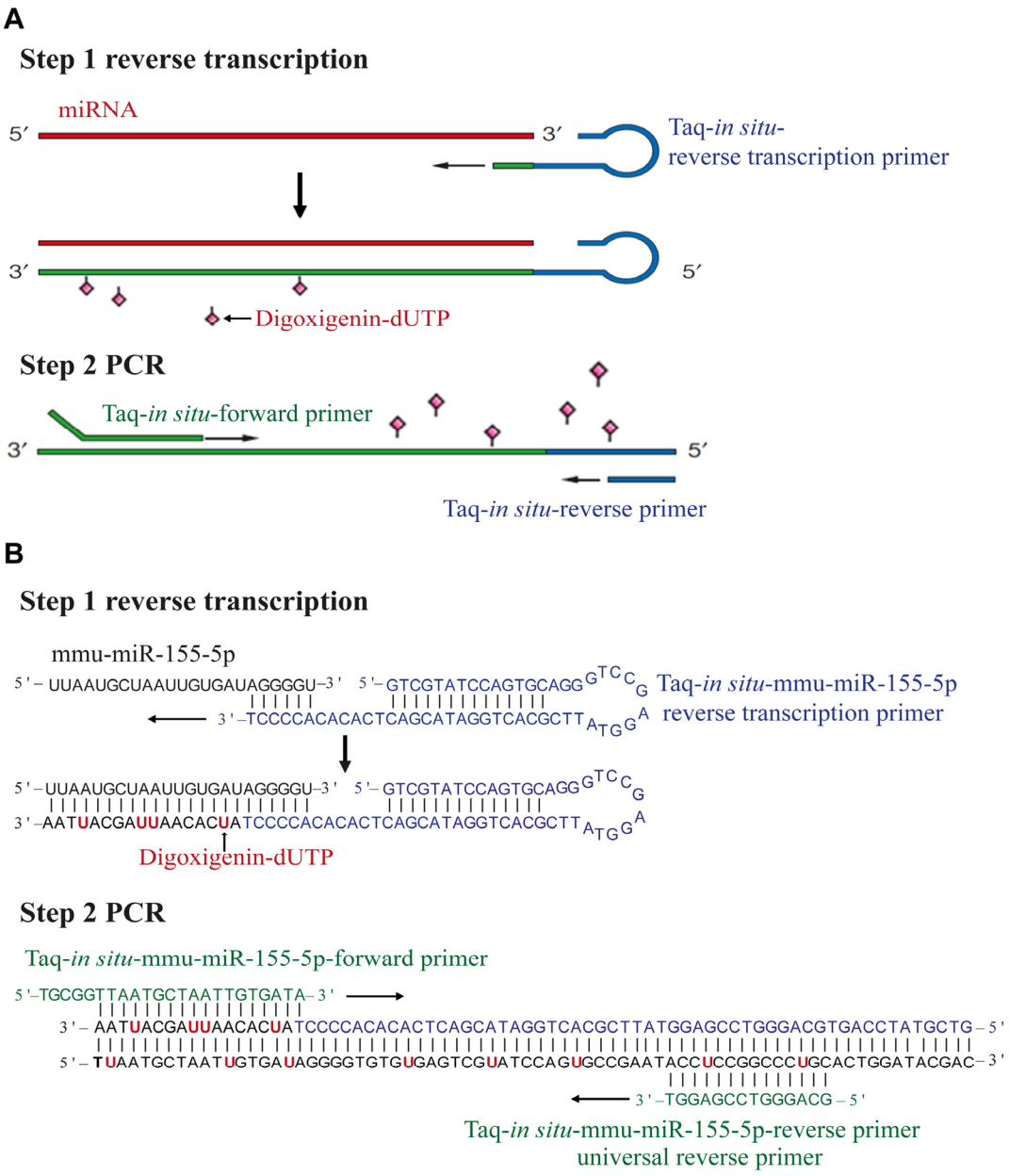

Figure 8. Schematic showing *in situ* reverse transcriptase PCRs. (**A**) In step 1, taq-*in situ*-reverse transcription primers bind to the 3' portion of miRNA molecules, initiating reverse transcription of the miRNA. In step 2, the reverse transcription product is amplified using miRNA specific taq-*in situ*-forward and -reverse primers. In both steps, the digoxigenin-dUTPs serve as reporter nucleotides that are incorporated into the synthesized DNA and detected using an anti-digoxigenin antibody. (**B**) Six nucleotides of 3′ end of the Taq-*in situ*-mmu-miR-155-5p-reverse transcription primer are complementary with the 3′ end of miR-155-5p (Step 1). Taq-*in situ*-mmu-miR-155-5p-forward and -reverse primers were designed for amplification (Step 2). The digoxigenin-dUTP is highlighted in red.

PAXgene-fixed pancreatic sections (7 μm thick) were deparaffinized (**Table 9**), covered by hybridization chambers (SecureSeal™ hybridization chambers-8-9mm Dia. X 1.0 mm Depth, Grace Bio-Labs, Oregon, USA) and treated with RNase-free DNase (Roche Diagnostics GmbH) for 16 h at 37 °C (**Figure 9**). After removing the tissue hybridization chambers, the DNase was removed by flushing the slides 2 – 3 times with DEPC-treated water. Subsequently, the slides were quickly dipped in RNase-free ethanol (100%) and air-dried.

Table 9. Deparaffinization for *in situ* PCR.

Step	Reagent	Time
1	Xylene	5 min
2	Xylene	5 min
3	100% Ethanol	3 min
4	100% Ethanol	3 min
5	96% Ethanol	3 min
6	70% Ethanol	3 min
7	100% Ethanol	5 s
8	air-dry	2 min

Figure 9. Approximately 50 μL of the DNase was added to each section through the hole of the hybridization chamber and covered RNase-free adhesive film. The slides were then incubated at 37 °C in the Thermoblocks or Thermal cyclers.

One-step reverse transcriptase *in situ* PCR was performed using gene-specific Taq-*in situ*-mmu-miR-155-5p primers (Sigma-Aldrich) (**Table 10** and Figure XX), the SuperScript One-Step RT-PCR System with Platinum Taq DNA Polymerase (Thermo Fisher Scientific), and digoxigenin-11-dUTPs (Roche Diagnotics GmbH) (**Table 11**). The worm-specific microRNA cel-miR-39 was used as negative control.

Table 10. Primer sequences for *in situ* PCR.

Gene	Primer sequences
Taq-in situ-mmu-miR-155–reverse transcription	5'-GTCGTATCCAGTGCAGGGTCCGAGG TATTCGCACTGGATACGACTCACACACCCCT-3'
Taq-*in situ*-mmu-miR-155–Forward	5'-TGCGGTTAATGCTAATTGTGATA-3'
Taq-*in situ*-mmu-miR-155–Reverse	5'-GTGCAGGGTCCGAGGT-3'
Taq-*in situ*-cel-miR-39–reverse transcription	5'-GTCGTATCCAGTGCAGGGTCCGAGG TATTCGCACTGGATACGACCAAGC-3'
Taq-*in situ*-cel-miR-39–Forward	5'-GCCCTCACCGGGTGTAAAT-3'
Taq-*in situ*-cel-miR-39–Reverse	5'-GTGCAGGGTCCGAGGT-3'

Two serial sections were placed on the same slide, one of which was used for negative control staining. SecureSeal™ hybridization chambers were attached to the slides and 50 μL reaction mix (**Table 11**) was added through access ports to the microwells formed by the hybridization chambers. The slides were then placed in a thermal cycler (Eppendorf Master Cycler Nexus) and reverse transcription and amplification was performed (**Table 12**). After completing the cycles, slides were rinsed first with xylene and then with ethanol (100%), before air-drying.

Table 11. Preparation of *in situ* reverse transcriptase PCR reaction mix.

Reagents	Volume (μL)
Platinum Taq DNA Polymerase (SuperScript One-Step RT-PCR System)	1
2xReaction mix buffer (SuperScript One-Step RT-PCR System)	25
2% BSA	1.6
Digoxigenin-11-dUTPs (1 mM)	0.6
RNase inhibitor	1.4
Taq-*in situ*- reverse transcription primer (100 μM)	1.2

Taq-*in situ*-Forward primer (100 μM)	0.9
Taq-*in situ*-Reverse primer (100 μM)	0.9
RNase-free water	17.4

Table 12. Thermal cycling conditions.

Steps	Cycles	Temperature	Time
1	1	55° C	30 min
2	1	95° C	3 min
3	25	95° C	15 s
		55° C	30 s
		72° C	20 s
4	1	72° C	5 min
5	1	10° C	hold

After stringent washing with SSC buffer (2x SSC with 2% BSA and 0.2x SSC with 2% BSA; 15 min each), the sections were incubated in Tris-NaCl blocking (TNB) buffer (**see section 2.4**) for 30 min and avidin/biotin blocking solutions (avidin/biotin blocking kit, Vector Laboratories). The sections were then incubated with horseradish peroxidase-conjugated anti-digoxigenin sheep F'ab fragments (Fab fragments from sheep, 1:100; Roche Diagnostics GmbH) for 1 h at 37 °C. Probes were visualized using a tyramide-based amplification system (TSA Plus Biotin; PerkinElmer Inc., Waltham, MA, USA) and Dylight 549-labeled streptavidin (1:200; Kirkegaard & Perry Laboratories). Images were acquired using a Leica-DM6000 B microscope (Leica microsystems) connected to a CCD camera (DFC365FX, Leica microsystems) and the LAS AF software (version 3.2.0.9652).

2.13 Laser microdissection (LMD)

Laser microdissection (LMD) is a method for isolating specific populations of cells from microscopic regions of cells, tissues, and organs [141,142]. Murine pancreata from *Mir155*$^{+/+}$*Ldlr*$^{-/-}$ mice fed a DDC or a ND for 24 wk were fixed using PAXgene tissue containers (Qiagen) and embedded in paraffin. Sections (7 μm thick) were collected on polyester-membrane frames slides (0.9 μm thickness, Leica Microsystems). Before

LMD, sections were deparaffinized under RNase-free conditions (Xylene and 100% Ethanol; 3 min each) and air-dried.

Laser microdissection was performed using a laser microdissection system (CTR 6000, Leica Microsystems) attached to an inverted microscope (LMD 7000, Leica Microsystems). Islets from approximately 60 pancreatic sections were collected from each mouse into the lysis buffer (TM1) of the PAXgene Tissue miRNA isolation kit (PreAnalytix, Switzerland) (**Figure 10**). RNA was isolated according to the manufacturer's instructions. All the steps were performed in the RNase-free condition to preserve RNA integrity.

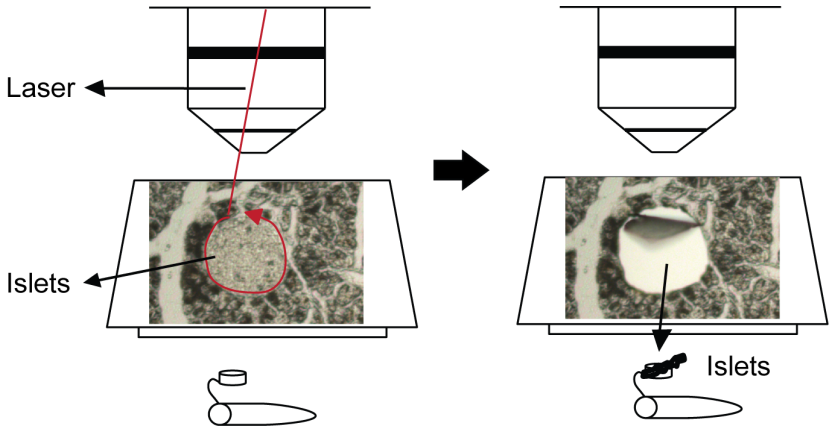

Figure 10. Laser microdissection system. Islets were dissected by laser from polyester-membrane frames slides and collected in the lid of a microfuge tube containing lysis buffer.

2.14 *In vitro* experiments

2.14.1 MIN6 cell culture

Mouse pancreatic insulinoma cell line MIN6 (passage 18 – 24)[143], which is a mixed cell line with other pancreatic endocrine hormones (e.g., glucagon and somatostatin)[144] and exhibits characteristics similar to isolated pancreatic islets,[145] are kindly provided by Prof. Ingo Rustenbeck (University of Braunschweig, Germany, originally from Prof. Jun-Ichi Miyazaki Osaka University, Japan). MIN6 cells were cultured in Dulbecco's Modified Eagle's Medium (DMEM) containing 25 mM glucose (Thermo Fisher Scientific), supplemented with 10% volume per volume (v/v) heat-inactivated FBS

(Sigma-Aldrich), 50 μg/mL Glutamine (Thermo Fisher Scientific) and 5 μL/L β-mercaptoethanol (Sigma-Aldrich). Cells were maintained in appropriate culture vessels (**Table 13**) at 37 °C under 5% (v/v) CO_2 and passaged using Accutase solution (Thermo Fisher Scientific, **Table 13**) when they reached around 80% confluency. The culture medium was changed every 48 – 72 h.

Table 13. Seeding and confluent density and volumes of dissociation solutions for various sizes of culture vessels.

	Seeding density (cells per well)	**Confluent density (cells per well)**	**Accutase (mL)**	**Growth Media (mL)**
Culture plates				
6-well	3-5 x 10^5	1.2 x 10^6	0.8	2
12-well	2 x 10^5	4 x 10^5	0.5	1
24-well	0.5 x 10^5	2 x 10^5	0.3	0.5
Flasks				
T-25	0.7 x 10^6	2.8 x 10^6	2	5
T-75	2.1 x 10^6	8.4 x 10^6	4	8 – 15

2.14.2 Transfection

MIN6 cells were transfected with locked nucleic acid (LNA)-miR-155-5p inhibitors (50 nM, miRCURY LNA™ microRNA inhibitors; Exiqon, Vedbaek, Denmark), miR-155-5p mimics (15 nM, mirVanaTM mimics; Thermo Fisher Scientific), *155*/Mafb target site blockers (50 nM miRCURY LNA™ microRNA target site blockers; Exiqon), or scrambled controls (mirVana™ miRNA Mimic, Negative Control, Thermo Fisher Scientific; miRCURY LNA™ microRNA inhibitor control and miRCURY LNA™ microRNA target site blockers control, Exiqon) using Lipofectamine2000 (Thermo Fisher Scientific).

One day before transfection, MIM6 cells were seeded in 6-well plates at 2 – 3 x 10^5 cells/mL or in 12-well plates at 2 x 10^5 cells/mL. The cells were transfected when the confluency reached 80-85% and the oligomer-Lipofectamine complexes were prepared. for each transfection sample (**Table 14**).

Table 14. Preparetion of oligomer-Lipofectamine complexes for transfection.

Reagent A		
	6-well (μL)	**12-well (μL)**
miR-155-5p inhibitors or control inhibitors (15 nM) *or* miR-155-5p mimics or control mimics (50 nM) *or* 155/Mafb TSBs or control TSBs (50 nM)	0.6 2 2	0.3 1 1
FBS and supplement free medium	250	125
Reagent B		
	6-well (μL)	**12-well (μL)**
Lipofectamin 2000	5	2.5
FBS and supplement free medium	250	125

Each reagent was gently mixed and incubated for 5 min at RT, before reagent A and B were combined, gently mixed and incubated for 20 min at RT. During the incubation, the medium was exchanged by fresh antibiotics-free growth medium. The miRNA inhibitor/mimic/TSB-Lipofectamine complexes were then added to each well and mixed gently by shaking the plate for 24 – 48 h before harvesting the cells. Total RNA was isolated by NucleoSpin microRNA Kit (Macherey-Nagel GmbH & Co. KG, Düren, Germany) and proteins were extracted using RIPA buffer (Sigma-Aldrich) containing protease inhibitors (cOmplete, EDTA-free protease inhibitor cocktail tablet, Roche Diagnostics GmbH). In all experiments, 5 – 6 biological replicates were studied.

2.14.3 Preparation of mildly oxidized LDL (moxLDL)

Human LDL (1 mg/mL, Calbiochem, Merck Millipor, Darmstadt, Germany) was incubated with 5 μM $CuSO_4$ at 37°C for 4 h. LDL oxidation was stopped by adding 10 μM EDTA and the LDL was passed through PD-10 desalting column (GE Healthcare, Uppsala, Sweden). Native LDL (nLDL) was treated in the same way as moxLDL except the addition of $CuSO_4$. The protein concentration was measured using a DC protein assay kit (Bio-Rad Laboratories GmbH) with BSA as a standard. The level of oxidation was determined by spectrophotometric quantification of thiobarbituric acid-reactive species formation (TBARS assay kit, Cayman Chemical, Michigan, USA) at 532 nm.

moxLDL and nLDL were stored at 4 °C and used for experiments within 14 d after preparation.

2.14.4 LPS or moxLDL stimulation

MIM6 cells were seeded in 12-well plates at 2 x 10^5 cells/mL and maintained at 37 °C for 24 h before stimulation with LPS (5, 20, or 50 ng/mL, from Escherichia coli 055:B5, Sigma-Aldrich), nLDL (100 μg/mL), moxLDL (100 μg/mL), or PBS for 6 h. Total RNA was isolated by NucleoSpin microRNA Kit (Macherey-Nagel GmbH & Co. KG, Düren, Germany). In all experiments, 5 – 6 biological replicates were studied.

2.14.5 IL-6 neutralization

MIN6 cells were cultured in 12-well plates and treated with neutralizing IL-6 antibodies (200 μg/mL, rat monoclonal Ab, Thermo Fisher Scientific) or isotype control antibodies (normal rat IgG, Santa Cruz Biotechnology) for 24 h. Then, cells were harvested, and RNA and protein was isolated using NucleoSpin microRNA Kit (Macherey-Nagel GmbH & Co. KG) and RIPA buffer (Sigma-Aldrich) with cOmplete, EDTA-free protease inhibitor cocktail tablet (Roche Diagnostics GmbH), respectively. For protein isolation, 3 wells were pooled for one biological replicate. The cell culture medium was collected and concentrated using the Amicon Ultra-2 mL Centrifugal Filters (Merck Millipore).

2.14.6 Cell cycle analysis

Cell cycle analysis of MIN6 cells was performed by flow cytometry. Briefly, MIN6 cells were cultured in 6-well plates and transfected with miR-155-5p mimics or miR-155-5p inhibitors for 24 h (**see also section 2.14.2**). Non-targeting oligonucleotides were used as control. Proliferation of these cells was assessed using flow cytometry by analyzing the DNA content after fixation with ice-cold 70% ethanol and staining with a solution containing propidium iodide (20 μg/mL), ribonuclease A (10 μg/mL) and 0.1% Triton-X 100 (all from Sigma-Aldrich). Sample acquisition and analysis was performed on the Attune Acoustic Focusing Cytometer (Thermo Fisher Scientific) according to the manufacturer's instructions.

2.15 RNA isolation and qPCR

Total RNA was isolated using mirVana miRNA kit (Thermo Fisher Scientific, Darmstadt, Germany), NucleoSpin microRNA kit (Macherey-Nagel) or PAXgene Tissue miRNA kit (Qiagen). The RNA concentration was determined by measuring the absorbance at 260 nm (A260) in a spectrophotometer (**see also section 2.1**). The absorbance at 280 nm (A280) was also measured to determine the RNA purity. The RNA quality was determined using a Fragment Analyzer™ (Advanced Analytical Technologies, Ankeny, lowa, USA). The RNA is separated according to fragment size, and results are returned as electropherograms and virtual gel images. An index for RNA quality, the RNA integrity number (RIN), is derived from the electrophoretic profile. RIN assigns an electropherogram a value of 1 to 10, with 10 being the least degraded, while a RIN value of 1 indicates massive degradation. For RIN calculation, the algorithm does not rely on the 28S/18S-rRNA ratio alone, but considers the entire electrophoretic profile (e.g., the fraction of short degraded RNA species). All samples were analyzed using High Sensitivity RNA Analysis kit (DNF-491-0500, Sizing range: 50 bp – 20,000 bp, Input concentration range: 50 pg/μL – 5,000 pg/μL, Agilent Technologies). RNA with an A260/A280 ratio of 1.7 – 2.1 and RNA integrity number (RIN) > 7 was used for qPCR.

miRNA was reverse-transcribed using TaqMan microRNA reverse transcription kit and quantitated by qPCR using the TaqMan Universal PCR Master Mix and TaqMan microRNA assays (both from Thermo Fisher Scientific). mRNA was reverse-transcribed by using the high-capacity cDNA reverse transcription kit and the expression of mRNA was determined using TaqMan universal PCR master mix and TaqMan gene expression assays (all from Thermo Fisher Scientific) or the SYBR green technology (GoTaq qPCR Master Mix, Promega GmbH, Mannheim, Germany) and self-designed, gene-specific primers (Sigma-Aldrich) (**Table 15**).

All qPCRs were run on a 7900HT real-time PCR system (Thermo Fisher Scientific). Relative expression levels were normalized to a single or multiple reference genes (small nucleolar RNA (sno)-135, sno-202, or U6 for miRNAs and glyceraldehyde 3-phosphate dehydrogenase (*Gapdh*), beta-actin (*Actb*) or hypoxanthine guanine

phosphoribosyl transferase (*Hprt1*) for mRNAs), and scaled to the sample with of the lowest expression and logarithmically transformed (Log10) using Qbase^{PLUS} software (Biogazelle NV, Zwijnaarde, Belgium).

Table 15. Primer sequences used in real-time RT-PCR analysis.

Gene	Primer	Primer sequences	Location	Product size (bp)	GenBank Accession numbers
Mafb	Forward	5'-GTAGTGTGGAGGACCGCTTC-3'	1003-1022	160	NM_010658.3
	Reverse	5'-TTATACCTGCACGACTGGGC-3'	1162-1143		
Glucagon	Forward	5'-CTGGTGAAAGGCCGAGGAAG-3'	467-486	89	NM_008100.4
	Reverse	5'-GAGAAGGAGCCATCAGCGTG-3'	555-536		
Insulin	Forward	5'-TGGCTTCTTCTACACACCCA-3'	229-248	197	NM_008387.5
	Reverse	5'-TCTAGTTGCAGTAGTTCTCCA-3'	425-405		
Il6	Forward	5'-CCACTTCACAAGTCGGAGGC-3'	218-237	78	NM_031168.2
	Reverse	5'-TGCCATTGCACAACTCTTTTCT-3'	295-274		
Pcsk1	Forward	5'-GTGAATGTTGTGGAGAAGCGG-3'	1945-1965	147	NM_013628.2
	Reverse	5'-TTGTAGGAGTCGCAGCATGG-3'	2091-2072		
Pcsk2	Forward	5'-GGTACTGACCCTCAAAACAAATGCATGTG-3'	1810-1838	127	NM_008792.4
	Reverse	5'-GGAGGTCATGTTGATGTTCAGGTCTCC-3'	1936-1910		
Arx	Forward	5'-GGCCGGAGTGCAAGAGTAAAT-3'	259-279	157	NM_007492.4
	Reverse	5'-TGCATGGCTTTTTCCTGGTCA-3'	415-395		
Med12l	Forward	5'-CAGAATCAGGGGTTGGGGAC-3'	2411-2430	182	NM_177855.3
	Reverse	5'-GGATGTTCCAGACGCAAAGC-3'	2590-2573		
Somatostatin	Forward	5'-ATGCTGTCCTGCCGTCTC-3'	101-118	194	NM_009215.1
	Reverse	5'-TTCTCTGTCTGGTTGGGCTC-3'	294-275		

Sema5a	Forward	5'-CAGGACCCTTACTGTGGCTG-3'	2156-2175	111	NM_009154.2
	Reverse	5'-ATTTCTGGTCGGACAGGTGG-3'	2266-2247		
Stmn2	Forward	5'-CTTGAAGCCACCATCTCCCAT-3'	256-276	127	NM_025285.2
	Reverse	5'-CTCTTGAGACTTTCTTCGCTCCT-3'	382-360		
Auh	Forward	5'-CTCTGCAAAAATGGGCCTGG-3'	564-583	70	NM_016709.2
	Reverse	5'-TAATCTCTGTGTCCCTCCTCCG-3'	633-612		
Nos2	Forward	5'-TCATTGGGCCTGGTACGGGCA-3'	3173-3193	105	NM_010927.4
	Reverse	5'-ACACCAAGCTCATGCGGCCTC-3'	3277-3257		
Mrc1	Forward	5'-AATGCTGACCTCCTGAGTGT-3'	850-869	158	NM_008625.2
	Reverse	5'-CAGTTCAGATACCGGAATGG-3'	1007-988		
Arg1	Forward	5'-TGGGCAACCTGTGTCCTTTCTCCT-3'	525-548	136	NM_007482.3
	Reverse	5'-TTCCCCAGGGTCTACGTCTCGCA-3'	660-638		
Gapdh	Forward	5'-CATGGCCTTCCGTGTTCCTA-3'	924-943	104	NM_008084.3
	Reverse	5'-CCTGCTTCACCACCTTCTTGAT-3'	1027-1006		
Actb	Forward	5'-GGCTGTATTCCCCTCCATCG-3'	193-212	154	NM_007393.5
	Reverse	5'-CCAGTTGGTAACAATGCCATGT-3'	346-325		
Hprt	Forward	5'-TCAGTCAACGGGGGACATAAA-3'	470-490	142	NM_013556.2
	Reverse	5'-GGGGCTGTACTGCTTAACCAG-3'	611-591		

2.16 Protein quantitation

2.16.1 Total protein quantification

Murine pancreatic islets isolated from *Mir155*$^{-/-}$*Ldlr*$^{-/-}$ and *Mir155*$^{+/+}$*Ldlr*$^{-/-}$ mice and MIN6 cells transfected with miR-155-5p inhibitors, miR-155-5p mimics, *155*/Mafb target site, or scrambled controls were lysed in RIPA buffer containing protease inhibitors (**see also section 2.14.2**). Total protein concentration was determined using a modified Lowry assay kit (DC protein assay kit, Bio-Rad Laboratories), which is based on the reaction of protein with an alkaline copper tartrate solution and Folin's reagent. The method combines the reactions of copper ions with the peptide bonds under alkaline conditions with the oxidation of aromatic protein residues[146]. Absorbance was measured at 750 nm by a microplate reader (Infinite F200 PRO). Different standard concentrations (**Table 16**) were prepared using UltraPure™ BSA solution (50 mg/mL, Thermo Fisher Scientific).

Table 16. Preparation of different standard concentrations.

Standard (mg/mL)	BSA	RIPA buffer (μL)
2	2 μL of 50 mg/mL BSA	48
1.6	1.6 μL of 50 mg/mL BSA	48.4
1	15 μL of 2 mg/mL BSA	15
0.8	25 μL of 1.6 mg/mL BSA	25
0.4	25 μL of 0.8 mg/mL BSA	25
0.2	25 μL of 0.4 mg/mL BSA	25
0.1	25 μL of 0.2 mg/mL BSA	25
0.05	25 μL of 0.1 mg/mL BSA	25
0	0 μL	50

2.16.2 Enzyme-linked immunosorbant assay (ELISA)

The concentrations of insulin in plasma from *Mir155*$^{-/-}$*Ldlr*$^{-/-}$ and *Mir155*$^{+/+}$*Ldlr*$^{-/-}$ mice fed a DDC for 24 wk, or *Mir155*$^{-/-}$*Ldlr*$^{-/-}$ and *Mir155*$^{+/+}$*Ldlr*$^{-/-}$ mice (10 – 12 wk old) fed a ND were determined after a 5 – 6 h fasting period using an ultra sensitive mouse insulin ELISA kit (dynamic range 0.1 – 64.0 ng/mL, Crystal Chem Inc. Downers

Grove, IL, USA) according to the manufacturer's instructions. The absorbance was measured at 405 nm by a microplate reader (Infinite F200 PRO).

For IL-6 protein measurement, MIN6 cells transfected with miR-155-5p inhibitors, miR-155-5p mimics, or scrambled controls were lysed in cell lysis buffer. Moreover, the cell culture medium was collected and concentrated using the Amicon Ultra-2 mL Centrifugal Filters (Merck Millipore). The concentrations of IL-6 in cell lysates and concentrated supernatants were quantified using a commercially available mouse IL-6 ELISA kit (RayBiotech, Inc., Norcross GA, USA) according to the manufacturer's instructions. The data were normalized to the total protein concentration determined using the DC Protein assay kit (cat. no. 5000116, Bio-Rad Laboratories, Inc.) (**see section 2.16.1**). The absorbance was measured at 405 nm by a microplate reader (Infinite F200 PRO).

2.16.3 Luminex's xMAP bead-based multiplex assays

Luminex's xMAP technology is bead based multiplexing, where beads are internally dyed with fluorescent dyes to produce a specific spectral address. Biomolecules (such as an oligonucleotide or antibody) can be conjugated to the surface of beads to capture analytes of interest. This technology uses flow cytometric or imaging technologies for characterization of the beads. Because the beads can be distinguished by their speical addresses and each address can be linked with a specific target, the beads can be combined in a single reaction to measure multiple targets simultaneously.

The Luminex's MAGPIX system (**Table 17**) was used to detect protein concentrations, which utilizes a flow cell and robust light-emitting diode (LED)/CCD-based optics, supports multiplexing of up to 50 tests in a single reaction volume using MagPlex beads. The reacted magnetic beads are sent through a flow cell into an imaging chamber where a magnetic actuator pulls the beads out of suspension and holds them in place for optical analysis. Red LEDs (635 nm) excite the fluorescent dyes contained within the microspheres and green LEDs (525 nm) excite the reporter fluorochrome bound to the bead surface. A CCD camera identifies the bead region and quantifies the bound reporter (**Figure 11**).

Table 17. Information of Luminex's MAGPIX system.

Instrument	**MAGPIX® System**
Software	xPONENT® 4.2
Optic	LED/ CCD camera
Hardware	Fluorescent imager
Bead compatibility	Magnetic
Multiplex capacity	50
Read time	~ 60 min/96-well plate
Applications	Protein/ Nucleic acid
Microtiter plate	96-well

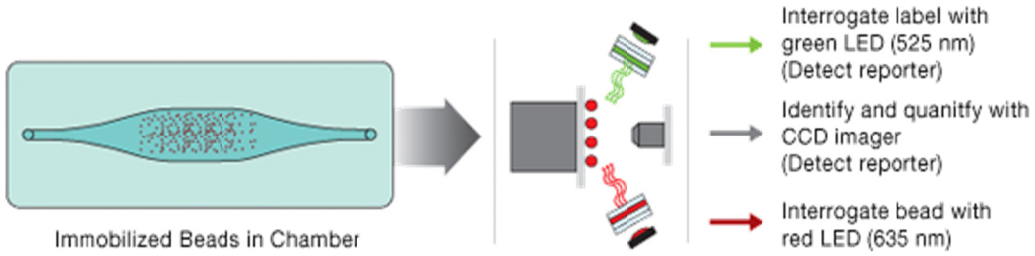

Figure 11. LED/image-based analysis. Dyed beads are pushed through a detection chamber in a single file or magnetically immobilized. The red classification laser (635 nm) or LED interrogates the internal dyes to identify bead regions. The green reporter laser (532 nm) or LED interrogates the fluorescent reporter to measure analyte concentration.

Insulin, glucagon and GLP-1 protein concentrations were determined using a Bio-Plex Pro Mouse Diabetes assay Luminex kit (Bio-Rad Laboratories) according to the manufacturer's instructions. Briefly, the capture antibody-coupled beads were first incubated with antigen standards or samples. The plate was then washed to remove unbound materials and incubated with biotinylated detection antibodies. After washing away the unbound detection antibodies, the beads were incubated with a reporter streptavidin-phycoerythrin conjugate (SA-PE). Following removal of excess SA-PE, the beads were passed through the Luminex array reader (MAGPIX® Multiplex Reader), which measures the fluorescence of the bound SA-PE (**Figure 12**). The results were analyzed using xPONENT® software version 4.2 (both from Luminex Corporation, Austin, TX, USA). Plasma insulin, glucagon and GLP-1 levels in mice were determined after a 5 – 6 h fasting period. The data from MIN6 cells and islet samples were

normalized to the total protein concentration determined using a modified Lowry assay (**see also section 2.16.1**).

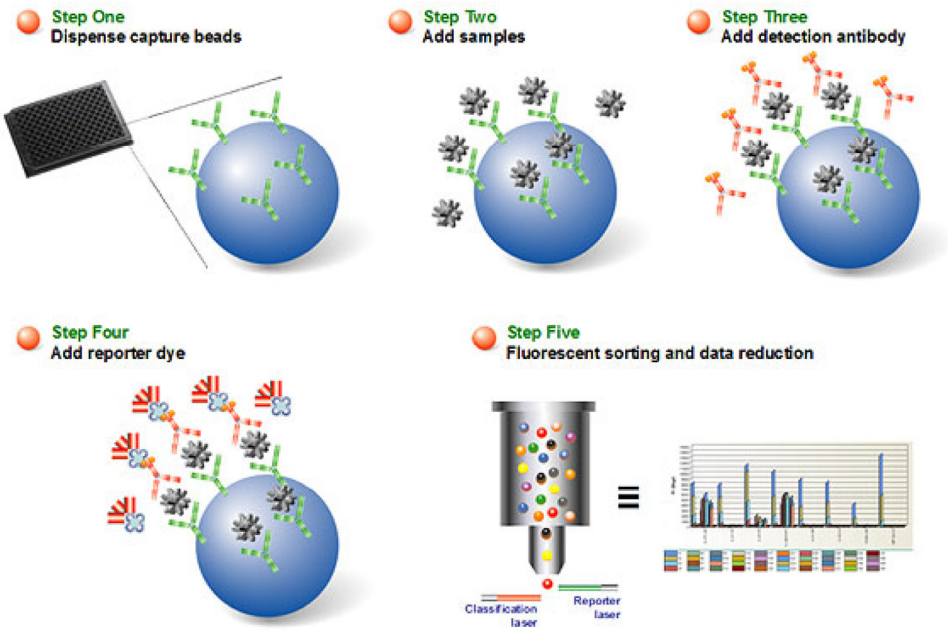

Figure 12. Schematic representation of an immunoassay sandwich-based assay workflow. Figure modified from http://www.bio-rad.com/de-de/applications-technologies/bio-plex-multiplex-immunoassay

2.17 Endotoxin activity

Endotoxin activity in serum, nLDL and moxLDL was determined by the limulus amebocyte lysate (LAL) assay (Pierce™ LAL endotoxin quantitation kit, Thermo Fisher Scientific) according to the manufacturer's instructions. Briefly, samples were heat-shocked at 70 °C for 15 min and incubated with LAL at 37 °C for 10 min, followed by incubation with the chromogenic substrate at 37 °C for 6 min. The absorbance was measured at 405 nm by a microplate reader (Infinite F200 PRO, Tecan Trading AG, Männedorf, Switzerland).

2.18 Global gene expression analysis

Murine pancreatic islets were isolated from *Mir155*$^{-/-}$*Ldlr*$^{-/-}$ and *Mir155*$^{+/+}$*Ldlr*$^{-/-}$ mice (10 – 12 wk old) fed a ND after a 5 – 6 h fasting period (**see also section 2.7.2**). Total RNA was isolated using the NucleoSpin microRNA kit and the RNA quality was determined by capillary electrophoresis using an Agilent 2100 Bioanalyzer (Agilent Technologies, Santa Clara, CA, USA). The samples with a RIN ≥ 7.7 were used for the array (**see also section 2.15**). Agilent SurePrint G3 Mouse Gene Expression Microarrays (8x60K format, Agilent) were used in combination with a one-color based hybridization protocol (IMGM Laboratories GmbH, Martinsried, Germany). Raw signals on the microarrays were scanned using the Agilent DNA Microarray Scanner. Quantile normalization and analysis of the raw data were performed using GeneSpring GX 13.0 software (both from Agilent Technologies).

2.19 Prediction of miR-155-5p target genes

Among the genes significantly upregulated (≥1.5-fold and $p<0.05$) in pancreatic islets of *Mir155*$^{-/-}$*Ldlr*$^{-/-}$ mice compared to *Mir155*$^{+/+}$*Ldlr*$^{-/-}$ mice (as determined by global gene expression analysis), miR-155-5p targets and the conservation of the miR-155-5p binding sites across species were predicted by Targetscan software (http://www.targetscan.org/). The probability of conserved targeting is indicated by the P_{CT} value.

2.20 Ingenuity® pathway analysis

Microarray gene expression data were analysed by Ingenuity® Pathway Analysis software (IPA, http://www.ingenuity.com/products/ipa, Qiagen) to predict gene connectivity and upstream regulators of differentially expressed genes[147]. Briefly, an input file containing gene identifiers, corresponding expression values, p-values and fold changes of all probe sets was uploaded into the IPA system. Each gene identifier was mapped to its corresponding gene object in the Ingenuity® Knowledge Base. These genes were loaded into a global molecular network developed from information

contained in the Ingenuity® Knowledge Base (**Figure 13**). Networks of these genes were then algorithmically generated based on their connectivity.

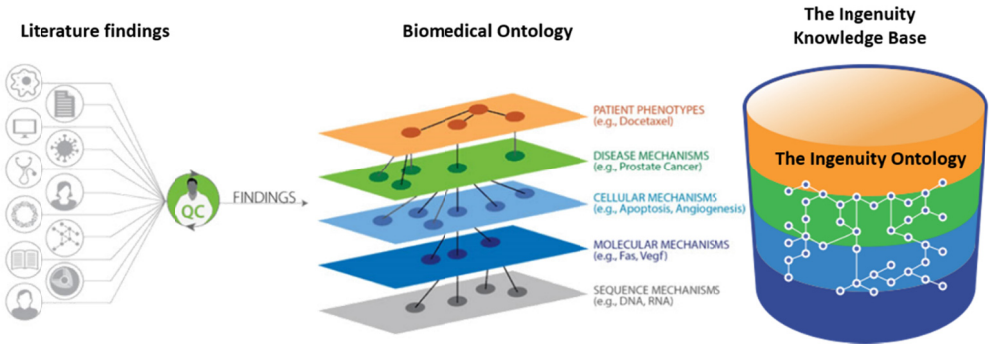

Figure 13. Schematic representation of Ingenuity® Knowledge Base.[147] The Ingenuity® Knowledge Base composed of experimental findings mainly taken from peer-reviewed journals and manually reviewed information from commonly used third party databases. All this information is pulled together to make connections between diseases, genes, drugs/compounds, pathways, and pathway regulators. IPA then uses this information to run its predictive algorithms and the user can directly pull out relevant information.

IPA Upstream Regulator Analysis is a tool to identify the cascade of upstream transcriptional regulators that can explain the observed gene expression changes in a dataset and illuminate the biological activities occurring in the tissues or cells being studied. For each potential transcriptional regulator two statistical measures, an overlap p-value and an activation z- score are computed. Firstly, the overlap p-value measures whether there is a statistically significant overlap between the target genes of this transcriptional regulator and the differentially expressed genes. It is calculated using Fisher's Exact Test, and significance is generally attributed to p-values < 0.01. Then, the analysis compares the direction of changes of the differentially expressed genes with the expected changes of these genes according to the IPA knowledge base. This prediction is derived from an activation z-score that quantifies the consistency between the expected (in the knowledge base) and observed (in the microarray data) directions of changes. A positive z-score represents activation and a negative z-score represents inhibition of an upstream regulator.[147]

2.21 MicroRNA target identification and quantification system (MirTrap)

MirTrap System was used to identify specific miR-155-5p targets in MIN6 cells. The system utilizes a dominant negative mutation of the miRNA-induced silencing complex (miRISC) protein subunit GW182, which is integrated into the endogenous Argonaute (Ago)/miRISC complex and locks a microRNA/target mRNA pair in the complex and limits further processing[148]. The DYKDDDDK (FLAG epitope) tag on the dominant negative GW182 protein allows capture and isolation of the entire Ago/RISC complex containing the trapped miRNA/target mRNA pair. This permits effective immunoprecipitation of the micRNA with its targets, which can then be identified or quantified by sequencing or qPCR (**Figure 14**).

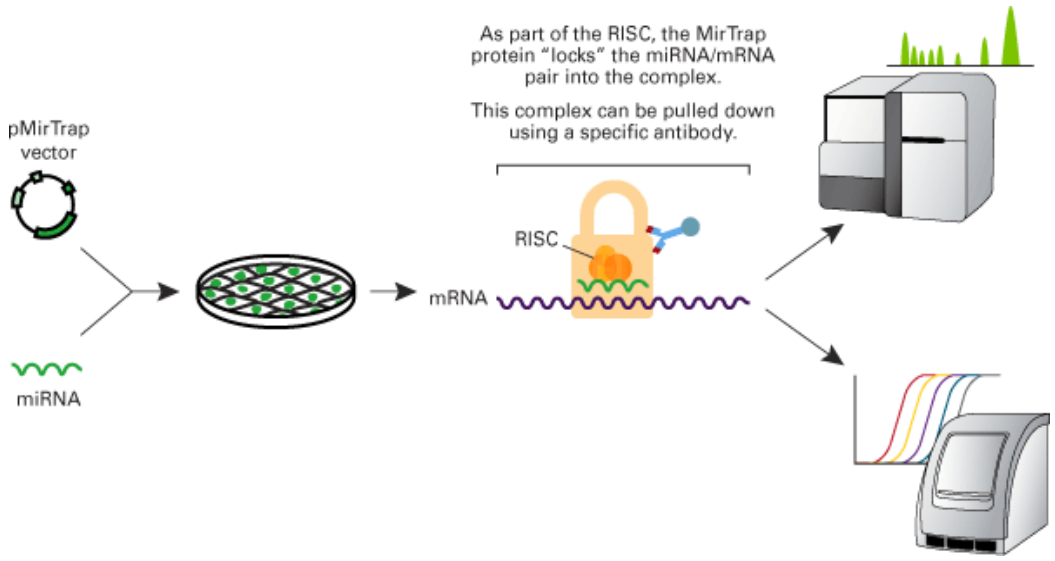

Figure 14. Experimental workflow for microRNA transfection and isolation of target mRNAs using the MirTrap System.[148] The MirTrap System utilizes a mutant RISC complex that locks the miRNA/mRNA pair into the RISC and limits further processing. A DYKDDDDK tag on the MirTrap protein allows for immunoprecipitation of the complex, which can then be efficiently pulled down without losing the miRNA/target mRNA pairs along the way. Upon isolation of the complex, the microRNA target can be identified and quantified by next-gene sequencing or quantitative PCR methods.

MIM6 cells were seeded in T-75 flasks (Corning Inc., NY, USA) at 3 x 10^6 cells/mL 24 h before the transfection (at a cell density of 75 – 80%) with miR-155-5p

mimics (15 nM, Thermo Fisher Scientific) and the pMirTrap vector expressing the DYKDDDDK-tagged GW182 protein using the Xfect™ microRNA transfection reagent in combination with Xfect Polymer (all from Clontech, aint-Germain-en-Laye, France) (**Table 18**)

Table 18. Reagents for Xfect™ microRNA transfection.

Reagent A (miRNA and pMirTrap vector)	
	Volume
miR-155-5p mimics or control mimics	5 μL (500 pM)
pMirTrap Vector	60 μL (30 μg)
Xfect Reaction Buffer	535 μL
Total volume	*600 μL*
Reagent B (Transfection Polymers)	
	Volume
Xfect Polymer	10 μL
Xfect Reaction Buffer	530 μL
Combine,vortex,and then add:	
Xfect MicroRNA Transfection Polymer	60 μL
Total volume	*600 μL*

Transfection efficiency was determined by a control transfection using miR-132 mimics, the pMirTrap positive control vector, which expresses an AcGFP1 fluorescein protein containing miR-132 recognition elements in its 3'-UTR or the empty pMirTrap vector (all from MirTrap System, **Table 19**).

Table 19. Reagents for Xfect™ microRNA transfection of positive control.

Reagent A (miRNA and pMirTrap vector)	
	Volume
miR-132 mimics	5 μL (500 pM)
pMirTrap Vector	60 μL (30 μg)
pMirTrap Control Vector	20 μL (10 μg)
Xfect Reaction Buffer	515 μL
Total volume	*600 μL*

Reagent B (Transfection Polymers)	
	Volume
Xfect Polymer	12 μL
Xfect Reaction Buffer	528 μL
Combine,vortex,and then add:	
Xfect MicroRNA Transfection Polymer	60 μL
Total volume	*600 μL*

Reagent A and reagent B were combined and incubated for 20 min at RT to form the miRNA/pMirTrap vector complexes. The nanoparticle complexes were then added to flasks with 10 mL of fresh antibiotics-free growth media and mixed gently by shaking the flask.

MIN6 cells were harvested after 24 h, washed in ice-cold PBS (Thermo Fisher Scientific), and incubated in lysis buffer (MirTrap System) supplemented with protease inhibitors (Roche). The cell lysates were centrifuged and input RNA was extracted from the supernatant using the NucleoSpin RNA XS kit (Macherey-Nagel). Anti-DYKDDDDK-conjugated magnetic beads (Clontech) were washed twice with 1× lysis/wash buffer containing 1 mM DTT, 0.1 unit/μL RNase inhibitor and protease inhibitors (Roche), and blocked for 3 h at 4 °C with 1.25 mg/mL tRNA solution and 1.25 mg/mL bovine serum albumin. Cell lysates were incubated with anti-DYKDDDDK beads for 2 h at 4 °C. After incubation, the beads were washed twice with 1× lysis/wash buffer and the RNA was isolated using the NucleoSpin RNA XS kit (Macherey-Nagel).

RNA from the input and immunoprecipitated samples was reverse transcribed using the high-capacity cDNA reverse transcription kit (Thermo Fisher Scientific), and amplified by qPCR with gene-specific primers (**Table 15**) and SYBR Green PCR Master Mix (Promega GmbH, Mannheim, Germany) using a 7900HT fast real-time PCR system (Thermo Fisher Scientific). Fold enrichment of the AcGFP1 control (transfected with miR-132 mimics and the pMirTrap positive control vector) or miR-155-5p predicted target genes in the GW182-immunoprecipitates was normalized to that of *Gapdh* according to the manufacturer's protocol.

2.22 Luciferase reporter assays

2.22.1 *Il6* promoter reporter clones

To investigate the effect of miR-155-5p-mediated targeting of *Mafb* on IL-6 expression, luciferase reporter assays were performed in MIN6 cells. The Gaussia Luciferase (GLuc) -Secreted Alkaline Phosphatase (SEAP) dual-reporter vector pEZX-PG04 containing the promoter region of mouse *Il6* gene (*Il6* promoter vector, MPRM26589-PG04) and the empty vector (Non-promoter sequence negative control in dual-reporter vector, NEG-PG04) (**Figure 15; Table 20**) were purchased from GeneCopoeia (GeneCopoeia, Vienna, Austria).

Table 20. Information of the *Il6* promoter vector and the empty vector

Information	**Promoter clone for gene *Il6***	**Negative control**
Vector	pEZXPG04	PG04CT
Whole plasmid size	7940 bp	6730 bp
Antibiotic	Kanamycin	Kanamycin
Stable selection marker	Puromycin	Puromycin
Reporter gene	GLuc	GLuc
Tracking gene	SEAP	SEAP
Promoter length	1229 bp	N/A
Gene accession	NM_031168	N/A

The *Il6* promoter vector contains a modified GLuc as the reporter gene, which can generate a highly stable signal. The secondary reporter SEAP, serves as an internal control and enables transfection normalization for accurate cross-sample comparison.

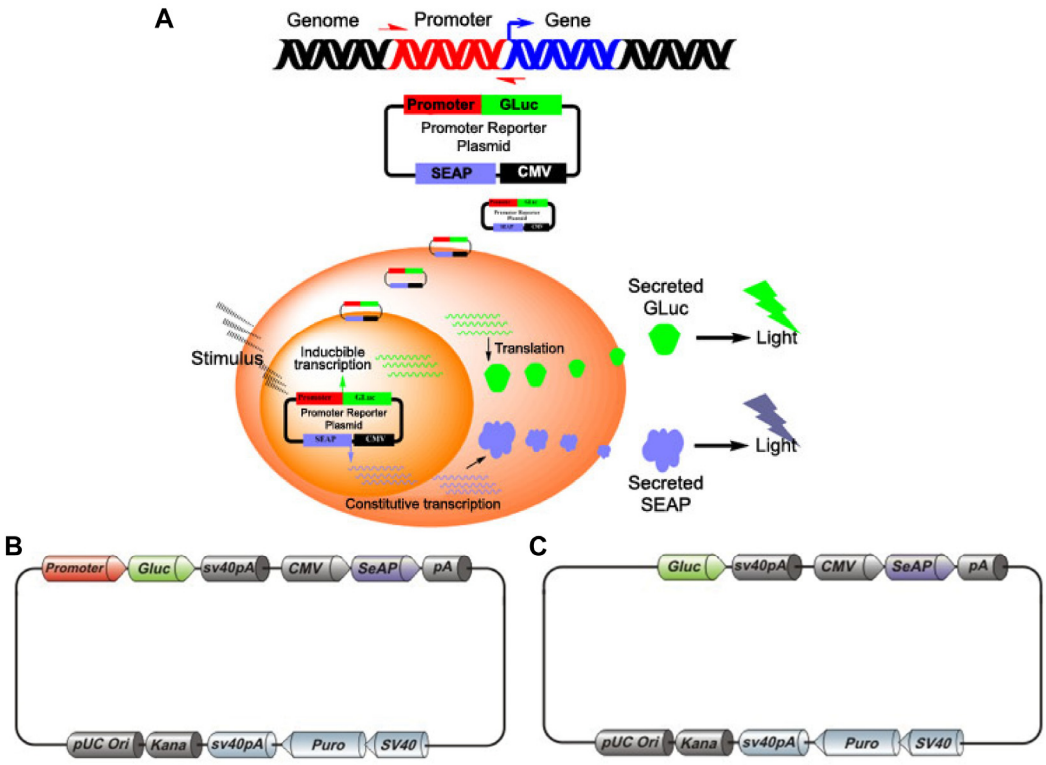

Figure 15. Principle of GLuc-ON promoter clones. (**A**) The promoter clone is placed upstream of the GLuc reporter gene. The putative cis-acting enhancer elements are expected to exist in the cloned promoter region, and the luciferase activity observed during the assay closely resembles the actual promoter regulation of these genes. (**B**) Structure of GLuc-SEAP dual-reporter vector pEZX-PG04 (*Il6* promoter vector). (**C**) Structure of the vector PG04CT (empty vector).

2.22.2 Site-directed mutagenesis

Putative binding sites for MafB were predicted at position 30012038 (*Il6* promoter-*Mafb*1) and at position 30012863 (*Il6* promoter-*Mafb*2) of the *Il6* promoter by TRANSFAC database (version 7.0, Qiagen, http://www.biobase.international.com, **Table 21**). [149,150] The *Il6* promoter-*Mafb*1 and *Il6* promoter-*Mafb*2 sequences were mutated using QuickChange site-directed mutagenesis kit (Agilent Technologies), specific primers (Sigma-Aldrich) (**Table 22**), Q5 high-fidelity DNA polymerase (New England Biolabs, Ipswich, MA, USA) and a PCR cycler (Mastercycler nexus, Eppendorf, Hamburg, Germany). The PCR product was treated with *Dpn*I restriction enzyme (Thermo Fisher Scientific) to digest the parental DNA template[151]. The vector DNA containing the desired mutation was transformed into XL10-Gold Ultra

component cells (Agilent Technologies) and the plasmid was isolated using the EndoFree Plasmid Maxi Kit (Qiagen).

Table 21. Putative MafB binding sites in the Il6 promoter region.

Factor name	Position	Core score	Matrix score	Sequence
MAF	30012863 (+)	1	1	gctgAGTCAc
MAF	30012038 (-)	0.941	0.96	tTGACCcagc

Table 22. Primer sequences used in luciferase reporter assays.

Primer	Primer sequences
Il6 promoter-PG04–Forward	5'-AGTTACTTAAGCTCGGGCCC-3'
Il6 promoter-PG04–Reverse	5'-TTGTTCTCGGTGGGCTTGGC-3'
Il6 promoter-Δ*Mafb1*–Forward	5'-AGAAGTCTGTTTAAGTTACTGGGTGCCTAGAAGACTTGA-3'
Il6 promoter-Δ*Mafb1*–Reverse	5'-ACCCAGTAACTTAAACAGACTTCTTCCCTTTGGTTAG-3'
Il6 promoter-Δ*Mafb2*–Forward	5'-TCAAGACATGCTCAAGTGGATCCAGACTTTTAAAGAAA-3'
Il6 promoter-Δ*Mafb2*–Reverse	5'-CTGGATCCACTTGAGCATGTCTTGATGGGAAAGAAAACT-3'

2.22.3 Secrete-pair dual luminescence assay

MIN6 cells were co-transfected with the GLuc-SEAP dual-reporter vector pEZX-PG04 containing the promoter region of mouse *Il6* gene (*Il6 promoter vector,* GeneCopoeia, Vienna, Austria) or luciferase reporter constructs harboring site-directed mutations in the predicted *Mafb* binding sites of the *Il6* promoter region (*Il6* promoter-Δ*Mafb*1 and *Il6* promoter-Δ*Mafb*2) together with LNA-miR-155-5p inhibitors or non-targeting LNA oligonucleotides (control inhibitors) using Lipofectamine 2000 (Thermo Fisher Scientific). The empty vector (dual-reporter vector without the *Il6* promoter sequence, GeneCopoeia) was used as control. The GLuc and SEAP activities were assayed by microplate reader (Infinite F200 PRO, Tecan) 48 h after the transfection using the Secrete-Pair Dual Luminescence Assay Kit (GeneCopoeia). The luminescence intensities of Gaussia luciferase were normalized to the activity of SEAP.

2.23 *In vivo* TSB treatment

10-wk-old *Ldlr*$^{-/-}$ mice fed a ND were injected intravenously via the tail vein with *155/Mafb* TSBs (5'-TTAATGCAGATTTTCG-3') or control TSBs (5'-GCTCCCTTCAATCCAA-3') (each 0.4 mg/20 g per injection; miRCURY LNA^{TM} Target Site Blocker, *in vivo* use; Exiqon). The fasting glucose levels (6 h fast) and body weights were measured every 3 d. Blood cell numbers, and plasma insulin, glucagon and GLP-1 levels were determined 21 d after the treatment after a 5 – 6 h fast. Tissues were harvested after 21 d and either embedded in Tissue-Tek O.C.T. Compound (Sakura Finetek) and immediately frozen on dry ice for cryostat sections or preserved in RNAlater (Thermo Fisher Scientific) for RNA purification.

2.24 Statistical analysis

Sample size (number of mice) was determined on the basis of previous studies.[103,126,152] Mice were not randomized to experimental groups. For most mouse experiments, the investigators were blinded when assessing the results without knowing the mouse genotypes. In some cases, selected samples were excluded from specific analyses because of technical issues during sample processing or data acquisition. The number of biological (non-technical) replicates for each experiment is indicated in the figure legends. Data represent the mean ± SEM. Statistical analysis of microarray data was performed by a modified t-test using GeneSpring software (GX13, Agilent Technologies). Student's t-tests and one-way ANOVAs followed by the Newman-Keuls post-hoc test was used for statistical comparisons between groups using Prism 6 software (GraphPad). The variance is similar between the groups that are being statistically compared. $p < 0.05$ was considered statistically significant.

3 RESULTS

3.1 Effects of *Mir155* deficiency on metabolic disease in *Ldlr*$^{-/-}$ mice

3.1.1 Obesity

To study the role of miR-155-5p in obesity-related metabolic disease, male *Mir155*$^{+/+}$*Ldlr*$^{-/-}$ and *Mir155*$^{-/-}$*Ldlr*$^{-/-}$ mice were fed a DDC (0.15% w/w cholesterol and 36.5% total fat) or a ND for 24 wk. The body weights were measured every 2 wk. eWAT was harvested after the 24-wk DDC feeding period. Compared to ND-fed *Ldlr*$^{-/-}$ mice, feeding the DDC increased the body weight of both *Mir155*$^{+/+}$*Ldlr*$^{-/-}$ and *Mir155*$^{-/-}$*Ldlr*$^{-/-}$ mice **(Figure 16A)**. While *Mir155*$^{-/-}$*Ldlr*$^{-/-}$ mice and *Mir155*$^{+/+}$*Ldlr*$^{-/-}$ mice gained similar body weight in the first 20 wk of DDC feeding, the body weight of *Mir155*$^{-/-}$*Ldlr*$^{-/-}$ mice increased more than that of *Mir155*$^{+/+}$*Ldlr*$^{-/-}$ mice during the last 4 wk of the DDC feeding period (**Figure 16A**). This increased body weight gain in *Mir155*$^{-/-}$*Ldlr*$^{-/-}$ mice was associated with an increase in epididymal fat pads weight after the 24-wk DDC feeding period (**Figure 16B**).

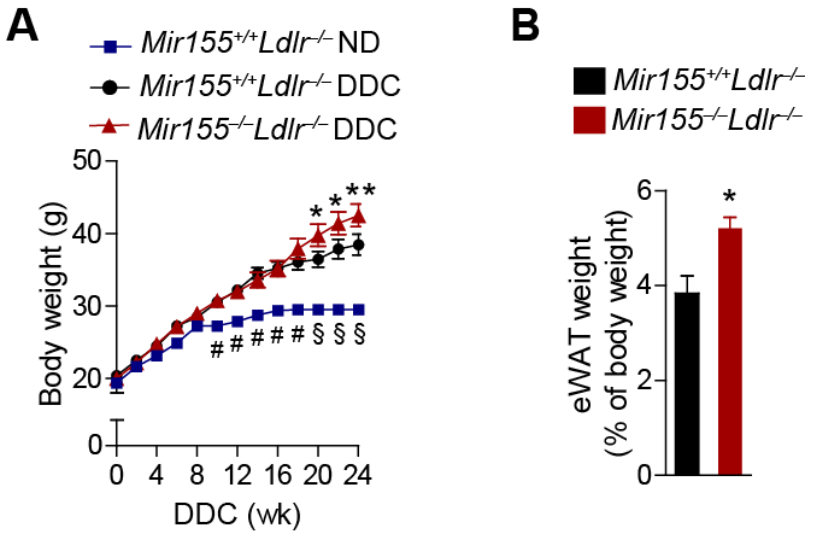

Figure 16. Effects of *Mir155* knockout on body weight and epididymal white adipose tissue weight in *Ldlr*$^{-/-}$ mice. (**A**) Body weight gain of mice fed a DDC (n = 15 mice per group) or a ND (n = 10 mice per group) for 24 wk. (**B**) Quantitation of eWAT weight in mice fed the DDC for 24 wk (n = 10 mice per

group). Data are represented as mean ± SEM. *p<0.05, **p<0.01, and ***p<0.001 compared to *Mir155*$^{+/+}$*Ldlr*$^{-/-}$ mice fed a DDC. $^{\#}$p<0.01 and §p<0.001 compared to mice fed the DDC.

To determine the effect of *Mir155* knockout on adipose tissue morphology, hematoxylin and eosin stain were performed in eWAT.[136] The average adipocyte cross-sectional area was increased in *Mir155*$^{-/-}$*Ldlr*$^{-/-}$ mice compared with *Mir155*$^{+/+}$*Ldlr*$^{-/-}$ mice after 24-wk DDC feeding (**Figure 17A**). Because macrophage accumulation in adipose tissue has been implicated in obesity-associated adipose tissue inflammation[153], the presence of macrophages within eWAT was analyzed by Mac2 immunostaining, a marker for mature macrophages. The fraction of Mac2-expressing cells was higher in *Mir155*$^{-/-}$*Ldlr*$^{-/-}$ mice than in *Mir155*$^{+/+}$*Ldlr*$^{-/-}$ mice (**Figure 17B**), indicating that *Mir155* knockout promotes adipose tissue inflammation by increasing adipocyte size and macrophage infiltration in eWAT from *Ldlr*$^{-/-}$ mice fed a DDC for 24 wk.

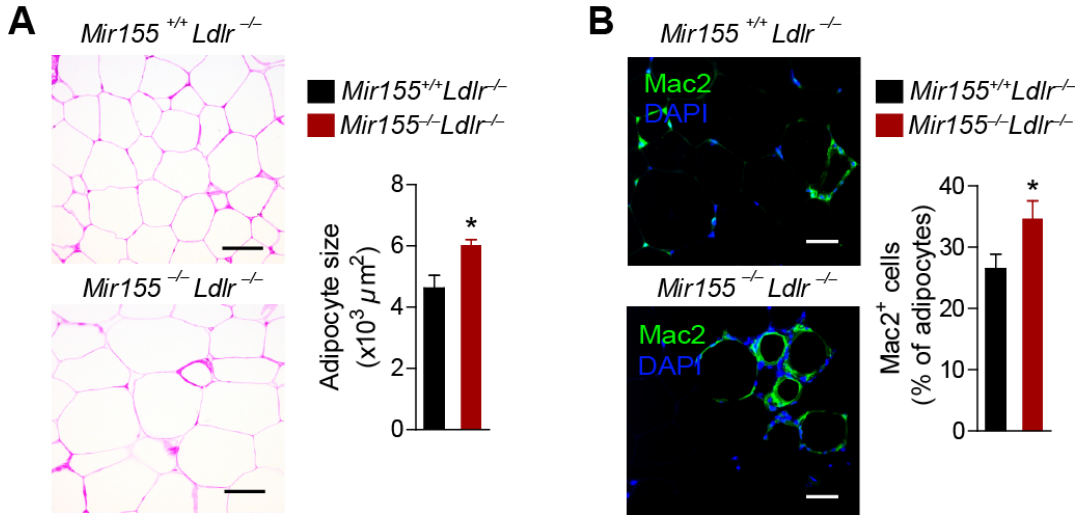

Figure 17. Effects of *Mir155* knockout on adipocyte size and macrophage infiltration in *Ldlr*$^{-/-}$ mice. (**A**) Quantitation of average adipocyte cross-sectional area in hematoxylin- and eosin-stained eWAT sections from mice fed the DDC for 24 wk determined by (n = 8 – 10 mice per group). Scale bars: 100 μm. (**B**) Macrophage accumulation in eWAT from mice after the 24-wk DDC feeding period assessed by Mac2 immunostaining (n = 9 mice per group). The nuclei were counterstained with DAPI. Scale bars: 50 µm. Data are represented as mean ± SEM. *p < 0.05.

In addition, the effect of *Mir155* knockout on adipose tissue gene expression was studied by qPCR. The expression of adiponectin (*Adipoq*) and leptin (*Lep*) was downregulated and up-regulated, respectively, in the eWAT of *Mir155*$^{-/-}$*Ldlr*$^{-/-}$ mice

(**Figure 18**). The expression of the proinflammatory macrophage-related gene nitric oxide synthase 2 (*Nos2*) and the anti-inflammatory macrophage marker mannose receptor, C type 1 (*Mrc1*) was not different between the groups (**Figure 18**). Deletion of *Mir155* did not alter interleukin 6 (*Il6*) mRNA expression, but increased tumor necrosis factor (*Tnf*) expression in eWAT (**Figure 18**). These data indicate that miR-155-5p limits adipose tissue dysfunction in obese $Ldlr^{-/-}$ mice.

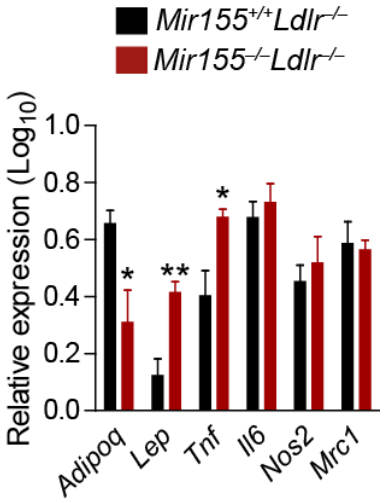

Figure 18. Effect of *Mir155* knockout on gene expression in adipose tissue in $Ldlr^{-/-}$ mice. Quantitation of gene expression by qPCR in eWAT from $Mir155^{+/+}Ldlr^{-/-}$ and $Mir155^{-/-}Ldlr^{-/-}$ mice fed a DDC for 24 wk (n = 4 – 6 mice per group). *Adipoq*, Adiponectin; *Lep*, leptin; *Tnf*, tumor necrosis factor; *Il6*, interleukin 6; *Nos2*, nitric oxide synthase 2; *Mrc1*, mannose receptor, C type 1. Data are represented as mean ± SEM; *p < 0.05 and **p < 0.01.

3.1.2 Lipid metabolism

Next, lipid levels were studied in the blood of $Mir155^{+/+}Ldlr^{-/-}$ and $Mir155^{-/-}Ldlr^{-/-}$ mice fed a DDC for 24 wk. Total cholesterol and triglyceride plasma levels were higher in $Mir155^{-/-}Ldlr^{-/-}$ mice than those in $Mir155^{+/+}Ldlr^{-/-}$ mice after the 24-wk DDC feeding period (**Figure 19A**), measured by cholesterol and triglyceride fluorescent assay kits, respectively. In $Mir155^{-/-}Ldlr^{-/-}$ mice, the cholesterol level was increased in the VLDL and LDL lipoprotein fraction and reduced in the HDL fraction, determined by high-performance liquid chromatography (**Figure 19B**).

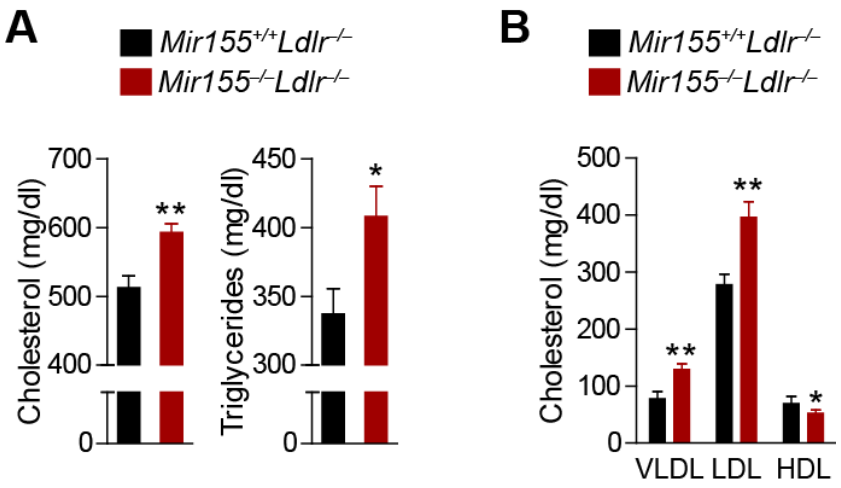

Figure 19. Effects of *Mir155* knockout on lipids and lipoproteins in *Ldlr*$^{-/-}$ mice. (**A**) Plasma cholesterol and triglyceride levels in *Mir155*$^{+/+}$*Ldlr*$^{-/-}$ and *Mir155*$^{-/-}$*Ldlr*$^{-/-}$ mice after a 24-wk DDC feeding period (n = 10 mice per group) measured by cholesterol and triglyceride fluorescent assay kits, respectively. (**B**) Cholesterol levels in VLDL, LDL and HDL fractions from mice after the 24-wk DDC feeding period analyzed by HPLC (n = 8 mice per group). Data are represented as mean ± SEM; *p < 0.05 and **p < 0.01.

3.1.3 Atherosclerosis

To assess the role of *Mir155* deficiency in atherosclerosis in the context of obesity and T2DM, the lesion size and necrotic core area in aortic roots from obese *Mir155*$^{-/-}$*Ldlr*$^{-/-}$ and *Mir155*$^{+/+}$*Ldlr*$^{-/-}$ mice were analyzed by EVG stain. The atherosclerotic lesion size and the lesional necrotic core area were increased in *Mir155*$^{-/-}$*Ldlr*$^{-/-}$ mice compared with *Mir155*$^{+/+}$*Ldlr*$^{-/-}$ mice after 24-wk DDC feeding (**Figure 20A**). To characterize the changes in atherosclerotic lesion formation, the accumulation of macrophages and smooth muscle cells in aortic root lesions was quantified by combined Mac2 and SMA immunostaining. Lesions in *Mir155*$^{-/-}$*Ldlr*$^{-/-}$ mice contained less macrophages than in *Mir155*$^{+/+}$*Ldlr*$^{-/-}$ mice, whereas the lesional smooth muscle cell content was similar in both groups (**Figure 20B**).

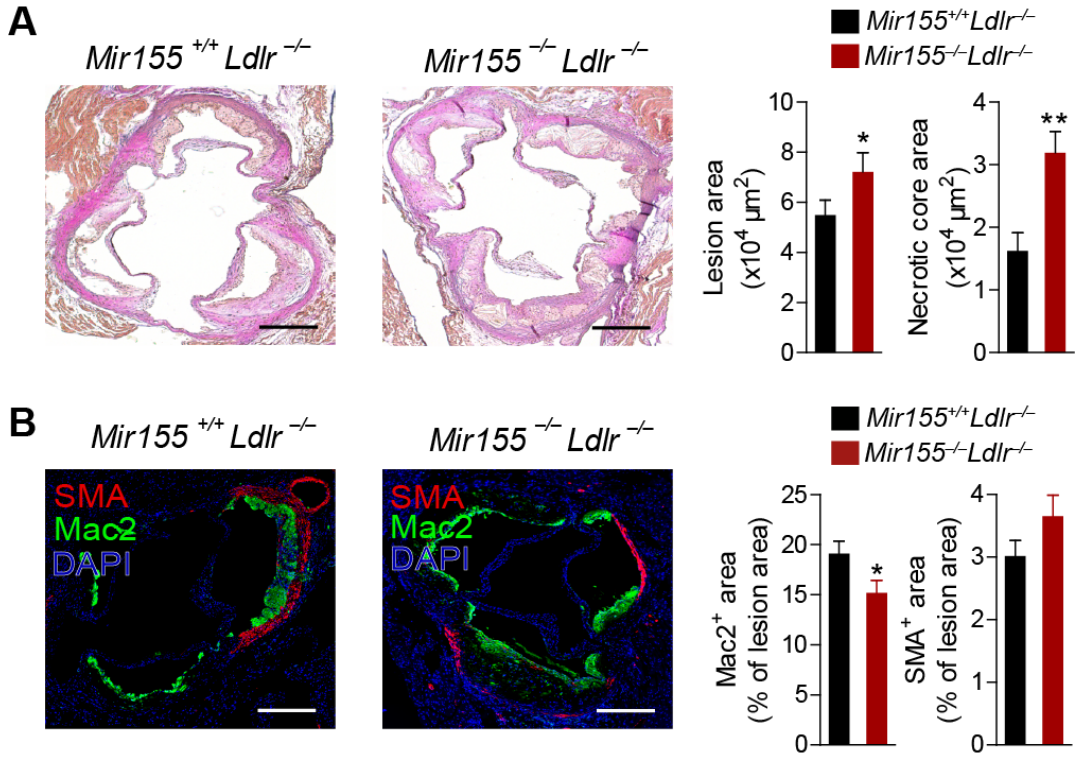

Figure 20. Effects of *Mir155* deficiency on atherosclerosis in DDC-fed *Ldlr*$^{-/-}$ mice. (**A**) Lesion and necrotic core areas in aortic roots from *Mir155*$^{+/+}$*Ldlr*$^{-/-}$ and *Mir155*$^{-/-}$*Ldlr*$^{-/-}$ mice after the 24-wk DDC feeding period determined by EVG stain (n = 10 mice per group). Scale bars: 100 μm. (**B**) Accumulation of macrophages and smooth muscle cells in aortic root lesions from *Mir155*$^{+/+}$*Ldlr*$^{-/-}$ and *Mir155*$^{-/-}$*Ldlr*$^{-/-}$ mice fed a DDC for 24 wk determined by combined Mac2 and SMA immunostaining, respectively (n = 10 mice per group). The nuclei were counterstained with DAPI. Scale bars: 100 μm. Data are represented as mean ± SEM; *p < 0.05 and **p < 0.01.

3.1.4 Fasting blood glucose concentrations

To investigate the role of *Mir155* deficiency in glucose homeostasis, FBG concentrations in *Mir155*$^{+/+}$*Ldlr*$^{-/-}$ and *Mir155*$^{-/-}$*Ldlr*$^{-/-}$ mice were measured every 4 wk during the 24-wk DDC feeding period. Notably, the FBG levels were already higher in lean *Mir155*$^{-/-}$*Ldlr*$^{-/-}$ mice compared with *Mir155*$^{+/+}$*Ldlr*$^{-/-}$ mice before DDC feeding (0 wk) (**Figure 21**). During the DDC feeding period, FBG levels remained higher in *Mir155*$^{-/-}$*Ldlr*$^{-/-}$ mice and increased steadily at a similar rate in both groups of mice. The differences in FBG levels between *Mir155*$^{+/+}$*Ldlr*$^{-/-}$ and *Mir155*$^{-/-}$*Ldlr*$^{-/-}$ mice occurred before those in body weight gain, lipid levels and atherosclerosis, which

indicates that miR-155-5p-mediated improvement of glucose homeostasis in *Ldlr*$^{-/-}$ mice limits obesity and atherosclerosis.

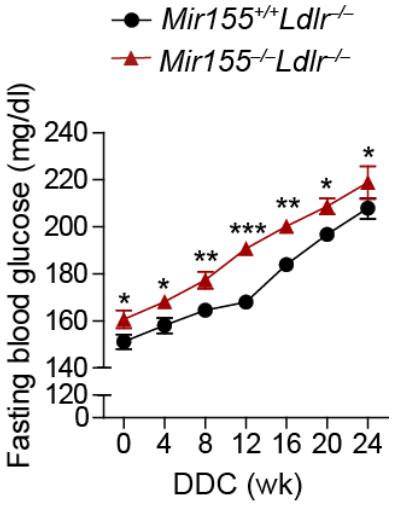

Figure 21. Effects of *Mir155* deficiency on fasting blood glucose concentrations in *Ldlr*$^{-/-}$ mice. FBG concentrations were measured after 6 h of fasting in mice during the 24-wk DDC feeding period (n = 10 mice per group). Data are represented as mean ± SEM. *p < 0.05, **p < 0.01 and ***p < 0.001.

3.2 Effects of miR-155-5p on islet function in hyperlipidemic mice

3.2.1 Insulin and glucagon levels

Insulin and glucagon are crucial regulators of glucose metabolism. To investigate the mechanism by which miR-155-5p affects glucose homeostasis, the effect of *Mir155* knockout on insulin and glucagon plasma levels were studied in *Mir155*$^{-/-}$*Ldlr*$^{-/-}$ and *Mir155*$^{+/+}$*Ldlr*$^{-/-}$ mice before and after a 24-wk DDC feeding program. The concentrations of insulin and glucagon in plasma were determined after 5 – 6 h of fasting using an ultra-sensitive mouse insulin ELISA kit or the Luminex's MAGPIX system. Notably, fasting plasma insulin levels were lower (**Figure 22A**), whereas glucagon levels were higher (**Figure 22B**) in *Mir155*$^{-/-}$*Ldlr*$^{-/-}$ mice than in *Mir155*$^{+/+}$*Ldlr*$^{-/-}$ mice fed the ND and after the 24-wk DDC feeding period, indicating that loss of miR-155-5p compromises islet cell function.

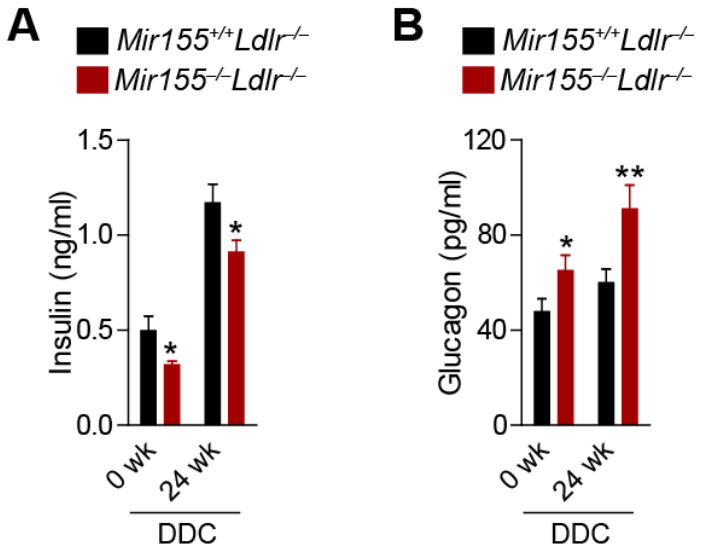

Figure 22 Effects of *Mir155* deficiency on insulin and glucagon plasma levels in *Ldlr*$^{-/-}$ mice. Fasting insulin (**A**) and glucagon (**B**) plasma concentrations were measured after 6 h of fasting in mice before (0 wk DDC) and after 24-wk feeding the DDC (n = 6 – 7 mice per group). Data are represented as mean ± SEM. *p < 0.05 and **p < 0.01.

3.2.2 Islet morphology

To gain insight into the function of miR-155-5p in pancreatic islets, the morphology of islets was investigated in ND-fed *Mir155*$^{+/+}$*Ldlr*$^{-/-}$and *Mir155*$^{-/-}$*Ldlr*$^{-/-}$ mice. Deletion of *Mir155* in *Ldlr*$^{-/-}$ mice did not affect the size and number of the pancreatic islets (data not shown). However, β-cell hypertrophy and a reduced islet cell density was observed in *Mir155*$^{-/-}$*Ldlr*$^{-/-}$ mice, determined in pancreatic sections stained with H&E stain (**Figure 23**).

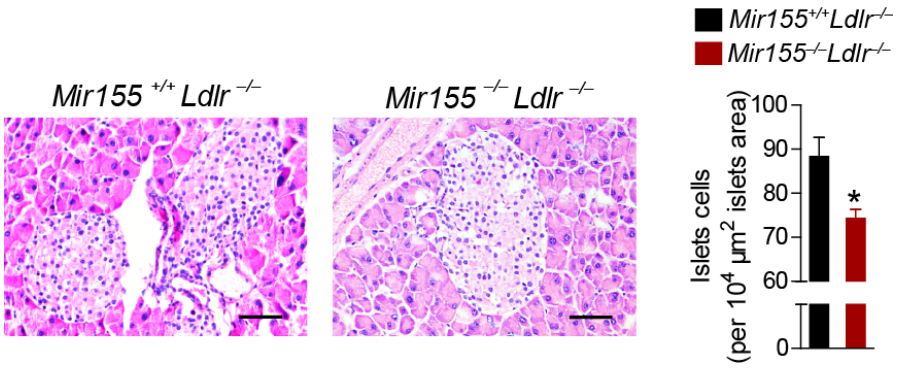

Figure 23. Effects of *Mir155* deficiency on islet morphology in ND-fed *Ldlr*$^{-/-}$ mice. Morphological characteristics of pancreatic islets determined by H&E staining of pancreas sections (n = 15 – 20 mice per group). Data are represented as mean ± SEM. *p < 0.05.

3.2.3 Islet insulin and glucagon content

To study the effect of miR-155-5p on islet cell composition and insulin and glucagon production, the percentage of insulin or glucagon-producing cells and the concentrations of insulin and glucagon were determined by immunostaining and Luminex multiplex analysis, respectively. In islets from ND-fed *Mir155*$^{-/-}$*Ldlr*$^{-/-}$ mice, the percentage of insulin-expressing cells and the insulin content were reduced compared with those in *Mir155*$^{+/+}$*Ldlr*$^{-/-}$ mice (**Figure 24A**). Conversely, the percentage of glucagon-expressing cells and the glucagon protein content were higher in islets from *Mir155*$^{-/-}$*Ldlr*$^{-/-}$ mice (**Figure 24B**), resulting in an elevated α-to-β-cell ratio.

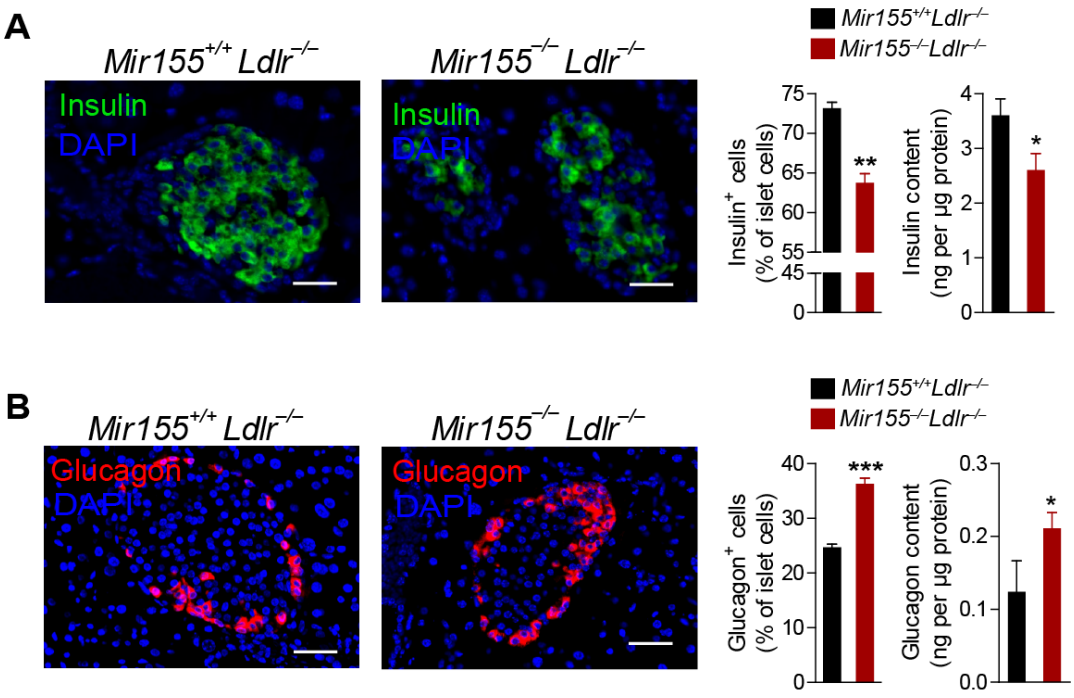

Figure 24. Effect of miR-155-5p on islet insulin and glucagon content in ND-fed *Ldlr*$^{-/-}$ mice. (**A**) Quantitation of the percentage of insulin-expressing β-cells per total islet cells (n = 15 – 18 mice per group) and islet insulin concentrations (n = 6 per group) by immunostaining and Luminex multiplex analysis, respectively, in 10 – 12 wk old mice fed a ND. The nuclei were counterstained with DAPI. Scale bars: 50 μm. (**B**) Quantitation of the percentage of glucagon-expressing α-cells per total islet cells (n = 15

– 18 mice per group) and islet glucagon concentrations (n = 6 per group) by immunostaining and Luminex multiplex analysis, respectively, in 10–12 wk old mice fed a ND. The nuclei were counterstained with DAPI. Scale bars: 50 μm. Data are represented as mean ± SEM. *p < 0.05, **p < 0.01 and ***p < 0.001.

3.2.4 Islet gene expression

To investigate how miR-155-5p regulates insulin and glucagon production in islets, the mRNA expression of candidate genes was analyzed in islets isolated from *Mir155*$^{+/+}$*Ldlr*$^{-/-}$ and *Mir155*$^{-/-}$*Ldlr*$^{-/-}$ mice by qPCR. Insulin *(Ins)* and proprotein convertase subtilisin/kexin type *(Pcsk) 1* mRNA expression was reduced in islets from *Mir155*$^{-/-}$*Ldlr*$^{-/-}$ mice, whereas islet glucagon (*Gcg*) and *Pcsk2* mRNA expression levels were elevated in these mice compared with *Mir155*$^{+/+}$*Ldlr*$^{-/-}$ mice. By contrast, the expression of somatostatin (*Sst*), and of the β-cell transcription factors ISL LIM homeobox 1 (*Isl1*), aristaless related homeobox (*Arx*), pancreatic and duodenal homeobox 1 (*Pdx1*), paired box 6 (*Pax6*), neurogenic differentiation 1 (*Neurod1*), and forkhead box A1 (*Foxa1*) in islets was not different between the groups (**Figure 25**).

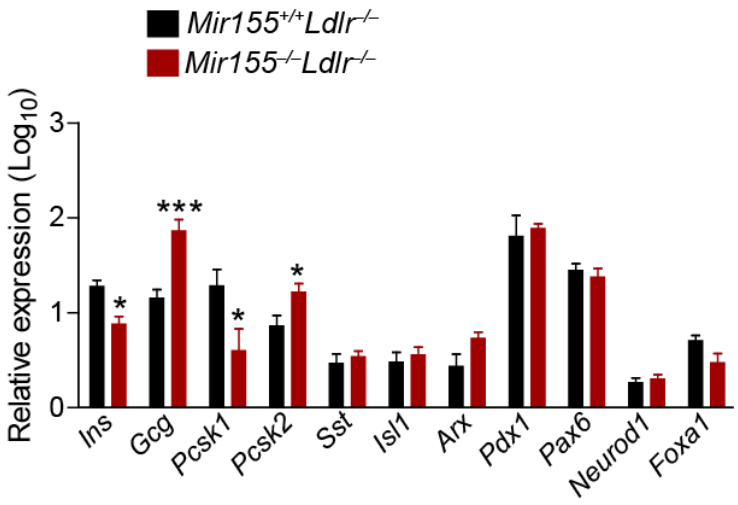

Figure 25. Effect of *Mir155* deficiency on islet gene expression in ND-fed *Ldlr*$^{-/-}$ mice. Quantitation of gene expression in murine islets isolated from 10 – 12 wk old mice fed a ND determined by qPCR. insulin (*Ins),* glucagon *(Gcg)*, and proprotein convertase subtilisin/kexin type *(Pcsk) 1*, *Sst,* somatostatin; *Isl1,* ISL LIM homeobox 1; *Arx,* aristaless related homeobox; Pdx1, pancreatic and duodenal homeobox 1; Pax6, paired box 6; Neurod1, neurogenic differentiation 1; Foxa1, forkhead box A1. (n = 6–8 mice per group). Data are represented as mean ± SEM. *p < 0.05 and ***p < 0.001.

3.2.5 GLP-1 levels

Proglucagon is processed to glucagon and GLP-1 by PC 2 (encoded by the *Pcsk2* gene) and PC1/3 (encoded by the *Pcsk1* gene), respectively[41,45,50]. GLP-1 can be generated locally in pancreatic α-cells, and increases islet insulin and reduces glucagon secretion[45]. Therefore, the effect of *Mir155* knockout on GLP-1 expression was studied. The islet GLP-1 protein content was reduced in ND-fed *Mir155*$^{-/-}$*Ldlr*$^{-/-}$ mice (**Figure 26A**). Plasma GLP-1 levels determined by Luminex analysis were lower in *Mir155*$^{-/-}$ *Ldlr*$^{-/-}$ mice than in *Mir155*$^{+/+}$*Ldlr*$^{-/-}$ mice fed a ND or the DDC for 24 wk (**Figure 26B**).

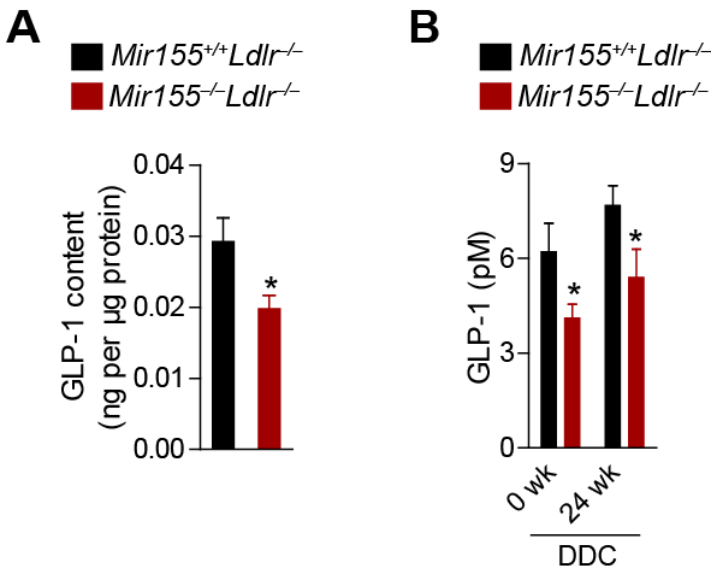

Figure 26. Effect of miR-155-5p on GLP-1 levels in *Ldlr*$^{-/-}$ mice. (**A**) Islet GLP-1 protein concentration in 10 – 12 wk old mice fed a ND determined by Luminex analysis (n = 6 per group). (**B**) Fasting GLP-1 plasma concentrations in mice fed a ND (0 wk DDC) and after the 24-wk DDC feeding period (n = 6 – 7 mice per group). Data are represented as mean ± SEM. *p < 0.05.

3.2.6 Proliferation and apoptosis of islet cells

Next, the role of miR-155-5p in proliferation and apoptosis of islet cells were studied in pancreatic sections from ND-fed *Mir155*$^{+/+}$*Ldlr*$^{-/-}$ and *Mir155*$^{-/-}$*Ldlr*$^{-/-}$ mice by immunostaining of Ki67 and activated Caspase3, respectively. Deletion of *Mir155* in *Ldlr*$^{-/-}$ mice reduced the percentage of Ki67^{+} islet cell numbers (**Figure 27A**), indicating

that miR-155-5p promotes islet cell proliferation. By contrast, islet cell apoptosis was negligible in both groups of mice (**Figure 27B**).

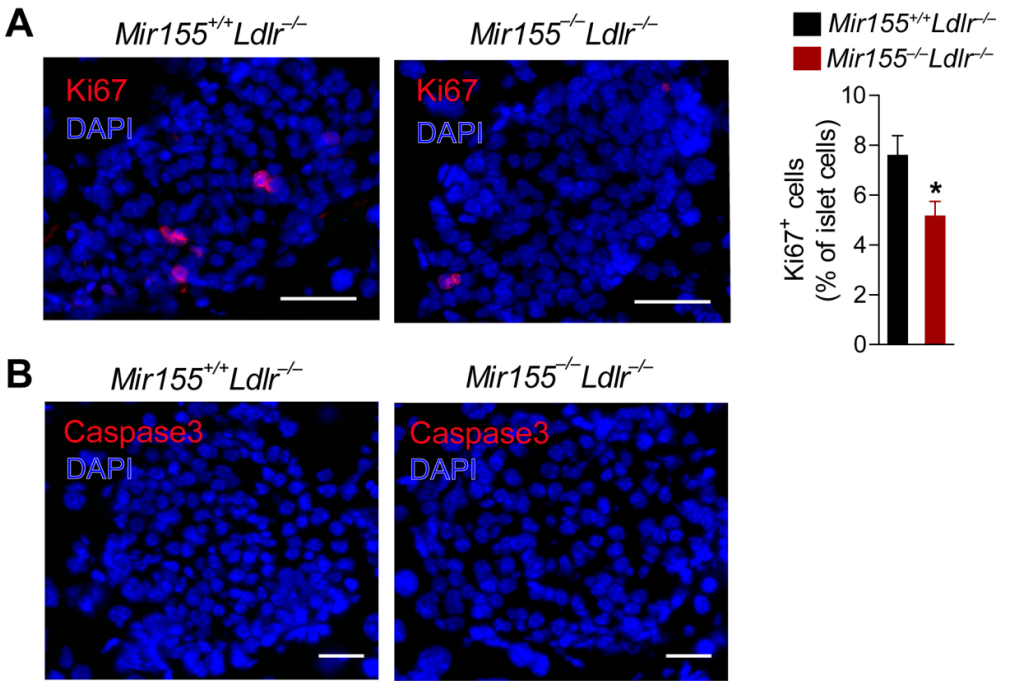

Figure 27. Effect of miR-155-5p on proliferation and apoptosis in pancreas. (**A**) Islet cell proliferation assessed by Ki67 immunostaining (n = 10 mice per group) in pancreatic sections from 10 – 12 wk old *Mir155*$^{+/+}$*Ldlr*$^{-/-}$ and *Mir155*$^{-/-}$*Ldlr*$^{-/-}$ mice fed a ND. The nuclei were counterstained with DAPI. Scale bars: 100 μm. Data are represented as mean ± SEM. *p < 0.05. (**B**) Islet cell apoptosis determined by immunostaining of activated Caspase3, Representative images are shown. The nuclei were counterstained with DAPI. Scale bars: 50 μm.

3.2.7 Inflammation in pancreatic islets

Because miR155-5p has been implicated as a central regulator of the immune system,[103,121,154,155] the effect of miR-155-5p on inflammation in pancreatic islets was studied. The accumulation of macrophages or T-cells in murine islets detected by combined Mac2 and CD3 immunostaining was negligible in both groups of mice (**Figure 28A**). Moreover, the expression of the proinflammatory genes *Nos2* and *Tnf* genes, and the anti-inflammatory genes *Mrc1* and Arginase 1 (*Arg1*) was not different between the groups (**Figure 28B**), indicating that the effects of miR-155-5p on islets are independent of inflammatory response.

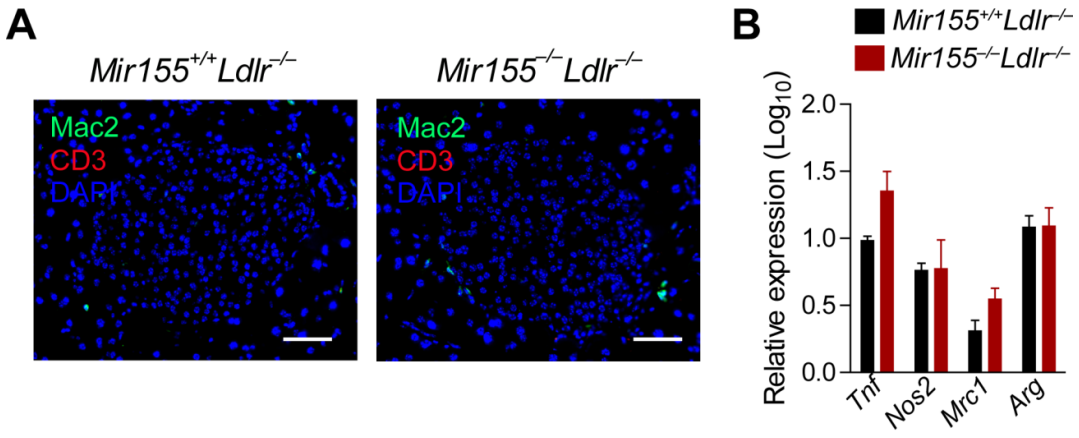

Figure 28. Effect of miR-155-5p on inflammation in pancreatic islets in *Ldlr*$^{-/-}$ mice. (**A**) Macrophages and T-cells in murine islets detected by combined Mac2 and CD3 immunostaining. Representative images are shown. The nuclei were counterstained with DAPI. Scale bars: 50 μm. (**B**) Quantitation of gene expression by qPCR in islets isolated from 10 – 12 wk old mice fed a ND (n = 4 – 6 samples per group). *Arg1*, Arginase 1. Data are represented as mean ± SEM.

3.2.8 Glucose tolerance

To test the role of hyperlipidemia in the regulation of glucose homeostasis by miR-155-5p, IPGTT was performed in *Mir155*$^{-/-}$ mice in the absence and presence of hyperlipidemia. *Mir155* knockout increased blood glucose levels following intraperitoneal glucose challenge in male and female *Ldlr*$^{-/-}$ (**Figures 29A and 29B**) or *Apoe*$^{-/-}$ mice (**Figures 29C and 29D**) fed a ND. Notably, glucose tolerance was not affected by *Mir155* knockout in male ND-fed *Ldlr*$^{+/+}$ mice (**Figure 29E**). Thus, miR-155-5p improved glucose homeostasis only under hyperlipidemic conditions.

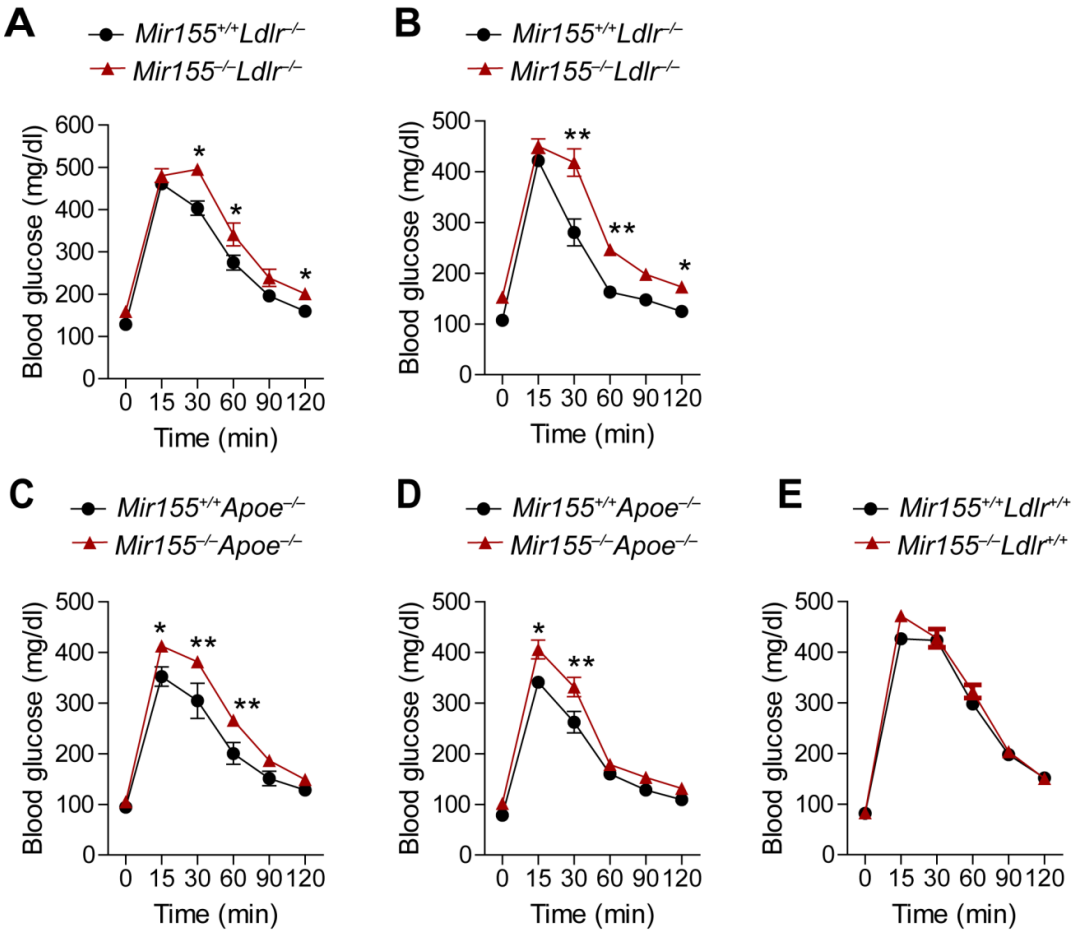

Figure 29. Effect of miR-155-5p on glucose tolerance. (**A** – **E**) Comparison of glucose tolerance between male *Mir155*$^{+/+}$*Ldlr*$^{-/-}$ and *Mir155*$^{-/-}$*Ldlr*$^{-/-}$ mice (**A**, n = 8 – 10 mice per group), female *Mir155*$^{+/+}$*Ldlr*$^{-/-}$ and *Mir155*$^{-/-}$*Ldlr*$^{-/-}$ mice (**B**, n = 4 mice per group), male *Mir155*$^{+/+}$*Apoe*$^{-/-}$ and *Mir155*$^{-/-}$*Apoe*$^{-/-}$ mice (**C**, n = 4 – 5 mice per group), female *Mir155*$^{+/+}$*Apoe*$^{-/-}$ and *Mir155*$^{-/-}$*Apoe*$^{-/-}$ mice (**D**, n = 4 – 6 mice per group) and male *Mir155*$^{+/+}$*Ldlr*$^{+/+}$ and *Mir155*$^{-/-}$*Ldlr*$^{+/+}$ mice (**E**, n = 6 – 8 mice per group), at 10 – 12 wk of age fed a ND. Data are represented as mean ± SEM. *p < 0.05 and **p < 0.01.

3.3 Effects of miR-155-5p on murine insulinoma cell line

3.3.1 Insulin and glucagon expression in MIN6 cells

To address the role of miR-155-5p in insulin and glucagon production, gain-and-loss-of-function experiments were performed in murine pancreatic β-cells (MIN6).[143]

Treatment with miR-155-5p inhibitors (**Figure 30A, left**) up-regulated *Gcg* and *Pcsk2* expression and down-regulated *Pcsk1* expression in MIN6 cells compared with non-targeting oligonucleotides (**Figure 30A, middle**). At the protein level, miR-155-5p inhibitor treatment resulted in lower insulin and GLP-1 concentrations, and higher glucagon levels in MIN6 cell lysates than control treatment (**Figure 30A right**). Conversely, miR-155-5p mimic treatment (**Figure 30B, left**) down-regulated *Gcg* and *Pcsk2* mRNA expression, and up-regulated *Pcsk1* mRNA expression compared with non-specific oligonucleotides (**Figure 30B, middle**). In contrast to miR-155-5p inhibitor treatment, overexpressing miR-155-5p in MIN6 cells increased insulin and GLP-1 expression, but reduced glucagon expression at the protein level (**Figure 30B, right**). Hence, these results indicate that miR-155-5p regulates insulin and glucagon production in pancreatic islets and promotes islet GLP-1 production by up-regulating *Pcsk1*.

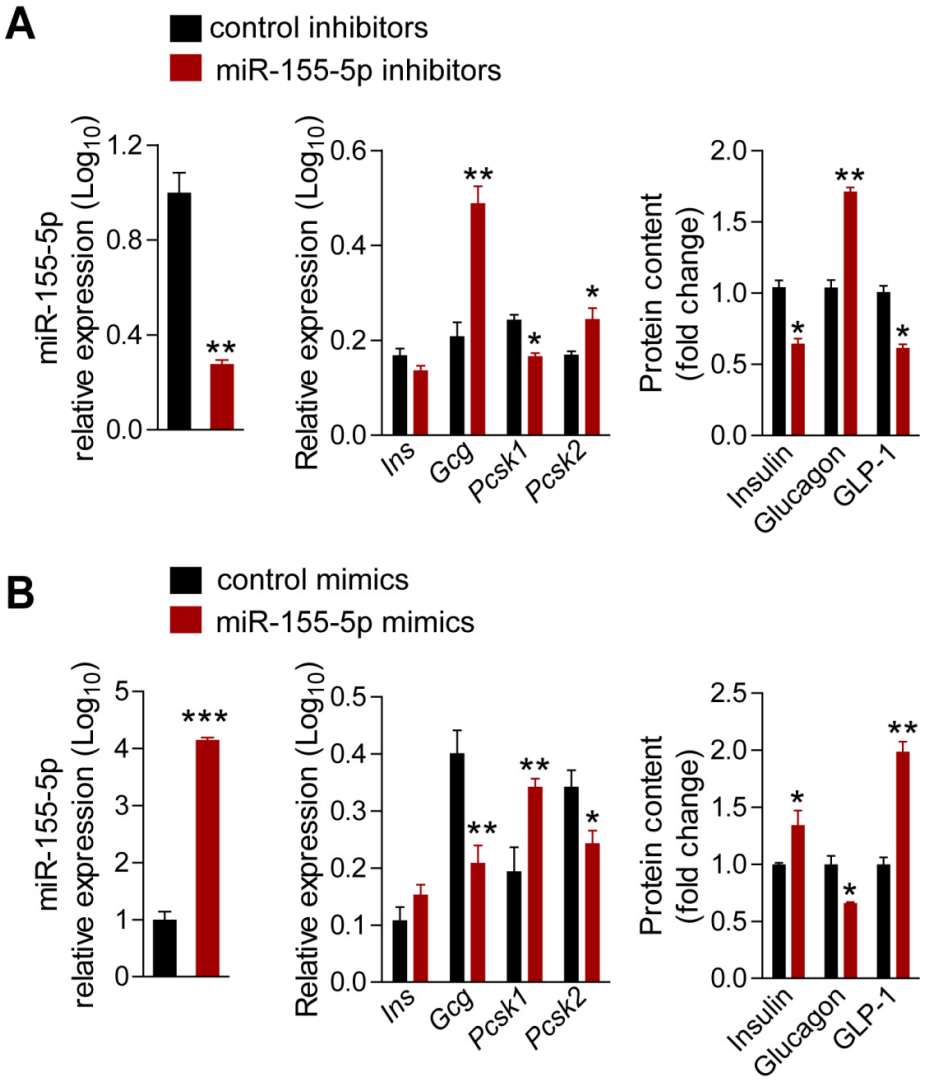

Figure 30 Effect of miR-155-5p on insulin and glucagon production in MIN6 cells. (**A** and **B**) *Ins, Gcg, Pcsk1* and *Pcsk2* mRNA expression levels (n = 4 – 6 per group) determined by qPCR, and insulin, glucagon and GLP-1 protein levels (n = 4 per group) measured by Luminex multiplex analysis in MIN6 cells treated with miR-155-5p inhibitors (**A**) or miR-155-5p mimics (**B**) for 24 h. Non-targeting oligonucleotides were used as control (control inhibitors or control mimics). Data are represented as mean ± SEM. *p < 0.05, **p < 0.01 and ***p < 0.001.

3.3.2 MIN6 cell proliferation

Because islet cell proliferation was down-regulated in *Mir155*$^{-/-}$*Ldlr*$^{-/-}$ mice compared to *Mir155*$^{+/+}$*Ldlr*$^{-/-}$ mice, cell cycle analysis was performed in MIN6 cells by flow cytometry. miR-155-5p mimic treatment increased, whereas miR-155-5p inhibitor

treatment reduced MIN6 cell proliferation compared to control oligonucleotides (**Figures 31A and 31B**), indicating that miR-155-5p promotes pancreatic β-cells proliferation.

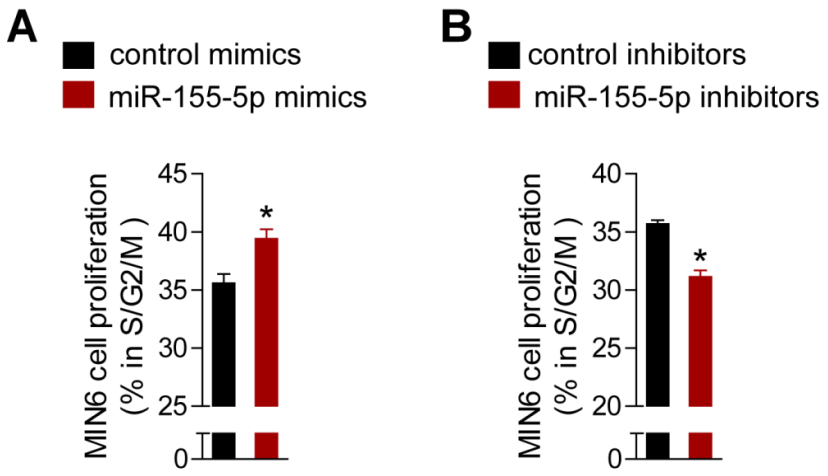

Figure 31. Effect of miR-155-5p on MIN6 cellular proliferation. (**A** and **B**) Cell cycle analysis of miR-155-5p mimics- (**A**) or miR-155-5p inhibitors-(**B**) treated MIN6 cells stained with propidium iodide by flow cytometry (n = 4 – 5 per group). Non-targeting oligonucleotides were used as control. Data are represented as mean ± SEM. *p < 0.05.

3.4 Role of hyperlipidemia-related endotoxemia in islet miR-155-5p expression

3.4.1 Regulation of miR-155-5p expression in pancreatic islets

Because *Mir155* knockout affected glucose homeostasis only in hyperlipidemic mice, the regulation of islet miR-155-5p expression by hyperlipidemia and LPS was studied by qPCR and *in situ* PCR. Feeding *Ldlr*$^{-/-}$ mice the DDC for 24 wk increased plasma lipid levels (**Figure 32A**), circulating endotoxin activity and islet miR-155-5p expression (**Figure 32B**) compared to ND feeding (**Figure 32B**). In ND-fed *Ldlr*$^{-/-}$ mice, miR-155-5p was mainly detectable in glucagon^{-} islet cells by combined glucagon immunostaining and miR-155-5p *in situ* PCR (**Figure 32C**). Similar to the effect of feeding the DDC, hyperlipidemia in 10 – 12 wk old, ND-fed *Ldlr*$^{-/-}$ mice (**Figure 32D**) is associated with increased plasma endotoxin activity (**Figure 32E**) and upregulation of islet miR-155-5p expression (**Figure 32E**) compared with normolipidemic *Ldlr*$^{+/+}$ mice.

Notably, knockout of *Ldlr* in ND-fed mice also resulted in deposition of oxLDL in islets (**Figure 32F**).These results indicate that hyperlipidemia-associated endotoxemia induces islet miR-155-5p expression in *Ldlr*$^{-/-}$ mice.

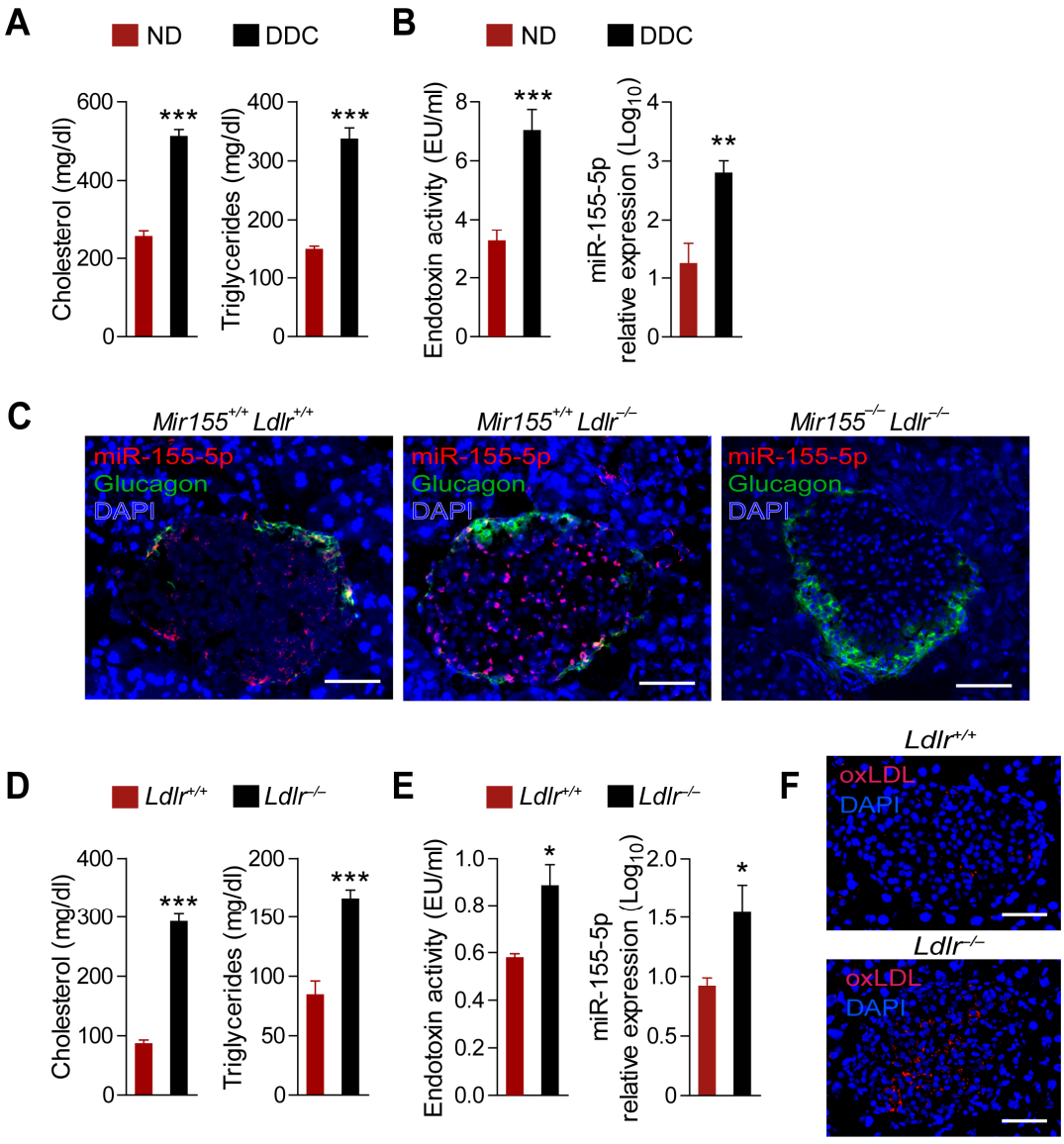

Figure 32. Regulation of miR-155-5p expression in pancreatic islets. (**A**) Plasma cholesterol and triglyceride levels in *Ldlr*$^{-/-}$ mice fed the ND or the DDC for 24 wk (n = 7 – 10 mice per group) measured by cholesterol and triglyceride fluorescent assay kits, respectively. (**B**) Serum endotoxin levels (left, n = 6 per group) and miR-155-5p expression level in laser-microdissected islets (right, n = 4 – 5 per group) in mice fed the ND or the DDC for 24 wk. (**C**) Localization of miR-155-5p expression in islets from ND-fed mice (10 – 12 wk of age) determined by *in situ* PCR and glucagon immunostaining. The nuclei were counterstained with DAPI. Scale bars: 50 μm. (**D**) Plasma cholesterol and triglyceride levels in ND-fed

Ldlr$^{+/+}$ or *Ldlr*$^{-/-}$ mice (10 – 12 wk of age, n = 7 – 10 mice per group). (**E**) Serum endotoxin levels in 10 – 12 wk old mice fed a ND determined by LAL test (left, n = 6 mice per group). Quantitation of miR-155-5p expression by qPCR in isolated murine islets from ND-fed mice (10 – 12 wk of age) (right, n = 6 mice per group). (**F**) oxLDL immunostaining in islets from ND-fed mice (10 – 12 wk of age). The nuclei were counterstained with DAPI. Scale bars: 50 μm. Data are represented as mean ± SEM. *p < 0.05, **p < 0.01 and ***p < 0.001.

3.4.2 Regulation of miR-155-5p expression in MIN6 cells

Because LPS and moxLDL induce miR-155-5p selectively in macrophages[103,104,152], the regulation miR-155-5p expression by LPS and moxLDL was studied in pancreatic β-cells. MIN6 cells were treated with LPS (5, 20, or 50 ng/mL), nLDL (100 μg/mL), moxLDL (100 μg/mL), and phosphate-buffered saline (vehicle) for 6 h. LPS induced miR-155-5p expression in MIN6 cells in a dose-dependent manner (**Figure 33A**). In contrast to nLDL, moxLDL up-regulated miR-155-5p expression in MIN6 cells compared with vehicle treatment (**Figure 33B**). Notably, mild oxidative modification of LDL leads to increased endotoxin activity compared with nLDL (**Figure 33C**). These results demonstrated that LPS and moxLDL induce miR-155-5p expression in murine pancreatic β-cells.

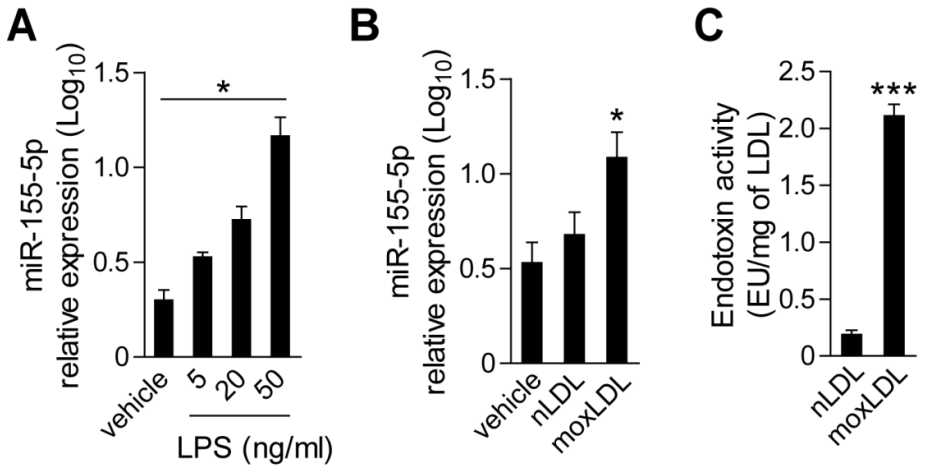

Figure 33. Regulation of miR-155-5p expression in MIN6 cells. (**A**) Quantitation of miR-155-5p expression in MIN6 cells treated with LPS or vehicle for 6 h (n = 5 – 6 per group) determined by qPCR. *p < 0.05 between each group. (**B**) Quantitation of miR-155-5p expression in MIN6 cells treated with nLDL, moxLDL or vehicle for 6 h (n = 5 – 6 per group) determined by qPCR. *p < 0.05. (**C**) Endotoxin

activity in nLDL or moxLDL determined by LAL test (n = 3 samples per group). ***p < 0.001. Data are represented as mean ± SEM.

3.4.3 Role of miR-155-5p in the effects of LPS on glucose homeostasis

Low-dose LPS infusion triggers GLP-1-mediated insulin secretion and lowers blood glucose levels in C57/BL6 mice.[48,75] To investigate whether the effect of LPS on glucose homeostasis is mediated by miR-155-5p, IPGTT was performed 6 h after LPS injection (2 mg/kg) into ND-fed *Ldlr*$^{-/-}$ mice. Low-dose LPS up-regulated islet miR-155-5p expression (**Figure 34A**), and increased insulin and GLP-1 plasma levels (**Figure 34B**). Moreover, the glucose-lowering effect of LPS following intraperitoneal glucose injection in *Ldlr*$^{-/-}$ mice (**Figure 34C**) was significantly reduced in *Mir155*$^{-/-}$ *Ldlr*$^{-/-}$ mice (**Figure 34C**), indicating that miR-155-5p is involved in LPS-triggered insulin secretion.

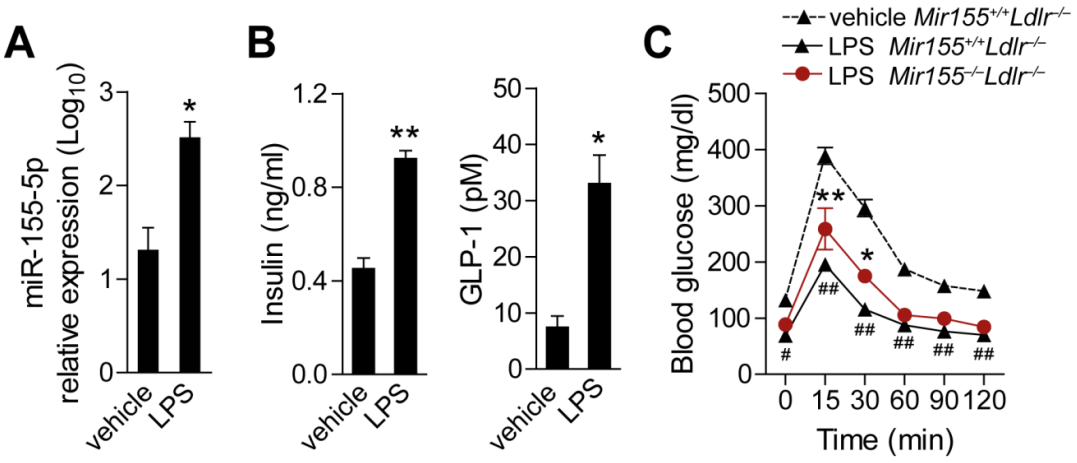

Figure 34. miR-155-5p mediates the effects of LPS on glucose homeostasis. (**A**) Quantitation of miR-155-5p expression by qPCR in islets isolated from ND-fed *Ldlr*$^{-/-}$ mice 6 h after injection of LPS (2 mg/kg) or vehicle (n = 6 mice per group). *p < 0.05. (**B**) Fasting insulin and GLP-1 plasma concentrations in ND-fed *Ldlr*$^{-/-}$ mice 6 h after injection of LPS (2 mg/kg) or vehicle determined by Luminex multiplex analysis (n = 6 – 7 mice per group). *p < 0.05, **p < 0.01 and ***p < 0.001. (**C**) IPGTT in *Ldlr*$^{-/-}$ mice 6 h after injection of LPS (2 mg/kg) or vehicle (n = 6 – 7 mice per group). *p < 0.05 and **p < 0.01 between LPS *Mir155*$^{-/-}$*Ldlr*$^{-/-}$ and LPS *Mir155*$^{+/+}$*Ldlr*$^{-/-}$; $^{\#}$p < 0.01 and $^{\#\#}$p < 0.001 between LPS *Mir155*$^{+/+}$*Ldlr*$^{-/-}$ and vehicle *Mir155*$^{+/+}$*Ldlr*$^{-/-}$. Data are represented as mean ± SEM.

3.5 Effect of miR-155 on global gene expression in pancreatic islets

To study the molecular mechanism by which miR-155-5p regulates islet function, genome-wide gene expression analysis was performed in islets from 10 – 12 wk old, ND-fed *Mir155*$^{+/+}$*Ldlr*$^{-/-}$ and *Mir155*$^{-/-}$*Ldlr*$^{-/-}$ mice by microarray analysis. In *Mir155*$^{-/-}$ *Ldlr*$^{-/-}$ mice, 239 genes were up-regulated and 420 genes were downregulated compared with *Mir155*$^{+/+}$*Ldlr*$^{-/-}$ mice ($p < 0.05$, absolute fold change ≥ 1.5, n = 3 samples per group).

To predict upstream regulators of miR-155-5p-dependent biological processes in islets, pathway analysis was performed using Ingenuity® Pathway Analysis (IPA) software.[147] Differentially regulated genes were enriched in the carbohydrate and lipid metabolism pathways and in pathways related to endocrine system function, cellular growth, DNA replication, and cell survival as determined by Ingenuity® Pathway Analysis software (**Figure 35**).

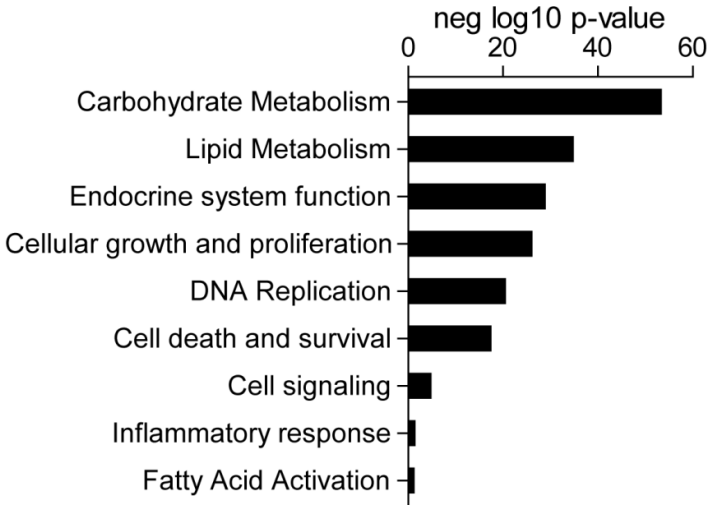

Figure 35. Pathway analysis. Gene expression profiling by microarrays in islets isolated from ND-fed *Mir155*$^{+/+}$*Ldlr*$^{-/-}$ and *Mir155*$^{-/-}$*Ldlr*$^{-/-}$ mice (10 – 12 wk of age) (n = 3 samples per group). Biological processes enriched with differentially regulated genes were predicted by Ingenuity® Pathway Analysis software ($p < 0.05$; fold change cutoff = 1.5).

Analysis of potential upstream regulators of differential gene expression in islets indicated cyclin-dependent kinase inhibitor (Cdkn)1 activation and cyclin-dependent kinases (Cdk)4 inhibition in *Mir155*$^{-/-}$*Ldlr*$^{-/-}$ mice, which may reduce islet cell proliferation (**Figure 36**).[156,157] Phosphatase and tensin homolog (PTEN) activation, which contributes to β-cell failure in mouse models of type 2 diabetes,[158] was increased in *Mir155*$^{-/-}$*Ldlr*$^{-/-}$ mice (**Figure 36**). Moreover, glucose transporter (Glut)2-dependent pathways and pathways related to cyclic adenosine monophosphate (AMP), GLP-1, and glucose-dependent insulinotropic polypeptide (GIP) signaling were inhibited, suggesting impaired glucose uptake and insulin secretion (**Figure 36**).[159,160]

Among the inflammatory pathways, IL-6 receptor activation was reduced and signaling pathways downstream of the IL-6 receptor, such as the janus kinase/signal transducer and activator of transcription (JAK/STAT) and extracellular signal–regulated kinase (ERK)1/2 pathways[161,162] were inhibited in *Mir155*$^{-/-}$*Ldlr*$^{-/-}$ mice (**Figure 36**). These data demonstrate that *Mir155* knockout results in transcriptional changes compatible with reduced β-cell function and proliferation.

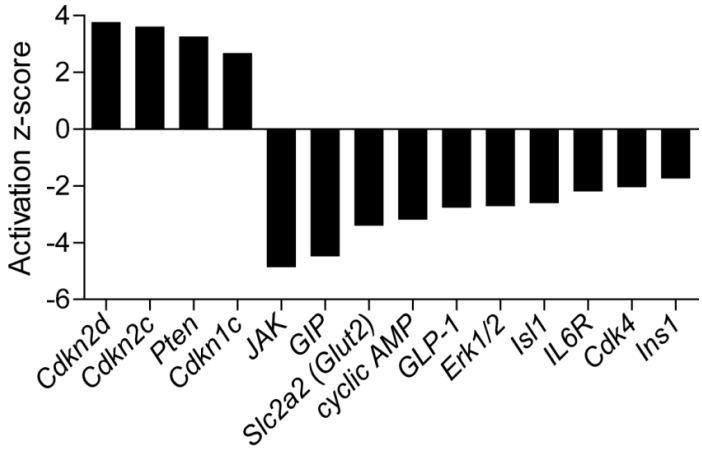

Figure 36. Analysis of potential upstream regulators. Gene expression profiling by microarrays in islets isolated from ND-fed *Mir155*$^{+/+}$*Ldlr*$^{-/-}$ and *Mir155*$^{-/-}$*Ldlr*$^{-/-}$ mice (10 – 12 wk of age) (n = 3 samples per group). Upstream regulators of differential gene expression predicted by Ingenuity® Pathway Analysis software ($p < 0.05$; fold change cutoff = 1.5).

3.6 Effect of miR-155-5p on IL-6 expression in β-cells

3.6.1 miR-155-5p positively regulates IL-6 expression in islets

IL-6 is physiologically expressed in islets, promotes islet cell proliferation, and increases insulin secretion and glucose tolerance by *Pcsk1*-mediated GLP-1 production.[163-165] In islets from *Mir155*$^{-/-}$*Ldlr*$^{-/-}$ mice, reduced IL-6 receptor signaling was predicted to play a causal role in the differential gene expression (**Figure 37**) and IL-6 showed the highest connectivity to other differentially regulated genes (**Figure 37**). Moreover, the positive regulation of IL-6 by miR-155-5p in macrophages and dendritic cells was shown in previous study,[152,154,166-168] therefore the effect of miR-155-5p on IL-6 expression in pancreatic islets was studied.

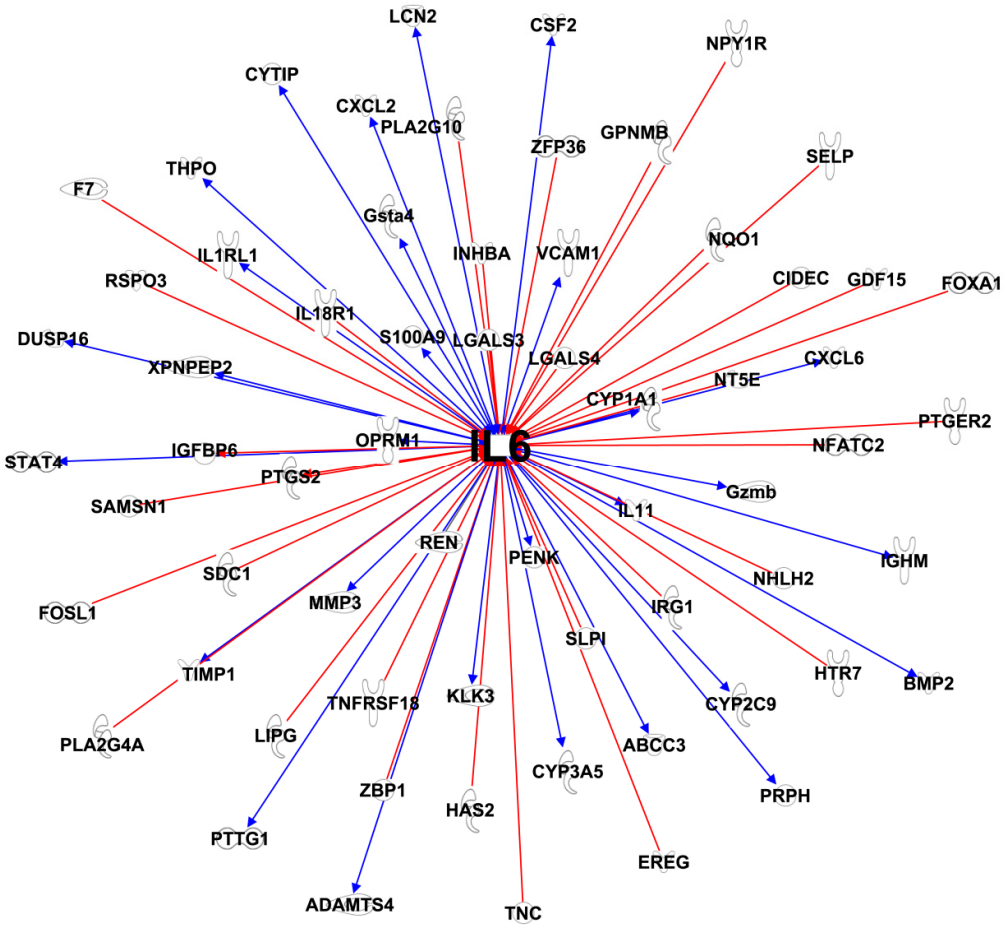

Figure 37. Connectivity of *Il6* with other differentially regulated genes. Connectivity of *Il6* with other differentially expressed mRNAs in islets from *Mir155*$^{+/+}$*Ldlr*$^{-/-}$ and *Mir155*$^{-/-}$*Ldlr*$^{-/-}$ mice fed a ND

analyzed by IPA and Ingenuity® iReport. Red lines indicate upstream regulators of *Il6* and blue lines indicate downstream genes regulated by *Il6* (n = 3 samples per group; P < 0.05; fold change cutoff = 1.5).

The expression of IL-6 was confirmed in the pancreatic islets from *Mir155*$^{+/+}$*Ldlr*$^{-/-}$ and *Mir155*$^{-/-}$*Ldlr*$^{-/-}$ mice. Accordingly, deficiency of miR-155-5p led to a marked reduction of the IL-6 mRNA and protein expression in islets determined by qPCR and ELISA, respectively (**Figure 38A**). Moreover, to investigate the cell-specific effect of miR-155-5p on IL-6 expression, combined IL-6 and insulin immunostaining was performed on pancreatic sections. The number of IL-6-producing β-cells were reduced in *Mir155*$^{-/-}$*Ldlr*$^{-/-}$ mice compared with *Mir155*$^{+/+}$*Ldlr*$^{-/-}$ mice (**Figure 38B**).

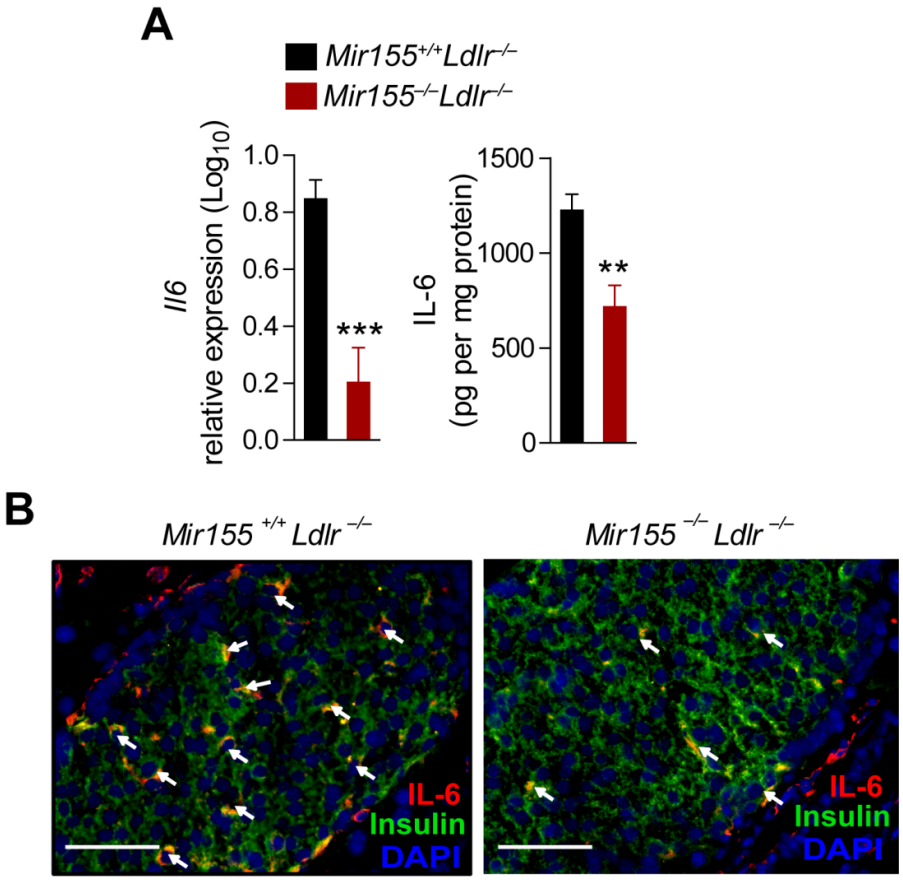

Figure 38. Regulation of IL-6 expression by miR-155-5p in islets. (**A**) Quantitation of IL-6 expression at the mRNA and protein level in islets isolated from ND-fed mice (10 – 12 wk of age) by qPCR and ELISA, respectively (*n* = 6 per group). (**B**) Combined IL-6 and insulin immunostaining in pancreatic sections from ND-fed mice (10 – 12 wk of age). Arrows indicate insulin^{+} cells expressing IL-6. Nuclei were counterstained with DAPI. Scale bars: 50 μm. Data are represented as mean ± SEM. **p < 0.01 and ***p < 0.001.

3.6.2 miR-155-5p up-regulates IL-6 expression in MIN6 cells

Next, to investigate the effect of miR-155-5p on IL-6 expression in β-cells, gain-and-loss-of-function experiments were performed in vitro. In MIN6 cells, miR-155-5p mimic treatment up-regulated *Il6* mRNA expression (**Figure 39A, left**), and increased IL-6 protein synthesis (**Figure 39A, middle**) and secretion (**Figure 39A, right**). Conversely, inhibition of miR-155-5p in MIN6 cells down-regulated *Il6* mRNA expression (**Figure 39B, left**), and reduced IL-6 protein synthesis (**Figure 39B, middle**) and secretion (**Figure 39B, right**). Thus, these results demonstrate that miR-155-5p positively regulates *Il6* mRNA and protein expression in MIN6 cells.

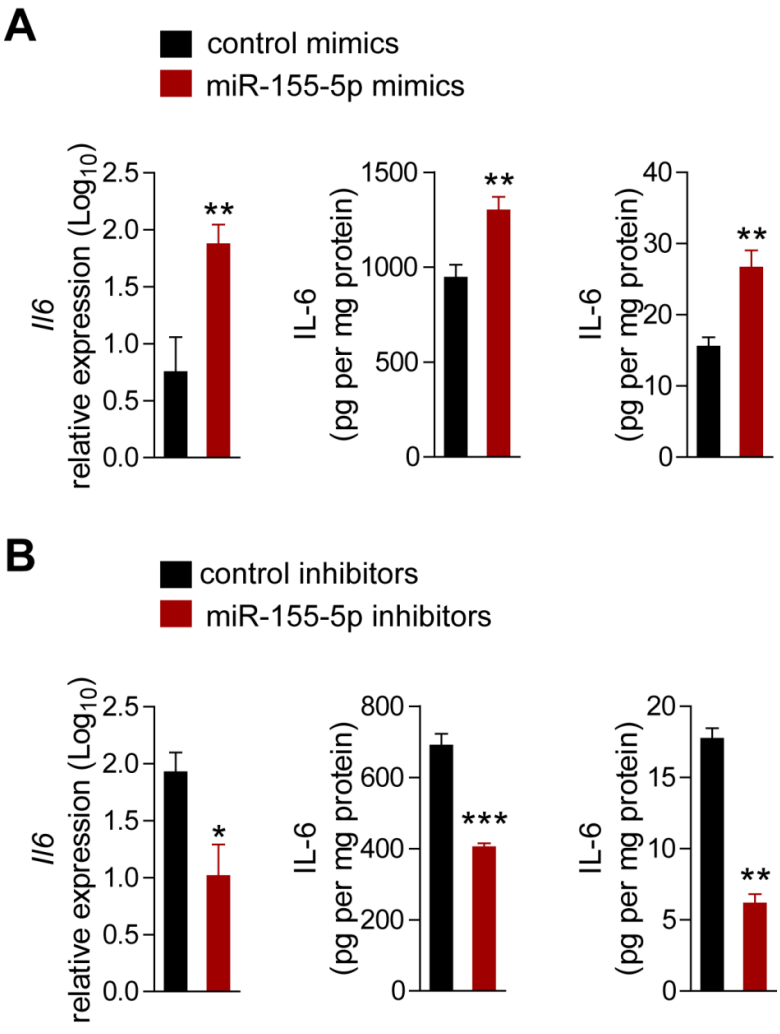

Figure 39. Regulation of IL-6 expression by miR-155-5p in MIN6 cells. (**A** and **B**) Quantitation of *Il6* mRNA expression (n = 6 per group, left), IL-6 cellular protein content (n = 4 per group, middle) and IL-6

protein secretion (n = 4 per group, right) by qPCR and ELISA after transfection of MIN6 cells with miR-155-5p mimics (**A**) or miR-155-5p LNA inhibitors (**B**). Non-targeting oligonucleotides were used as control. Data are represented as mean ± SEM. *p < 0.05, **p < 0.01 and ***p < 0.001.

To determine whether miR-155-5p transcriptionally regulation IL6 expression, MIN6 cells were co-transfected with Luciferase reporter constructs harboring the *Il6* promoter region and miR-155-5p mimics or miR-155-5p LNA inhibitors. Overexpression of miR-155-5p markedly increased the luciferase activity in cells expressing luciferase under the control of the *Il6* promoter, but not in cells treated with empty vector (**Figure 40A**), while inhibition of miR-155-5p had the opposite effect (**Figure 40B**). These data suggest that miR-155-5p promotes *Il6* gene transcription in MIN6 cells

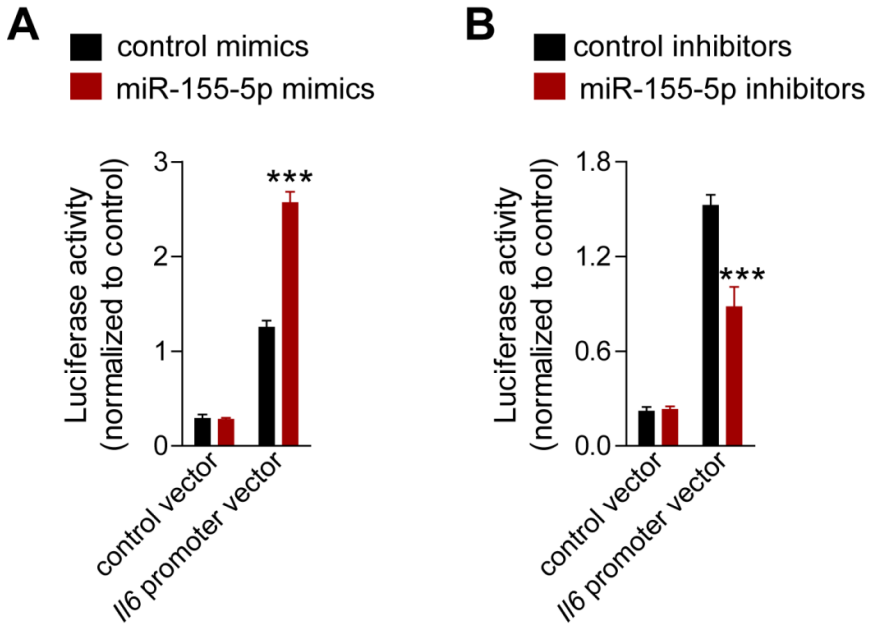

Figure 40. miR-155-5p promotes IL-6 transcription in MIN6 cells. (**A** and **B**) Luciferase activity in MIN6 cells co-transfected with Luciferase reporter constructs harboring *Il6* promoter region or the empty vector and miR-155-5p mimics (**A**) or miR-155-5p LNA inhibitors (**B**) Non-targeting oligonucleotides were used as control. (n = 4 per group). The empty vector was used as control. The luminescence intensities of Gaussian luciferase were normalized to the activity of secreted alkaline phosphatase. Data are represented as mean ± SEM. ***p < 0.001.

3.6.3 Effect of islet-derived IL-6 on islet gene expression

To study the effect of islet-derived IL-6 on islet gene expression, the secretion of IL-6 from MIN6 cells was blocked using a neutralizing IL-6 antibody. Treatment with the IL-6 antibody reduced *Ins* and *Pcsk1* expression and increased *Pcsk2* expression (**Figure 41**), determined by qPCR, as compared to an unspecific control antibody. Taken together, these results indicate that miR-155-5p increases IL-6 expression, which may enhance GLP-1 production through up-regulating *Pcsk1* expression.

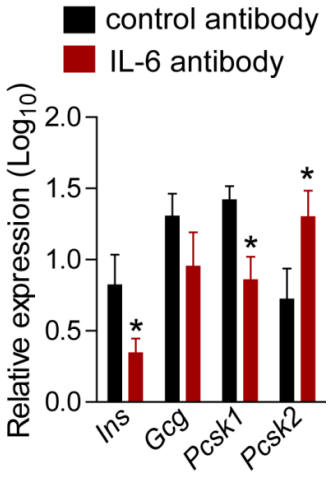

Figure 41. Effects of bloking secreted IL-6 in MIN6 cells. Effect of anti-IL-6 antibody treatment on the expression levels of *Ins*, *Gcg*, *Psck1* and *Pcsk2* in MIN6 cells compared to treatment with isotype control antibodies ($n = 4$ per group). Data are represented as mean ± SEM. *$p < 0.05$.

3.7 Targets of miR-155-5p in islets during hyperlipidemia

3.7.1 Prediction of miR-155-5p target genes in pancreatic islets

To determine the targets that mediate the effect of miR-155-5p on islet cell function, the 3'-UTR of the genes up-regulated in islets from *Mir155*$^{-/-}$*Ldlr*$^{-/-}$ mice was screened for miR-155-5p binding sites using the Targetscan (v7.0) prediction algorithm.[169] According to the prediction, 27 out of the 239 up-regulated genes, including *Mafb,*

semaphorin 5A (*Sema5a)* and mediator complex subunit 12-like (*Med12l),* contained miR-155-5p binding sites (**Table 23**). The miR-155-5p target sites in the *Mafb* and *Sema5a* 3'-UTRs were conserved among species, whereas the other 25 sites were poorly conserved. However, three of the poorly conserved sites were also found in humans, including the site in the AU RNA binding protein/enoyl-coenzyme A hydratase (*Auh)*, stathmin-like 2 (*Stmn2)* and *Med12l* mRNAs (**Table 23**). Moreover, the binding probability ($P_{CT} \geq 0.1$)[120] of the miR-155-5p site in the *Mafb*, *Sema5a*, *Med12l*, *Stmn2* and *Auh* mRNAs was higher than for the other 22 putative targets; therefore, the regulation of these five genes by miR-155-5p was studied.

Gene	**P_{CT}**	**Conservation**
Mafb	0.39	conserved
Sema5a	0.3	conserved
Med12l	0.15	poorly conserved[a]
Stmn2	0.13	poorly conserved[a]
Auh	0.12	poorly conserved[a]
F13a1	< 0.1	poorly conserved[b]
Dhfr	< 0.1	poorly conserved[b]
Klhl42	< 0.1	poorly conserved[b]
Ppp1r9a	< 0.1	poorly conserved[b]
Phf21a	< 0.1	poorly conserved[b]
Rab3c	< 0.1	poorly conserved[b]
Nedd4l	< 0.1	poorly conserved[b]
Homez	< 0.1	rodent-specific
Nrp1	< 0.1	rodent-specific
Pde4d	< 0.1	rodent-specific
Zkscan3	< 0.1	rodent-specific
Zfp14	< 0.1	rodent-specific
Bik	< 0.1	mouse-specific
Camkk2	< 0.1	mouse-specific
Clec1a	< 0.1	mouse-specific
Gpr179	< 0.1	mouse-specific
Htra3	< 0.1	mouse-specific

Myct1	< 0.1	mouse-specific
Scai	< 0.1	mouse-specific
Zfp111	< 0.1	mouse-specific
Zfp937	< 0.1	mouse-specific
Zscan20	< 0.1	mouse-specific

Table 23. Putative miR-155-5p target genes in pancreatic islets. Among the genes significantly upregulated (≥ 1.5-fold and p<0.05) in pancreatic islets of Mir155$^{-/-}$*Ldlr*$^{-/-}$ mice compared to Mir155$^{+/+}$*Ldlr*$^{-/-}$ mice (as determined by global gene expression analysis), miR-155-5p targets and the conservation of the putative miR-155-5p binding sites across species were predicted by Targetscan software (http://www.targetscan.org/). The probability of conserved targeting is indicated by P_{CT}. a: Conserved between human and rodent; b: Seed sequences are different in mouse and human.

3.7.2 Verification of the predicted miR-155-5p targets

To confirm the differential regulation of the predicted targets of miR-155-5p identified by global gene expression, the expression levels of *Mafb*, *Sema5a*, *Med12l*, *Stmn2* and *Auh* were quantified by qPCR in pancreatic islets from ND-fed *Mir155*$^{-/-}$*Ldlr*$^{-/-}$ and *Mir155*$^{+/+}$*Ldlr*$^{-/-}$ mice at 10 – 12 wk of age. All of the potential miR-155-5p targets were up-regulated in islets from *Mir155*$^{-/-}$*Ldlr*$^{-/-}$mice (**Figure 42**).

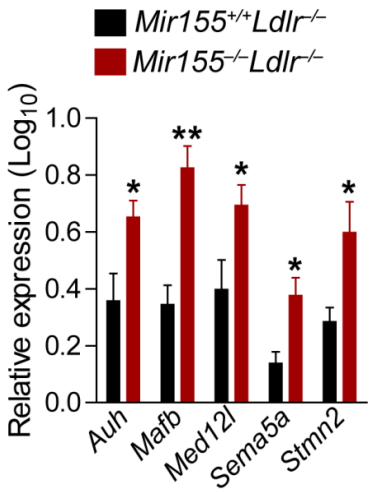

Figure 42. Confirmation of the up-regulation of potential miR-155-5p targets. Quantitation of predicted miR-155-5p target gene expression in islets isolated from ND-fed *Mir155*$^{-/-}$*Ldlr*$^{-/-}$ mice and

Mir155$^{+/+}$*Ldlr*$^{-/-}$ mice (10 – 12 wk of age) by qPCR (n = 6 – 8 per group). Data are represented as mean ± SEM. *p < 0.05and **p < 0.01.

Moreover, the regulation of predicted targets by miR-155-5p was also confirmed in MIN6 cells using gain-and-loss-of-function experiments. Treatment of MIN6 cells with miR-155-5p mimics (**Figure 43A**) and inhibitors (**Figure 43B**) up-regulated and down-regulated *Auh*, *Mafb*, *Med12l*, *Sema5a*, and *Stmn2* expression, respectively.

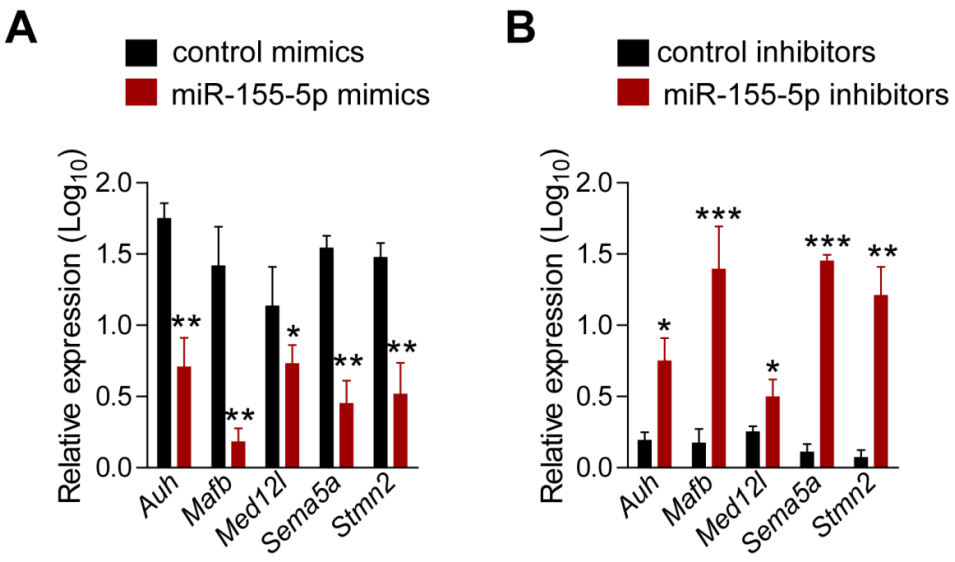

Figure 43. Regulation of predicted miR-155-5p targets in MIN6 cells. (**A** and **B**) Expression of predicted miR-155-5p targets in MIN6 cells after transfection with miR-155-5p mimics (**A,** n = 5 – 6 per group) or miR-155-5p LNA inhibitors (**B,** n = 5 – 6 per group). Non-targeting oligonucleotides were used as control (n = 5 – 6 per group). Data are represented as mean ± SEM. *p < 0.05, **p < 0.01 and ***p < 0.001.

3.7.3 miR-155-5p targets *Mafb* in islets cells

To further study the regulation of potential targets by miR-*155-5p*, immunoprecipitation of the miRISC was performed using extracts from MIN6 cells overexpressing FLAG-tagged GW182[148]. In the positive control group, AcGFP1 (Aequrea coerulescences green fluorescent protein) containing a miR-132 target sequence was expressed in MIN6 cells. Treatment with miR-132 mimics resulted in a 27-fold enrichment of the AcGFP1 mRNA in the miRISC as compared to *Gapdh*. Following miR-155-5p mimics

treatment, the enrichment of *Mafb* (60-fold) in the miRISC was higher than that of *Stmn2* (30-fold), *Auh* (9-fold), *Med12l* (8-fold) or *Sema5a* (15-fold) (**Figure 44**).

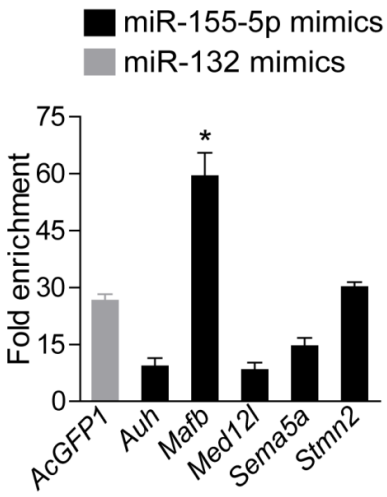

Figure 44. Immunoprecipitation-based miR-155-5p target identification in MIN6 cells. Enrichment of potential miR-155-5p targets in the Argonaute/RISC complexes from MIN6 cells determined by GW182 immunoprecipitation (MirTrap-IP) and qPCR ($n = 3$ per group). The results are expressed as fold enrichment of the transcripts in miR-155-5p mimics treated MIN6 cells compared to those treated with non-targeting, control mimics. The fold enrichment of the *AcGFP1* control in miR-132 mimics treated MIN6 cells was used as positive control. Data are represented as mean ± SEM. *$p < 0.05$.

The transcription factor MafB, a key activator of glucagon transcription, is highly expressed in α-cells.[170,171] Pdx1-mediated repression of MafB is required for maintenance of β-cell identity, and derepression of MafB in β-cell was responsible for glucagon induction and triggers a β-to-α-cell reprogramming.[172] The miR-155-5p binding site in the 3′–UTR of the *MAFB* mRNA has been previously verified in B-cell lymphoma cells (**Figure 45A**),[173] suggesting that MafB may mediate the effect of miR-155 on islets. The expression of MafB in islets from ND-fed *Mir155*$^{+/+}$*Ldlr*$^{-/-}$ and *Mir155*$^{-/-}$*Ldlr*$^{-/-}$ mice was quantified by combined MafB and insulin immunostaining. *Mir155* knockout increased the number of MafB-expressing cells, including β-cells (**Figure 45B**), indicating that miR-155-5p promotes a β-cell phenotype by repressing MafB.

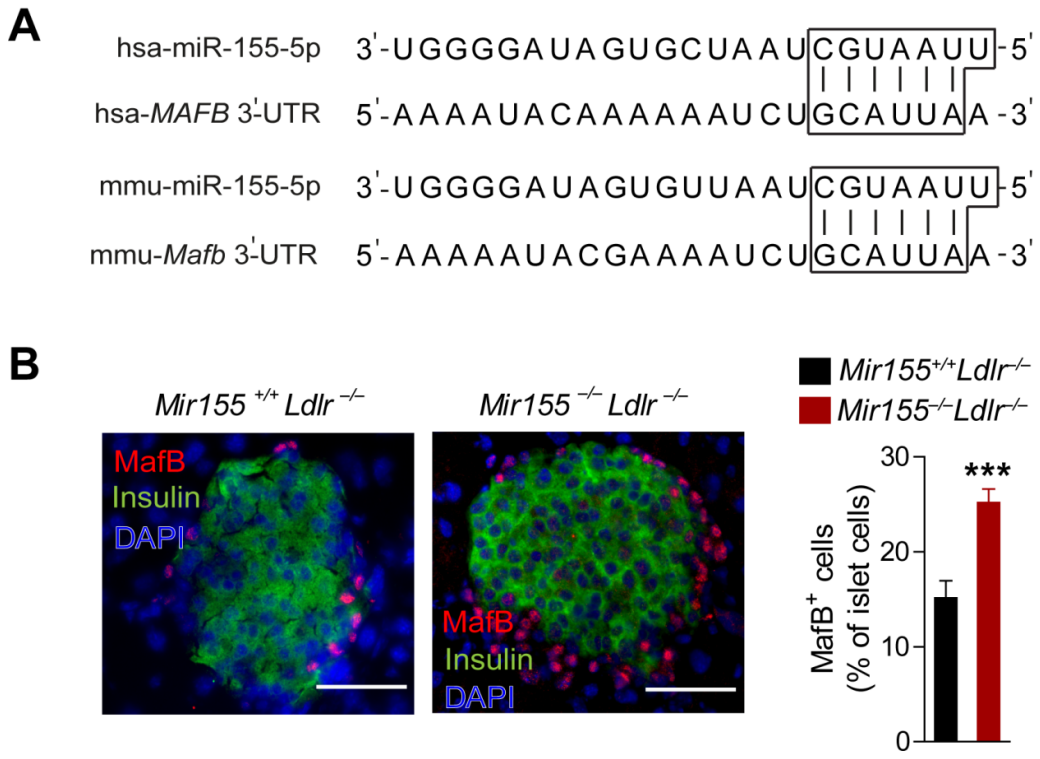

Figure 45. miR-155-5p targets *Mafb* in islets cells. (**A**) Conserved miR-155-5p binding site in the 3′–UTR of the *Mafb* mRNA in human (hsa) and mouse (mmu). The boxes indicate the interaction between miR-155-5p and *Mafb*. (**B**) Quantitation of MafB-producing islet cells from *Mir155*$^{+/+}$*Ldlr*$^{-/-}$ or *Mir155*$^{-/-}$*Ldlr*$^{-/-}$ mice at 10 – 12 wk of age fed a ND by combined MafB and insulin immunostaining (n = 10 mice per group). The nuclei were counterstained with DAPI. Scale bars: 50 μm. Data are represented as mean ± SEM. ***p < 0.001.

Next, to test the function of miR-155-5p binding site in the *Mafb* 3'-UTR, LNA-modified oligonucleotides that selectively inhibit the interaction between miR-155-5p and *Mafb* were designed (*155/Mafb* target site blocker, TSB) (**Figure 46A**). The MIN6 cells were transfected with *155/Mafb* TSB or non-targeting TSBs (control TSB) for 48 h and the expression of the candidate genes was determined by qPCR. Treatment with *155/Mafb* TSBs increased *Mafb, Gcg* and *Pcsk2* expression, and reduced *Ins* and *Pcsk1* expression compared with control TSBs (**Figure 46B**). These data indicate that the effects of miR-155-5p on islet cells are mainly mediated through targeting of *Mafb*.

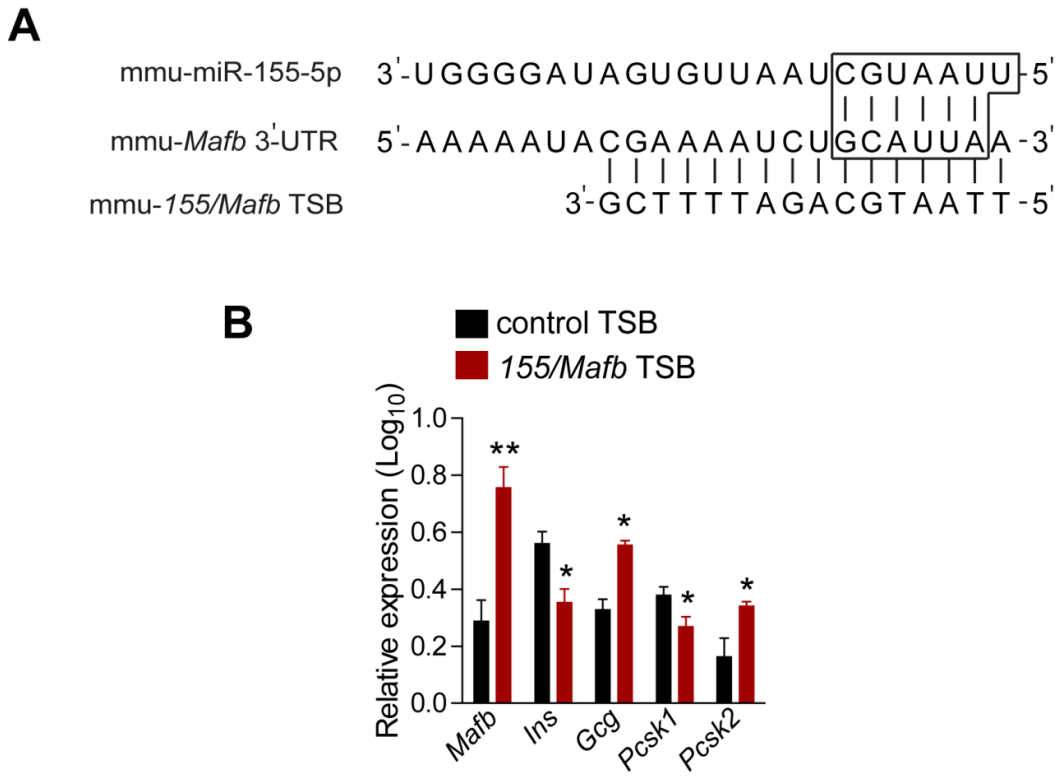

Figure 46. Effects of *155/Mafb* TSB *in vitro*. (**A**) Sequence of the *Mafb*-target site blocker oligonucleotide (*155/Mafb* TSB) complementary to the miR-155-5p binding site and its 5' flanking region in the *Mafb* 3′-UTR. The box indicates the interaction between miR-155-5p and *Mafb*. (**B**) Quantitation of *Mafb, Ins, Gcg, Pcsk1* and *Pcsk2* mRNA expression in MIN6 cells treated with oligonucleotides that block the interaction between miR-155-5p and the 3'-UTR of *Mafb* (target site blocker, *155/Mafb* TSB) or non-targeting TSBs (control TSB) by qPCR (n =5-6 per group). Data are represented as mean ± SEM. *$p < 0.05$ and **$p < 0.01$.

3.8 MafB mediated the effect of miR-155-5p on *Il6* expression

Next, to investigate whether miR-155-5p-induced IL-6 expression in islets is mediated by targeting MafB, IL-6 expression was measured in MIN6 cells treated with *155/Mafb* TSB. Blocking the interaction between miR-155-5p and MafB in MIN6 cells down-regulated *Il6* mRNA expression (**Figure 47, left**) and reduced IL-6 protein secretion (**Figure 47, right**), suggesting that miR-155-5p upregulates *Il-6* expression by targeting *Mafb*.

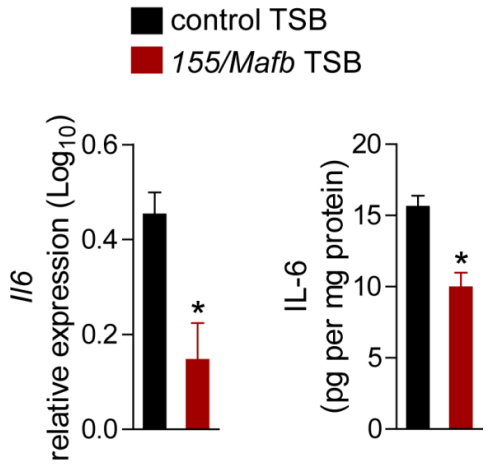

Figure 47. Effects of *155/Mafb* TSB on IL-6 expression *in vitro*. Quantitation of IL-6 expression at the mRNA and protein level in MIN6 cells treated with *155/Mafb* TSB or control TSB by qPCR and ELISA, respectively (n = 5 per group). Data are represented as mean ± SEM. *$p < 0.05$.

Two MafB binding sites were predicted in the *Il6* promoter region using TRANSFAC database (version 7.0, Qiagen, http://www.biobase.international.com) (**Figure 48A**, *Il6* promoter-*Mafb*1 refers to binding sites at position 30012038 and *Il6* promoter-*Mafb*2 refers to binding sites at position 30012038)[149,150].

To study whether MafB negatively regulates *Il6* expression via binding to putative binding sites in the Il6 promoter, MIN6 cells were transfected with a luciferase reporter vector containing the wildtype *Il6* promoter or the *Il6* promoter containing mutations in the predicted *Mafb* binding sites *Mafb1* and *Mafb2* (**Figure 48A**). Treatment with miR-155-5p inhibitors reduced the luciferase activity in cells expressing the wildtype promoter, but not in cells expressing the promoter containing the mutated *Mafb* binding sites (**Figure 48B**). These findings suggest that reduced transcriptional repression of IL-6 by MafB contributes to the effect of miR-155-5p on β-cell function.

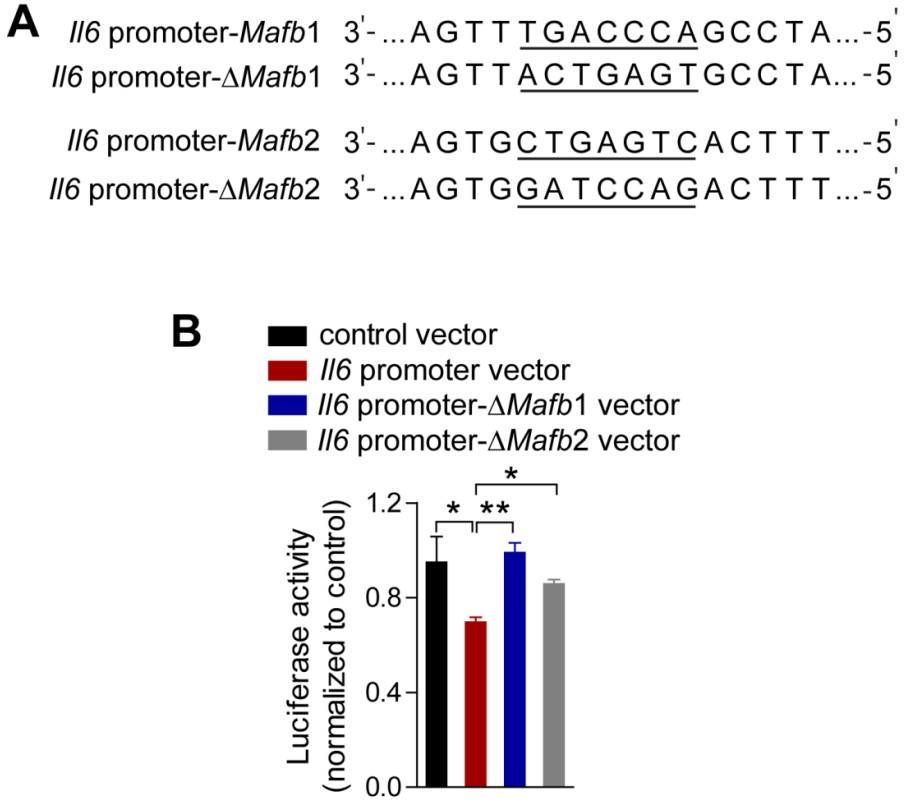

Figure 48. Targeting of MafB by miR-155-5p promotes IL-6 expression. (**A**) Wildtype (*Il6* promoter-*Mafb*1 and *Il6* promoter-*Mafb*2) and mutated (*Il6* promoter-Δ*Mafb*1 and *Il6* promoter-Δ*Mafb*2, underlined) sequences of putative *Mafb* binding sites in the *Il6* promoter region. (**B**) Luciferase activity in MIN6 cells cotransfected with luciferase reporter constructs harboring site-directed mutations in the predicted *Mafb* binding sites of the *Il6* promoter region (*Il6* promoter-Δ*Mafb*1 and *Il6* promoter-Δ*Mafb*2) and miR-155-5p LNA inhibitors or non-targeting LNA oligonucleotides (n = 4 per group). The empty vector was used as control. The luminescence intensities of Gaussia luciferase were normalized to the activity of secreted alkaline phosphatase. Data are represented as mean ± SEM. *p < 0.05, **p < 0.01 and ***p < 0.001.

3.9 *155/Mafb* TSB effects *in vivo*

To study whether the effect of hyperlipidemia-induced miR-155-5p in β-cells on glucose homeostasis is mediated by the suppression of *Mafb*, 10-wk-old *Ldlr*$^{-/-}$ mice fed a ND were treated with a single injection of *155/Mafb* TSBs or control TSBs (each 0.4 mg/20 g per injection, sequences were shown in **Figure 46A**). Body weights (**Figure 49A**) and differential blood counts (**Figure 49B**) were not different between the groups at 21 d after the treatment.

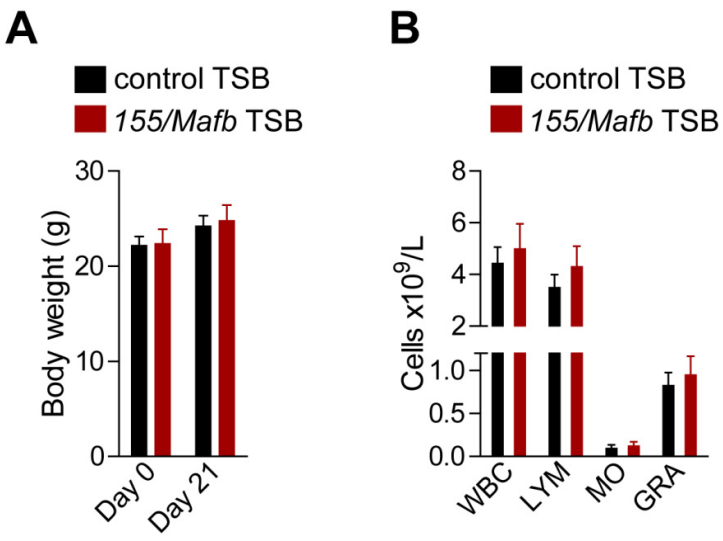

Figure 49. Effects of *155/Mafb* TSB on body weight and blood cell numbers in *Ldlr*$^{-/-}$ mice. (**A**) Body weight of *Ldlr*$^{-/-}$ mice before (Day 0) and 21 d (Day 21) after treatment with *155/Mafb* TSBs or control TSBs (n = 7 mice per group). (**B**) White blood cell (WBC), lymphocyte (LYM), monocyte (MO) and granulocyte (GRA) count in the blood of *Ldlr*$^{-/-}$ mice 21 d after injection of *155/Mafb* TSBs or control TSBs (n = 7 mice per group). Data are represented as mean ± SEM.

To assess whether the effect of the interaction between miR-155 and *Mafb* is specific in islets, tissues were harvested 21 d after injection of the TSBs. *Mafb* mRNA expression levels were increased in islets and spleen, but not in heart, liver and eWAT in *155/Mafb* TSB-treated mice (**Figure 50A**). *155/Mafb* TSB treatment did not affect islet *Auh*, *Med12l*, *Sema5a* and *Stmn2* expression levels (**Figure 50B**). Moreover, the protein level of MafB was determined in islets by combined MafB and insulin immunostaining. The percentage of MafB-expressing islet cells was higher in *155/Mafb* TSB-treated mice than in mice treated with control TSBs (**Figure 50C**), indicating that *155/Mafb* TSB specifically derepressed MafB in islets.

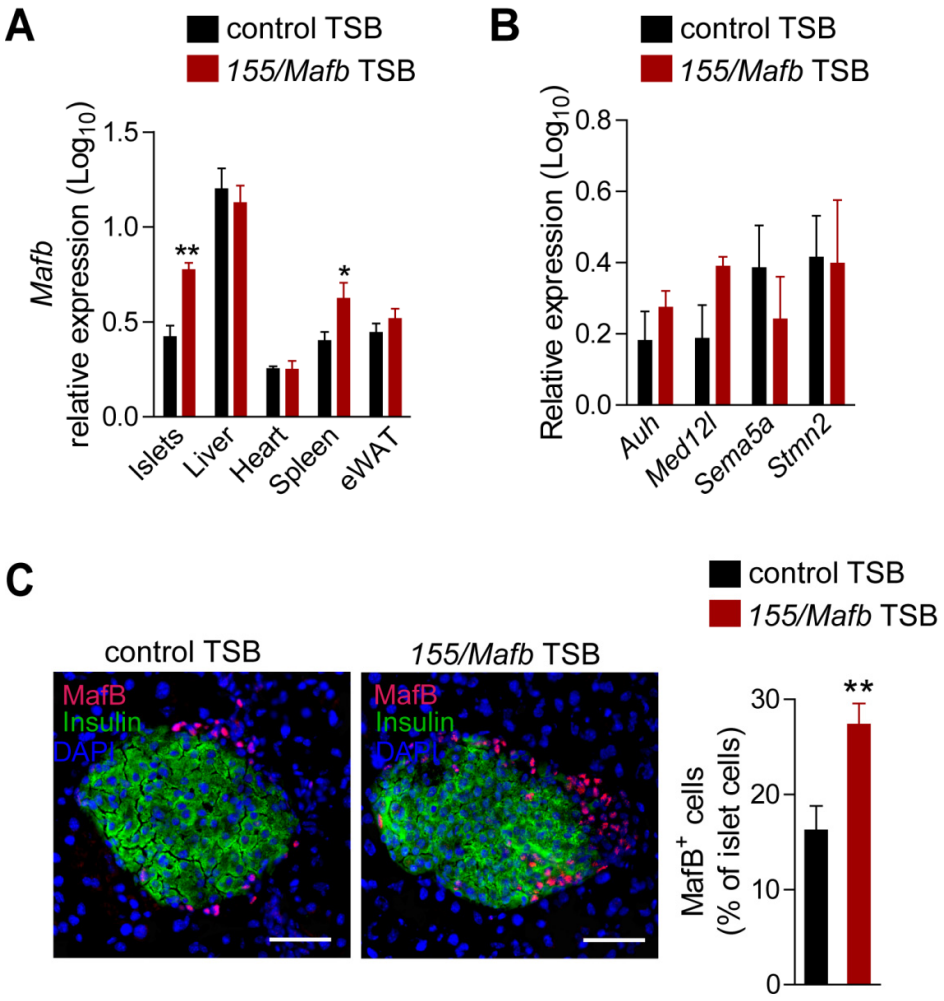

Figure 50. Effects of *155/Mafb* TSB on the expression of predicted targets of miR-155-5p in *Ldlr*$^{-/-}$ mice. (A) Quantitation of *Mafb* mRNA expression by qPCR in various tissues of ND-fed mice 21 d after the injection of *155/Mafb* TSBs or control TSBs (n = 4 per group). (**B**) Quantitation of MafB-expressing cells in murine islets 21 d after the injection of *155/Mafb* TSBs or control TSBs by combined MafB and insulin immunostaining (n = 6 or 7 mice per group). The nuclei were counterstained with DAPI. Scale bars: 50 µm. (**C**) Quantitation of putative miR-155-5p targets genes by qPCR in islets from *Ldlr*$^{-/-}$ mice 21 d after treatment with 155/Mafb TSBs or control TSBs (n = 4 per group). Data are represented as mean ± SEM. *$p < 0.05$ and **$p < 0.01$.

To further study the effect of the miR-155-5p-*Mafb* interaction on islets of *Ldlr*$^{-/-}$ mice, the expression of the candidate genes was assessed by qPCR. Blocking the interaction between miR-155-5p and *Mafb* up-regulated *Gcg* mRNA expression and down-regulated *Pcsk1* and *Il6* expression in islets (**Figure 51A**). Consistently, treatment with *155/Mafb* TSBs increased the percentage of α-cells, and reduced the percentage of

β-cells compared with control, determined by combined insulin and glucagon immunostaining (**Figure 51B**). This effect in *155/Mafb* TSB-treated mice was associated with reduced insulin and GLP-1 plasma levels, and increased glucagon plasma levels (**Figure 51C**), measured by Luminex assays.

Moreover, FBG levels and glucose tolerance were measured 21 d after injection of the TSBs. Blocking the interaction between miR-155 and *Mafb* elevated FBG levels (**Figure D**) and impaired glucose tolerance following intraperitoneal glucose injection (**Figure F**). This data indicates that hyperlipidemia-induced miR-155-5p expression improves β-cell adaptation and maintains glucose homeostasis by suppressing *Mafb*.

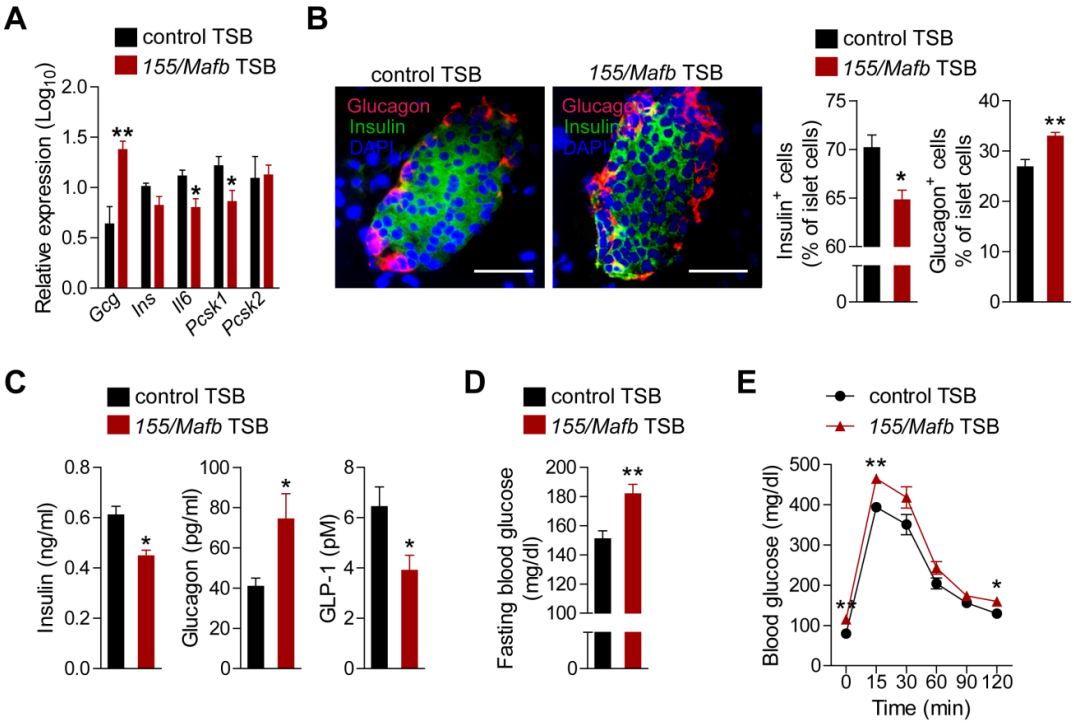

Figure 51. Effect of the interaction between miR-155-5p and *Mafb* on glucose homeostasis in *Ldlr*$^{-/-}$ mice. (**A**) Quantitation of gene expression by qPCR in islets isolated from ND-fed mice 21 d after injection of *155/Mafb* TSBs or control TSBs (n = 4 per group). (**B**) Quantitation of insulin- and glucagon-producing cells in islets from ND-fed mice 21 d after injection of *155/Mafb* TSBs or control TSBs by immunostaining (n = 6 or 7 mice per group). The nuclei were counterstained with DAPI. Scale bars: 50 μm. (**C**) Fasting insulin, glucagon, GLP-1 plasma concentrations by Luminex multiplex analysis in ND-fed mice 21 d after treatment with *155/Mafb* TSBs or control TSBs (n = 7 mice per group). (**D** and **E**) FBG levels (**D**) and glucose tolerance (**E**) in ND-fed mice 21 d after injection of *155/Mafb* TSBs or control TSBs (n = 7 mice per group)**.** Data are represented as mean ± SEM. *p < 0.05 and **p < 0.01.

4 DISCUSSION

4.1 Hyperlipidemia induces islet miR-155-5p expression

miRNAs, such as miR-375 and miR-184, play crucial roles in β-cell function and the adaptation of β-cells to insulin resistance.[174] Although miR-155-5p expression is low in normal islets compared to islet-enriched miRNAs,[175] increasing blood lipid levels by knocking out *Ldlr* in ND-fed mice upregulated islet miR-155-5p expression. More severe hyperlipidemia in *Ldlr*$^{-/-}$ mice fed the DDC was positively correlated with miR-155 expression levels in islets. In contrast to normolipidemic wildtype mice, knocking out Mir155 in hyperlipidemic *Ldlr*$^{-/-}$ and *Apoe*$^{-/-}$ mice improved glucose tolerance, indicating that hyperlipidemia-mediated miR-155 expression enhances islet cell function. In macrophages, hyperlipidemia also up-regulates miR-155-5p expression and enhances TLR4-dependent inflammatory activation.[104,129,176] Notably, absence of miR-155-5p expression in lean and obese *Ldlr*$^{-/-}$ mice deteriorated glucose homeostasis, and reduced insulin and enhanced glucagon production and secretion by islet cells. Insulin and glucagon are critical regulators for maintaining glucose homeostasis.[177,178] In addition to impaired or insufficient insulin secretion,[179] increased glucagon-to-insulin ratio are frequently observed in diabetic individuals and chronic hyperglucagonemia is correlated with hyperglycemia in T2DM.[180-182] Hence, *Mir155* knockout may lead to elevated plasma glucose levels in *Ldlr*$^{-/-}$ mice due to its effects on insulin and glucagon production in islets. Although chronic HFD feeding results in obesity and insulin-resistance, the short-term effects of HFD feeding include enhanced β-cell proliferation and hyperinsulinemia.[183,184] However, the role of hyperlipidemia independent of a HFD on glucose homeostasis is unclear. The results of the current study suggest that upregulation of islet miR-155 expression contributes to the effect of hyperlipidemia on insulin secretion.

4.2 miR-155-5p increases intra-islet GLP-1

The main mechanisms of β-cell failure in DM development involve dedifferentiation and impaired regeneration of β-cells.[10,18] Lineage-tracing studies in mice showed that metabolic stress-induced loss of β-cells is due to their dedifferentiation into stem/progenitor-like cells, which are devoid of the insulin-producing β-cell identity.[18] Of note, a subset of the dedifferentiated cells acquire features of α-cells that express the *Gcg* gene and increase the pancreatic α-cell mass, which results in elevated plasma glucagon levels and pancreatic glucagon content in mice.[18] In accordance with these results, *Mir155* knockout did not only increase plasma and glucagon levels but also reduced insulin expression, indicating that miR-155-5p in β-cells limits β- to α-cell conversion.

In addition to its effect on insulin and glucagon production, plasma and islet GLP-1 levels were reduced in *Mir155*$^{-/-}$*Ldlr*$^{-/-}$ mice. GLP-1 triggers glucose-dependent insulin secretion, suppresses glucagon secretion, increases insulin synthesis, promotes β-cell growth and neogenesis, and inhibits β-cell apoptosis.[41,45,50-53] β-cell-specific *Glp1r* knockout results in β-cell dysfunction and impaired intraperitoneal glucose tolerance in response to parenteral GLP-1 administration,[54] and selective restoration of the GLP-1R expression in the pancreas of *Glp1r*$^{-/-}$ mice promotes β-cell mass expansion and improves glucose tolerance.[55] In contrast to the important role of GLP-1R in β-cells, GLP-1 is predominantly expressed in a-cells in response to lipotoxic stress and hyperglycemia via upregulation of *Pcsk1* expression.[35,38,165,185] Because miR-155-5p upregulated *Pcsk1* in islet cells, enhanced GLP-1 production in a-cells may contribute to the effect of miR-155-5p on glucose homeostasis by stimulating insulin and reducing glucagon secretion.[45,50] Moreover, miR-155-5p reduced *Pcsk2* expression and thus switched the processing of proglucagon in α-cells from glucagon to GLP-1 production in response to hyperlipidemic stress. Although intestinal L-cells are the main source of circulating GLP-1 after oral glucose ingestion, the source of basal GLP-1 levels in the circulation is unknown. However, increased insulin levels can induce GLP-1 secretion from intestinal L-cells, suggesting that miR-155-5p may increase circulating GLP-1 levels by islet GLP-1-triggered insulin secretion.[186]

Although crucial roles of miR-155-5p in immune responses have been described previously,[103,121,154,155] the accumulation of immune cells (macrophages or T-cells) was negligible in islets of ND-fed mice, suggesting the inflammatory response is not, or at least not the primary effect of miR-155-5p on islets function.

4.3 Hyperlipidemia-related endotoxemia induces islet miR-155-5p expression

In addition to hyperlipidemia, LPS-induced TLR4 activation selectively increases miR-155-5p expression in macrophages. Low levels of LPS are physiologically present in the blood of humans and animals.[91] HFD feeding modulates the gut microbiota and increases intestinal permeability, which elevates LPS plasma concentrations.[71,72] In line with these results, LPS also increased miR-155-5p expression in murine pancreatic β-cells in vitro and in vivo. LPS predominantly binds to LDL in the circulation, which reduces its biological activity and promotes endotoxin removal.[135,187-191] The data of the current study show that mild oxidation increases the endotoxin activity of LDL, maybe by altering lipid-mediated interactions between LDL and LPS. Accordingly, treatment with moxLDL but not with nLDL upregulated miR-155-5p expression in β-cells. Moreover, hyperlipidemia in *Ldlr*$^{-/-}$ mice was accompanied by elevated serum endotoxin activity and by the deposition of oxLDL in islets. Taking together, these results indicate that hyperlipidemia results in the deposition of moxLDL in islets, which induces miR-155-5p expression in β-cells by its endotoxin activity.

Low-dose LPS injection reduces blood glucose levels by promoting GLP-1-mediated insulin secretion in C57/BL6 mice.[75] Similarly, the current study showed that treatment with low-dose LPS increased islet miR-155-5p expression and promoted GLP-1-induced insulin secretion in *Ldlr*$^{-/-}$ mice. Knockout of *Mir155* blunted the effect of LPS on glucose metabolism in *Ldlr*$^{-/-}$ mice, indicating that β-cell miR-155-5p contributes to LPS-induced insulin secretion.

4.4 IL-6 mediates the effect of miR-155-5p on GLP-1

Islet-derived GLP-1 is processed and secreted exclusively from rodent and human glucagon-containing α-cells;[192,193] however, induction of islet miR-155-5p expression by hyperlipidemia was mainly detectable in glucagon negative cells, indicating that miR-155-5p induces GLP-1 production in a paracrine manner. Of note, IL-6 is a key stimulator of GLP-1 production in a-cells, which highly express the IL-6 receptor, by upregulating Pcsk1 expression,[47,164] and thereby promotes insulin secretion and β-cell function.[34,35,47] Accordingly, the microarray results indicate that islet miR-155-5p expression activates IL-6 receptor signaling pathways, such as the JAK/STAT and ERK1/2 pathways, in the islets of *Ldlr*$^{-/-}$ mice. IL-6 is physiologically expressed in rodent pancreatic β-cells[163] and up-regulated upon stimulation of inflammatory cytokines,[163,194] which may protect pancreatic islets from inflammation-induced cell death and functional impairment.[195] The results of present study demonstrate that miR-155-5p positively regulated IL-6 expression and secretion in β-cells, which is similar to the effect observed in immune cells, such as macrophages, T-cells and dendritic cells.[102,129,152,166-168] Blocking IL-6 secreted from islet MIN6 cells increased *Pcsk1* expression and reduced *Pcsk2* expression, suggesting that miR-155-5p-induced IL-6 secretion from β-cells switches processing of proglucagon to GLP-1 in α-cells. Thus, hyperlipidemia-induced miR-155-5p may act as an upstream regulator of the IL-6/Pcsk1/GLP-1 pathway in islets that mediates the mutual crosstalk between α-cells and β-cells and improves β-cell adaptation to stress. However, the mechanism by which miR-155-5p regulates IL-6 expression is not clear.

4.5 MafB mediates the effects of miR-155-5p in islets

To determine the mechanism by which miR-155-5p regulates IL-6 expression in β-cells, a genome-wide expression analysis in murine islets was performed. Notably, 27 potential targets of miR-155-5p, including *Mafb* and *Sema5a,* were upregulated in islets from *Mir155* knockout mice. In contrast to the other 25 putative miR-155-5p targets, *Mafb* and *Sema5a* contain highly conserved miR-155-5p target sites in their 3'-UTRs, indicating that both may be targeted by miR-155-5p in islets. Whereas the miR-155-5p canonical 7-merA1 binding site in the *Mafb* 3'-UTR has been validated experimentally,

the target site in the *Sema5a* 3'-UTR has not been studied yet.[173] Accordingly, miR-155-5p enriched *Mafb* and *Sema5a* in the RISC, demonstrating that both are targets of miR-155-5p in islet cells. However, MafB may be the primary target of miR-155-5p, because the enrichment of *Mafb* was much higher than that of *Sema5a*. Hence, the effect of the interaction between miR-155-5p and *Mafb* was studied using *155/Mafb* TSBs. Importantly, *155/Mafb* TSBs strongly increased *Mafb* expression and led to similar alterations in islet gene expression as those of the miR-155-5p inhibitor treatment, indicating that targeting of *Mafb* plays a key role in the effects of miR-155-5p on islets function.

The members of the large Maf protein transcription factor family, MafA and MafB, play critical roles in the development and function of α- and β- cells. In adult rodent islets, MafA is only expressed in β-cells and promotes transcription of the insulin gene,[170,196-199] whereas MafB is primarily expressed in α-cells and activates the transcription of the *Gcg* gene.[197 200] In pregnant or obese mice, however, MafB expression is up-regulated in β-cell.[201] Notably, previous studies show that repression of MafB is required for maintenance of β-cell identity, because de-repression of MafB in the absence of the β-cell-specific transcription factor Pdx1 triggers a β-to-α-cell reprogramming[199] and thereby contributes to β-cell failure in T2DM.[172,202,203] In line with these evidences, the current data of the *Mir155*$^{-/-}$ mice show that hyperlipidemia-induced expression of miR-155-5p in β-cells limits *Mafb* expression, and maintains a β-cell phenotype as indicated by reduced α-cell-specific gene transcription in islets, and decreased plasma and islet glucagon levels. Accordingly, blocking the interaction between miR-155-5p and *Mafb* in hyperlipidemic mice increased *Gcg* transcription and the α-to-β-cell ratio, suggesting that the effect of miR-155-5p in islet function is due to the targeting of *Mafb*. Although the knockout of *Mir155* in *Ldlr*$^{-/-}$ mice is not islet cell specific and thus miR-155-5p may indirectly regulate islet *Mafb* expression, the finding that *155/Mafb* TSB treatment increased *Mafb* expression in islets demonstrates that miR-155 targets *Mafb* in islets. Taken together, these data indicate that hyperlipidemia-induced miR-155-5p expression maintains β-cell identity and improves β-cell adaptation by targeting *Mafb*.

In addition, blocking the interaction between miR-155-5p and *Mafb* in β-cells inhibited IL-6 expression, indicating that miR-155-5p upregulates IL-6 in β-cells by targeting MafB. As a member of the large Maf transcription family, MafB contains the basic leucine zipper (bZIP) DNA binding motifs and N-terminal activation domains.[204] In addition to serving as a key activator of the *Gcg* gene in α-cells,[197] MafB can acts as a repressor that inhibits gene transcription in myeloid cells,[205 206] osteoclasts[207] and human β-cells.[206] However, the role of MafB in the regulation of IL-6 expression was unclear, although two MafB binding sites were predicted in the *Il6* promoter region. The current study shows that miR-155-5p upregulates IL-6 by targeting *Mafb*, which transcriptionally inhibits *Il6* gene expression in β-cells. Consistent with the effect observed in *Mir155* knockout mice, inhibiting the interaction between miR-155-5p and *Mafb* in hyperlipidemic mice down-regulated the IL-6/Pcsk1/GLP-1 pathway in islets. Thus, reduced transcriptional repression of IL-6 by MafB contributes to the effect of miR-155-5p on β-cell function.

Taken together, the current data demostrate that hyperlipidemia-induced miR-155-5p maintains a β-cell phenotype and inhibits *Gcg* expression primarily by targeting *Mafb* in β-cells. In addition, my findings strongly suggest that targeting of *Mafb* by miR-155-5p promotes PC1/3-mediated GLP-1 production in α-cells due to enhanced secretion of IL-6 from β-cells. Thus, hyperlipidemia-induced miR-155-5p/MafB/IL-6 axis mediates a crosstalk between α-cells and β-cells, which may improve β-cell adaptation to obesity-related insulin resistance by up-regulating GLP-1 production (**Figure 52**).

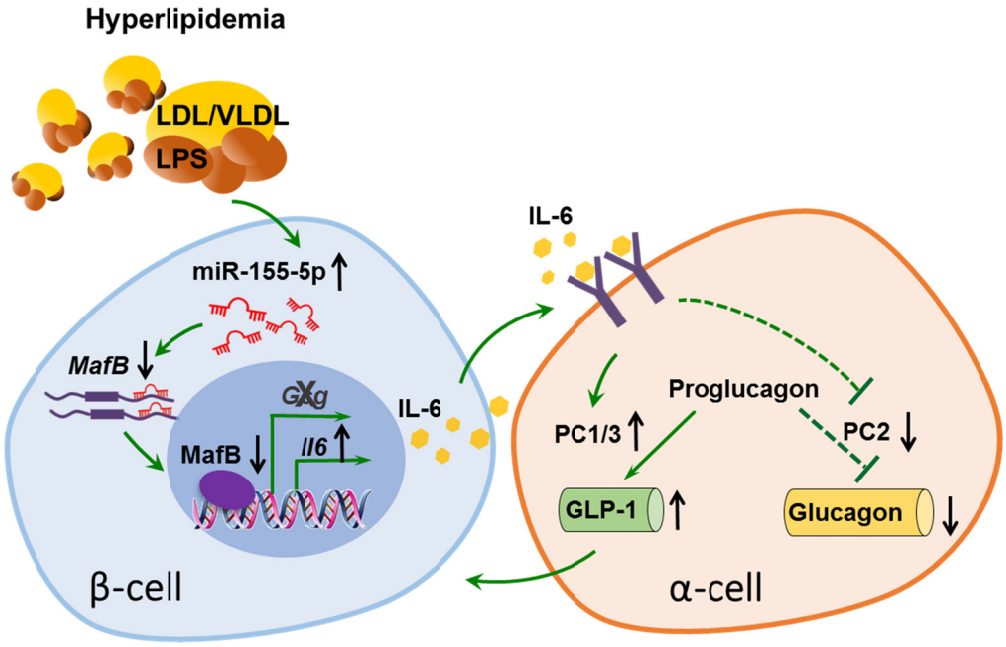

Figure 52. The role of miR-155-5p in islet function. Induction of miR-155-5p expression in β-cells by hyperlipidemia-associated endotoxemia promotes a β-cell phenotype by targeting the transcription factor Mafb, which results in de-repression of IL-6 gene transcription and increased production of GLP-1in α-cells.

4.6 miR-155-5p and the MetS: potential role of GLP-1

4.6.1 MetS

MetS is highly prevalent and strongly associated with T2DM, cardiovascular diseases and all-cause mortality.[13-15] However, the contribution of miR-155-5p to MetS-related disease conditions, such as central obesity, atherosclerosis dyslipidemia and insulin resistance is completely unclear.

Adipose tissue inflammation due to the accumulation of proinflammatory macrophages and adipocyte dysfunction characterized by enhanced leptin and TNF-a secretion play key roles in the progression of obesity and insulin resistance in the MetS.[208,209] To investigate the effect of miR-155-5p on obesity in the MetS, *Mir155*$^{-/-}$ *Ldlr*$^{-/-}$ mice were fed a DDC in the current study. Notably, *Mir155* knockout increased the progression of obesity and the accumulation of adipose tissue macrophages in *Ldlr*$^{-/-}$ mice, suggesting a protective role of miR-155-5p in the MetS. In line with these

results, *Mir155* knockout promotes obesity and increases white adipocyte hypertrophy in *Apoe*$^{-/-}$ mice.[210] Hence, although miR-155-5p is essential in the proinflammatory response in macrophages, which promotes obesity, the current findings do not indicate that macrophage miR-155-5p contributes to adipose tissue inflammation and obesity. This conclusion is supported by the finding that *Mir155* knockout did not change the macrophage polarization in adipose tissue of *Ldlr*$^{-/-}$. In contrast to the findings in *Ldlr*$^{-/-}$ and *Apoe*$^{-/-}$ mice, *Mir155* knockout reduces adipose tissue inflammation and prevents HFD-induced obesity in female C57/Bl6 mice.[131] This effect has mainly been attributed to enhanced adipose tissue browning by miR-155-5p expressed in adipocytes.[132] However, *Mir155* deficiency aggravated eWAT dysfunction including adipocyte hypertrophy, increased leptin and reduced adiponectin secretion in obese *Ldlr*$^{-/-}$ mice. This effect of Mir155 knockout is probably not mediated by miR-155-5p in adipocytes, because miR-155-5p promotes adipocytes dysfunction and inhibits adipogenesis[130].

The effect of *Mir155* knockout on atherosclerosis has been studied in different mouse models. In *ApoE*$^{-/-}$ mice, miR-155-5p is selectively induced in proinflammatory macrophages, which increases advanced atherosclerosis by impairing efferocytosis and promoting inflammatory activation, but reduces early lesion formation through inhibition of macrophage proliferation.[103,104,122,126-129] By contrast, the data of current study demonstrate that miR-155-5p limits advanced atherosclerosis and necrotic core formation in obese *Ldlr*$^{-/-}$ mice, although lesional macrophage accumulation was increased *Mir155*$^{+/+}$*Ldlr*$^{-/-}$ mice. Hence, the phenotype observed in obese *Ldlr*$^{-/-}$ mice is unlikely due to the role of miR-155-5p in macrophages. Compared with *Ldlr*$^{-/-}$ mice, *Apoe*$^{-/-}$ mice develop significantly less obesity, adipose tissue inflammation and insulin resistance during HFD feeding. This difference in the metabolic response may affect the mechanisms of plaque formation. Whereas atherosclerosis in *ApoE*$^{-/-}$ mice may be primarily driven by lesional macrophages, lesion formation in *Ldlr*$^{-/-}$ mice may be enhanced by obesity and insulin resistance. Accordingly, in contrast to *Mir155*$^{-/-}$*Apoe*$^{-/-}$ mice,[103,126] *Mir155*$^{-/-}$*Ldlr*$^{-/-}$ mice developed various metabolic imbalances, such as more severe adipose tissue inflammation, obesity and dyslipidemia, in the late stage of DDC feeding, which may in turn influence the atherosclerotic lesion formation. Together, the effects of miR-155-5p may differ in *Apoe*$^{-/-}$ mice and *Ldlr*$^{-/-}$ mice

probably owing to cell-type specific effects of this miRNA and the differences in metabolic status between the mouse models.

4.6.2 GLP-1

Whereas glucose homeostasis was impaired in lean and obese *Mir155*$^{-/-}$*Ldlr*$^{-/-}$ mice, *Mir155* knockout increased body weights only in obese mice, suggesting that the effects of miR-155-5p on islets implicate reduced weight gain. Notably, in addition to reduced intra-islet GLP-1 expression, *Mir155* knockout decreased plasma GLP-1 levels in *Ldlr*$^{-/-}$ mice. GLP-1 receptor agonists and overexpression of GLP-1 reduce obesity in humans and adipose tissue inflammation in mice, respectively.[211,212] By contrast, GLP-1 effect is impaired in obesity and postprandial GLP-1 secretion was found to be inversely proportional to body mass index.[24,25,213-219] Moreover, treatment with GLP-1 receptor agonists improves obesity-related dyslipidemia, probably by inhibiting hepatic VLDL production.[211,220] Therefore, reduced GLP-1 plasma levels may contribute to adipose tissue inflammation, obesity progression and dyslipidemia in *Mir155*$^{-/-}$*Ldlr*$^{-/-}$ mice. Consequently, elevated LDL and VLDL levels can promote the progression of atherosclerosis in obese *Mir155*$^{-/-}$*Ldlr*$^{-/-}$ mice. By contrast, *Mir155* knockout in mice with normal lipoprotein levels did not affect glucose tolerance, presumably due to the low islet miR-155-5p expression level in these mice.[131] Thus, the effect of miR-155-5p on obesity differs between mice with normal lipid levels and hyperlipidemia, likely because different cell types are affected.

In addition to adiposity and dyslipidemia, the anti-atherosclerotic effect of GLP-1 may also exert directly through GLP-1R signaling in relevant cells, such as endothelial cells, vascular smooth muscle cells, macrophages and monocytes.[221-224] A study described that GLP-1R agonists attenuate endoplasmic reticulum stress-induced cell death in aortic lesion macrophages;[225] partially supporting the present data that miR-155-5p has a protective effect against atherosclerosis in obese *Ldlr*$^{-/-}$ mice, which was associated with reduced necrotic core area.

Taken together, the present study indicates that in the *Ldlr*$^{-/-}$ mouse model, the effect of miR-155-5p in β-cells determines the outcome of HFD feeding. miR-155-5p limited the progression of obesity and adipose tissue inflammation, and reduced

hyperlipidemia and atherosclerosis in DDC-fed *Ldlr*$^{-/-}$ mice, probably due to elevated plasma GLP-1 levels.

4.7 Conclusion and Perspective

In conclusion, the results of current study showed that hyperlipidemia and LPS up-regulate miR-155-5p expression in β-cells, which improved glucose homeostasis by targeting *Mafb* and limited a β-to-α-cell reprogramming. In the absence of miR-155-5p, up-regulation of MafB by hyperlipidemia repressed IL-6 expression and thereby inhibited IL-6-mediated GLP-1 production in α-cells. In obese mice, miR-155-5p-induced GLP-1 production may limit atherosclerosis, dyslipidemia, and the progression of adiposity, and improve the adaptation of β-cells to insulin resistance. Hence, up-regulation of miR-155-5p represents a protective mechanism in the stress response of β-cells and improves the adaptation of β-cells to insulin resistance.

Similar to *Ldlr*$^{-/-}$ mice, hyperlipidemia in patients with familial hypercholesterolemia, which occurs due to mutations in the *Ldlr* gene,[226] protects from T2DM and obesity,[97] indicating that hyperlipidemia plays a so far undetermined metabolic role that might improve glucose metabolism. The data of current study strongly indicate that β-cell miR-155-5p may play a crucial role in mediating the effect of hyperlipidemia on obesity and glucose metabolism. Because heterozygote familial hypercholesterolemia is a rather common disease (the prevalence has been estimated at 1 in 200 to 1 in 500),[227] the findings regarding the role of hyperlipidemia in metabolic disease are highly relevant.

5 SUMMARY

A HFD increases intestinal permeability and promotes leakage of LPS into the circulation, where it primarily binds to lipoproteins and may promote GLP-1-mediated insulin secretion. Notably, patients with familial hypercholesterolemia have a reduced risk for T2DM. However, chronically elevated circulating LPS levels during HFD feeding also induce adipose tissue inflammation and obesity-induced insulin resistance. In macrophages, LPS and hyperlipidemia selectively induce miR-155-5p expression and trigger inflammatory activation. However, the role of miR-155-5p in obesity-related metabolic and cardiovascular diseases is poorly understood. Therefore, the aim of the current study was to determine whether miR-155-5p mediates the effects of hyperlipidemia on obesity and glucose homeostasis.

Hyperlipidemia-associated endotoxemia increased deposition of oxLDL and induced miR-155-5p expression in pancreatic islets of *Ldlr*$^{-/-}$ mice. Mild oxidative modification of LDL led to increased endotoxin activity and increased miR-155-5p expression in pancreatic β-cells. In *Mir155*$^{-/-}$*Ldlr*$^{-/-}$mice, glucose and plasma glucagon levels were increased, whereas plasma insulin and GLP-1 levels were reduced compared with Mir155$^{+/+}$*Ldlr*$^{-/-}$ mice. The α-to-β-cell ratio and the glucagon protein level were higher, whereas the insulin and GLP-1 protein content was reduced in islets from *Mir155*$^{-/-}$*Ldlr*$^{-/-}$mice. Treatment with low-dose LPS up-regulated islet miR-155-5p expression, increased insulin and GLP-1 plasma levels and lowered the glucose levels following intraperitoneal glucose injection in *Ldlr*$^{-/-}$ mice, and the effects of LPS on glucose metabolism were partially abolished by *Mir155* knockout. Microarray analysis revealed inhibition of insulin, GLP-1, and IL-6 signaling pathways and upregulation of putative miR-155 targets, including *Mafb*, *Sema5a, Med12l, Auh*, *and Stmn2* in islets from *Mir155*$^{-/-}$*Ldlr*$^{-/-}$mice. In murine β-cells, overexpression of miR-155-5p enriched *Mafb* mRNA in the RISC. Moreover, luciferase reporter assays showed that MafB suppressed *Il6* expression by binding to the *Il6* promoter region. In *Ldlr*$^{-/-}$ mice, blocking the interaction between miR-155-5p and MafB increased FBG levels and decreased the expression of *Il6,* the GLP-1 producing enzyme *Pcsk1*, and insulin production in islets. Probably due to elevated plasma GLP-1 levels, miR-155-5p limited

the progression of obesity and adipose tissue inflammation, and reduced hyperlipidemia and atherosclerosis in HFD-fed *Ldlr*$^{-/-}$ mice.

Taken together, hyperlipidemia-associated endotoxemia can improve glucose homeostasis by upregulating miR-155-5p expression in pancreatic β-cells. Targeting of MafB by miR-155-5p may limit β-to-α-cell reprogramming and promotes β-cell function likely through IL-6-induced GLP-1 production in α-cells. Hence, hyperlipidemia-induced miR-155-5p improves the adaptation of β-cells to insulin resistance. Increasing miR-155-5p levels in β-cell may be a valuable therapeutic strategy against diabetes and the MetS.

6 ZUSAMMENFASSUNG

Die Verfütterung eines „high fat“ Futters führt zu einer erhöhten Darmpermeabilität, die zu einer Steigerung der LPS Konzentration in der Zirkulation führt. Dort bindet LPS an Lipoproteine und stimuliert dadurch die GLP-1-vermittelte Sekretion von Insulin. Patienten mit familiären Hypercholesterinämie leiden seltener an T2DM. Die durch das „high fat“ Futter chronisch erhöhte LPS Konzentration in der Zirkulation induziert die Entzündung im adipösen Gewebe und die Adipositas-bedingte Insulinresistenz. LPS und Hyperlipidämie induzieren die Expression von miR-155-5p und rufen eine inflammatorische Aktivierung in Makrophagen hervor. Allerdings ist über die Rolle von miR-155-5p in mit Adipositas verbundenen metabolischen und kardiovaskulären Erkrankungen wenig bekannt. Das Ziel dieses Vorhabens ist die Effekte von miR-155-5p in Hyperlipidämie-vermittelter Adipositas und Glukose-Homöostase zu untersuchen.

Die Hyperlipidämie-assoziierte Endotoxämie erhöhte die Akkumulation von oxLDL und die Expression von miR-155-5p in den Langerhans-Inseln von *Ldlr*$^{-/-}$ Mäusen. Während die Glukose- und Glukagon Plasmawerte verglichen mit den Werten in Mir155$^{+/+}$*Ldlr*$^{-/-}$ Mäusen erhöht waren, wurde eine Reduktion der Insulin- und GLP-1 Plasmawerte in *Mir155*$^{-/-}$*Ldlr*$^{-/-}$ Mäusen detektiert. Das Verhältnis von α-zu-β Zellen und die Glukagon-Proteinwerte waren erhöht, wohingegen die Insulin- und GLP-1 Proteinwerte in den Langerhans-Inseln der *Mir155*$^{-/-}$*Ldlr*$^{-/-}$ Mäusen reduziert waren. Eine Behandlung mit niedrig dosiertem LPS erhöhte die Expression von miR-155-5p, steigerte die Insulin- und die GLP-1 Plasmawerte, reduzierte jedoch die Glukosewerte nach einer intraperitonealen Glukose-Injektion in *Ldlr*$^{-/-}$ Mäusen. Ferner ist die LPS-assoziierte Wirkung teilweise durch den *Mir155* Knockout aufgehoben. In den Langerhans-Inseln der*Mir155*$^{-/-}$*Ldlr*$^{-/-}$ Mäusen zeigte die Microarray-Analyse eine Inhibierung von Insulin, GLP-1 und dem IL-6 Signalweg sowie eine Erhöhung vermeintlicher miR-155 Targets, wie z.B. *Mafb*, *Sema5a, Med12l, Auh* und *Stmn2*. Die Überexpression von miR-155-5p führte zur Anreicherung der *Mafb* mRNA im RISC. Die Luciferase Reporter-Assay zeigte, dass MafB die Expression von *Il6* durch die Bindung an den *Il6* Promoter supprimiert. In *Ldlr*$^{-/-}$ Mäusen führte die Hemmung der Interaktion zwischen miR-155-5p und MafB zu erhöhten FBG Werten und zu

reduzierten Expressionen von *Il6*, GLP-1 produziertem Enzym *Pcsk1* und zur verringerten Insulin Produktion in den Langerhans-Inseln. MiR-155-5p reduzierte die Adipositas und die Inflammation im adipösen Gewebe wahrscheinlich aufgrund der erhöhten GLP-1 Konzentration im Plasma. Nach Verfütterung des „high fat“ Futters inhibierte miR-155-5p die Hyperlipidämie und die Entwicklung der Atherosklerose in *Ldlr*$^{-/-}$ Mäusen.

Zusammenfassend verbessert die Hyperlipidämie-assoziierte Endotoxämie die Glukose-Homöostase durch die gesteigerte Expression von miR-155-5p in den β-Zellen. Die Hemmung von MafB durch miR-155-5p reduzierte die β-α Zell Umprogrammierung und verbesserte die β-Zell Funktion durch eine IL-6-induzierte GLP-1 Produktion in den α-Zellen. Die Hyperlipidämie-vermittelte Induktion von miR-155-5p trägt zur Anpassung von β-Zellen an die Insulinresistenz bei. Die erhöhte Expression von miR-155-5p in den β-Zellen stellt einen vielversprechenden Ansatz in der Therapie des Diabetes und des MetS dar.

7 REFERENCES

1 International Diabetes Federation. IDF Diabetes Atlas, 7th edn. *Brussels, Belgium: International Diabetes Federation* (2015).

2 World Health Organization, editor. Global report on diabetes. *Geneva, Switzerland: World Health Organization* (2016).

3 World Health Organization, editor. Global health risks: mortality and burden of disease attributable to selected major risks. *Geneva, Switzerland: World Health Organization* (2009).

4 Alberti, K. G. & Zimmet, P. Z. Definition, diagnosis and classification of diabetes mellitus and its complications. Part 1: diagnosis and classification of diabetes mellitus provisional report of a WHO consultation. *Diabet. Med.* 15, 539-553, doi:10.1002/(SICI)1096-9136(199807)15:7<539::AID-DIA668>3.0.CO;2-S (1998).

5 Polonsky, K. S. The past 200 years in diabetes. *N. Engl. J. Med.* 367, 1332-1340, doi:10.1056/NEJMra1110560 (2012).

6 van Belle, T. L., Coppieters, K. T. & von Herrath, M. G. Type 1 diabetes: etiology, immunology, and therapeutic strategies. *Physiol. Rev.* 91, 79-118, doi:10.1152/physrev.00003.2010 (2011).

7 Todd, J. A. Etiology of type 1 diabetes. *Immunity* 32, 457-467, doi:10.1016/j.immuni.2010.04.001 (2010).

8 American Diabetes, A. Diagnosis and classification of diabetes mellitus. *Diabetes Care* 37 Suppl 1, S81-90, doi:10.2337/dc14-S081 (2014).

9 Beckman, J. A., Creager, M. A. & Libby, P. Diabetes and atherosclerosis: epidemiology, pathophysiology, and management. *JAMA.* 287, 2570-2581 (2002).

10 Prentki, M. & Nolan, C. J. Islet beta cell failure in type 2 diabetes. *J. Clin. Invest.* 116, 1802-1812, doi:10.1172/JCI29103 (2006).

11 Mokdad, A. H. *et al.* Prevalence of obesity, diabetes, and obesity-related health risk factors, 2001. *JAMA.* 289, 76-79 (2003).

12 Kahn, S. E., Hull, R. L. & Utzschneider, K. M. Mechanisms linking obesity to insulin resistance and type 2 diabetes. *Nature* 444, 840-846, doi:10.1038/nature05482 (2006).

13 Eckel, R. H., Grundy, S. M. & Zimmet, P. Z. The metabolic syndrome. *Lancet* 365, 1415-1428, doi:10.1016/s0140-6736(05)66378-7 (2005).

14 Grundy, S. M. Metabolic syndrome pandemic. *Arterioscler. Thromb. Vasc. Biol.* 28, 629-636, doi:10.1161/ATVBAHA.107.151092 (2008).

15 Despres, J. P. & Lemieux, I. Abdominal obesity and metabolic syndrome. *Nature* 444, 881-887, doi:10.1038/nature05488 (2006).

16 Gregor, M. F. & Hotamisligil, G. S. Inflammatory mechanisms in obesity. *Annu. Rev. Immunol.* 29, 415-445, doi:10.1146/annurev-immunol-031210-101322 (2011).

17 Wang, Z., York, N. W., Nichols, C. G. & Remedi, M. S. Pancreatic beta cell dedifferentiation in diabetes and redifferentiation following insulin therapy. *Cell Metab.* 19, 872-882, doi:10.1016/j.cmet.2014.03.010 (2014).

18 Talchai, C., Xuan, S., Lin, H. V., Sussel, L. & Accili, D. Pancreatic beta cell dedifferentiation as a mechanism of diabetic beta cell failure. *Cell* 150, 1223-1234, doi:10.1016/j.cell.2012.07.029 (2012).

19 Butler, A. E. *et al.* Beta-cell deficit and increased beta-cell apoptosis in humans with type 2 diabetes. *Diabetes* 52, 102-110 (2003).

20 Costes, S., Langen, R., Gurlo, T., Matveyenko, A. V. & Butler, P. C. beta-Cell failure in type 2 diabetes: a case of asking too much of too few? *Diabetes* 62, 327-335, doi:10.2337/db12-1326 (2013).

21 Weir, G. C. & Bonner-Weir, S. Five stages of evolving beta-cell dysfunction during progression to diabetes. *Diabetes* 53 Suppl 3, S16-21 (2004).

22 Goodpaster, B. H. & Wolf, D. Skeletal muscle lipid accumulation in obesity, insulin resistance, and type 2 diabetes. *Pediatr. Diabetes* 5, 219-226, doi:10.1111/j.1399-543X.2004.00071.x (2004).

23 Lugari, R. *et al.* Evidence for early impairment of glucagon-like peptide 1-induced insulin secretion in human type 2 (non insulin-dependent) diabetes. *Horm. Metab. Res.* 34, 150-154, doi:10.1055/s-2002-23199 (2002).

24 Muscelli, E. *et al.* Separate impact of obesity and glucose tolerance on the incretin effect in normal subjects and type 2 diabetic patients. *Diabetes* 57, 1340-1348, doi:10.2337/db07-1315 (2008).

25 Toft-Nielsen, M. B. *et al.* Determinants of the impaired secretion of glucagon-like peptide-1 in type 2 diabetic patients. *J. Clin. Endocrinol. Metab.* 86, 3717-3723, doi:10.1210/jcem.86.8.7750 (2001).

26 Kieffer, T. J. & Habener, J. F. The glucagon-like peptides. *Endocr. Rev.* 20, 876-913, doi:10.1210/edrv.20.6.0385 (1999).

27 Irwin, D. M. Molecular evolution of proglucagon. *Regul. Pept.* 98, 1-12 (2001).

28 Kreymann, B., Williams, G., Ghatei, M. A. & Bloom, S. R. Glucagon-like peptide-1 7-36: a physiological incretin in man. *Lancet* 2, 1300-1304 (1987).

29 Orskov, C. *et al.* Glucagon-like peptides GLP-1 and GLP-2, predicted products of the glucagon gene, are secreted separately from pig small intestine but not pancreas. *Endocrinology* 119, 1467-1475, doi:10.1210/endo-119-4-1467 (1986).

30 Orskov, C., Rabenhoj, L., Wettergren, A., Kofod, H. & Holst, J. J. Tissue and plasma concentrations of amidated and glycine-extended glucagon-like peptide I in humans. *Diabetes* 43, 535-539 (1994).

31 Kreymann, B. *et al.* Characterization of glucagon-like peptide-1-(7-36)amide in the hypothalamus. *Brain Res.* 502, 325-331 (1989).

32 Holst, J. J. *et al.* Proglucagon processing in porcine and human pancreas. *J. Biol. Chem.* 269, 18827-18833 (1994).

33 Rothenberg, M. E. *et al.* Processing of mouse proglucagon by recombinant prohormone convertase 1 and immunopurified prohormone convertase 2 in vitro. *J. Biol. Chem.* 270, 10136-10146 (1995).

34 Habener, J. F. & Stanojevic, V. Alpha cells come of age. *Trends Endocrinol Metab.* 24, 153-163, doi:10.1016/j.tem.2012.10.009 (2013).

35 Wideman, R. D. *et al.* Improving function and survival of pancreatic islets by endogenous production of glucagon-like peptide 1 (GLP-1). *Proc. Natl. Acad. Sci. U.S.A.* 103, 13468-13473, doi:10.1073/pnas.0600655103 (2006).

36 Kilimnik, G., Kim, A., Steiner, D. F., Friedman, T. C. & Hara, M. Intraislet production of GLP-1 by activation of prohormone convertase 1/3 in pancreatic alpha-cells in mouse models of ss-cell regeneration. *Islets* 2, 149-155 (2010).

37 Whalley, N. M., Pritchard, L. E., Smith, D. M. & White, A. Processing of proglucagon to GLP-1 in pancreatic alpha-cells: is this a paracrine mechanism enabling GLP-1 to act on beta-cells? *J. Endocrinol.* 211, 99-106, doi:10.1530/JOE-11-0094 (2011).

38 Nie, Y. *et al.* Regulation of pancreatic PC1 and PC2 associated with increased glucagon-like peptide 1 in diabetic rats. *J. Clin. Invest.* 105, 955-965, doi:10.1172/jci7456 (2000).

39 Wideman, R. D., Covey, S. D., Webb, G. C., Drucker, D. J. & Kieffer, T. J. A switch from prohormone convertase (PC)-2 to PC1/3 expression in transplanted alpha-cells is accompanied by differential processing of proglucagon and improved glucose homeostasis in mice. *Diabetes* 56, 2744-2752, doi:10.2337/db07-0563 (2007).

40 Hansen, A. M. *et al.* Upregulation of alpha cell glucagon-like peptide 1 (GLP-1) in Psammomys obesus--an adaptive response to hyperglycaemia? *Diabetologia* 54, 1379-1387, doi:10.1007/s00125-011-2080-1 (2011).

41 Sandoval, D. A. & D'Alessio, D. A. Physiology of proglucagon peptides: role of glucagon and GLP-1 in health and disease. *Physiol. Rev.* 95, 513-548, doi:10.1152/physrev.00013.2014 (2015).

42 Kuhre, R. E. *et al.* Fructose stimulates GLP-1 but not GIP secretion in mice, rats, and humans. *Am. J. Physiol. Gastrointest. Liver Physiol.* 306, G622-630, doi:10.1152/ajpgi.00372.2013 (2014).

43 Orskov, C., Jeppesen, J., Madsbad, S. & Holst, J. J. Proglucagon products in plasma of noninsulin-dependent diabetics and nondiabetic controls in the fasting state and after oral glucose and intravenous arginine. *J. Clin. Invest.* 87, 415-423, doi:10.1172/JCI115012 (1991).

44 Tolhurst, G. *et al.* Short-chain fatty acids stimulate glucagon-like peptide-1 secretion via the G-protein-coupled receptor FFAR2. *Diabetes* 61, 364-371, doi:10.2337/db11-1019 (2012).

45 Cho, Y. M., Fujita, Y. & Kieffer, T. J. Glucagon-like peptide-1: glucose homeostasis and beyond. *Annu. Rev. Physiol.* 76, 535-559, doi:10.1146/annurev-physiol-021113-170315 (2014).

46 Campbell, J. E. & Drucker, D. J. Pharmacology, physiology, and mechanisms of incretin hormone action. *Cell Metab.* 17, 819-837, doi:10.1016/j.cmet.2013.04.008 (2013).

47 Ellingsgaard, H. *et al.* Interleukin-6 enhances insulin secretion by increasing glucagon-like peptide-1 secretion from L cells and alpha cells. *Nat. Med.* 17, 1481-1489, doi:10.1038/nm.2513 (2011).

48 Kahles, F. *et al.* GLP-1 secretion is increased by inflammatory stimuli in an IL-6-dependent manner, leading to hyperinsulinemia and blood glucose lowering. *Diabetes* 63, 3221-3229, doi:10.2337/db14-0100 (2014).

49 Donath, M. Y. & Burcelin, R. GLP-1 effects on islets: hormonal, neuronal, or paracrine? *Diabetes Care* 36 Suppl 2, S145-148, doi:10.2337/dcS13-2015 (2013).

50 Campbell, J. E. & Drucker, D. J. Pharmacology, physiology, and mechanisms of incretin hormone action. *Cell Metab.* 17, 819-837, doi:10.1016/j.cmet.2013.04.008 (2013).

51 Buteau, J. GLP-1 receptor signaling: effects on pancreatic beta-cell proliferation and survival. *Diabetes Metab.* 34 Suppl 2, S73-77, doi:10.1016/S1262-3636(08)73398-6 (2008).

52 Tuduri, E., Lopez, M., Dieguez, C., Nadal, A. & Nogueiras, R. Glucagon-Like Peptide 1 Analogs and their Effects on Pancreatic Islets. *Trends Endocrinol Metab.* 27, 304-318, doi:10.1016/j.tem.2016.03.004 (2016).

53 Yusta, B. *et al.* GLP-1 receptor activation improves beta cell function and survival following induction of endoplasmic reticulum stress. *Cell Metab.* 4, 391-406, doi:10.1016/j.cmet.2006.10.001 (2006).

54 Smith, E. P. *et al.* The role of beta cell glucagon-like peptide-1 signaling in glucose regulation and response to diabetes drugs. *Cell Metab.* 19, 1050-1057, doi:10.1016/j.cmet.2014.04.005 (2014).

55 Lamont, B. J. *et al.* Pancreatic GLP-1 receptor activation is sufficient for incretin control of glucose metabolism in mice. *J. Clin. Invest.* 122, 388-402, doi:10.1172/jci42497 (2012).

56 Morton, G. J., Cummings, D. E., Baskin, D. G., Barsh, G. S. & Schwartz, M. W. Central nervous system control of food intake and body weight. *Nature* 443, 289-295, doi:10.1038/nature05026 (2006).

57 Baggio, L. L. & Drucker, D. J. Glucagon-like peptide-1 receptors in the brain: controlling food intake and body weight. *J. Clin. Invest.* 124, 4223-4226, doi:10.1172/JCI78371 (2014).

58 Finan, B. *et al.* Targeted estrogen delivery reverses the metabolic syndrome. *Nature Med.* 18, 1847-1856, doi:10.1038/nm.3009 (2012).

59 Sisley, S. *et al.* Neuronal GLP1R mediates liraglutide's anorectic but not glucose-lowering effect. *J. Clin. Invest.* 124, 2456-2463, doi:10.1172/JCI72434 (2014).

60 Drucker, D. J. The Cardiovascular Biology of Glucagon-like Peptide-1. *Cell Metab.* 24, 15-30, doi:10.1016/j.cmet.2016.06.009 (2016).

61 Ussher, J. R. & Drucker, D. J. Cardiovascular biology of the incretin system. *Endocr Rev.* 33, 187-215, doi:10.1210/er.2011-1052 (2012).

62 Fava, S. Glucagon-like peptide 1 and the cardiovascular system. *Curr. Diabetes Rev.* 10, 302-310 (2014).

63 Ban, K. *et al.* Cardioprotective and vasodilatory actions of glucagon-like peptide 1 receptor are mediated through both glucagon-like peptide 1 receptor-dependent and -independent pathways. *Circulation* 117, 2340-2350, doi:10.1161/CIRCULATIONAHA.107.739938 (2008).

64 Beiroa, D. *et al.* GLP-1 agonism stimulates brown adipose tissue thermogenesis and browning through hypothalamic AMPK. *Diabetes* 63, 3346-3358, doi:10.2337/db14-0302 (2014).

65 Vendrell, J. *et al.* Study of the potential association of adipose tissue GLP-1 receptor with obesity and insulin resistance. *Endocrinology* 152, 4072-4079, doi:10.1210/en.2011-1070 (2011).

66 Bjerre Knudsen, L. *et al.* Glucagon-like Peptide-1 receptor agonists activate rodent thyroid C-cells causing calcitonin release and C-cell proliferation. *Endocrinology* 151, 1473-1486, doi:10.1210/en.2009-1272 (2010).

67 Hadjiyanni, I., Siminovitch, K. A., Danska, J. S. & Drucker, D. J. Glucagon-like peptide-1 receptor signalling selectively regulates murine lymphocyte proliferation and maintenance of peripheral regulatory T cells. *Diabetologia* 53, 730-740 (2010).

68 Zietek, T. & Rath, E. Inflammation Meets Metabolic Disease: Gut Feeling Mediated by GLP-1. *Front Immunol.* 7, 154, doi:10.3389/fimmu.2016.00154 (2016).

69 Pyke, C. *et al.* GLP-1 receptor localization in monkey and human tissue: novel distribution revealed with extensively validated monoclonal antibody. *Endocrinology* 155, 1280-1290, doi:10.1210/en.2013-1934 (2014).

70 Cantini, G., Mannucci, E. & Luconi, M. Perspectives in GLP-1 Research: New Targets, New Receptors. *Trends Endocrinol Metab.* 27, 427-438, doi:10.1016/j.tem.2016.03.017 (2016).

71 Cani, P. D. *et al.* Changes in gut microbiota control metabolic endotoxemia-induced inflammation in high-fat diet-induced obesity and diabetes in mice. *Diabetes* 57, 1470-1481, doi:10.2337/db07-1403 (2008).

72 Cani, P. D. *et al.* Metabolic endotoxemia initiates obesity and insulin resistance. *Diabetes* 56, 1761-1772, doi:10.2337/db06-1491 (2007).

73 Amar, J. *et al.* Energy intake is associated with endotoxemia in apparently healthy men. *Am. J. Clin. Nutr.* 87, 1219-1223 (2008).

74 Cani, P. D. *et al.* Endocannabinoids--at the crossroads between the gut microbiota and host metabolism. *Nat. Rev. Endocrinol.* 12, 133-143, doi:10.1038/nrendo.2015.211 (2016).

75 Nguyen, A. T. *et al.* Lipopolysaccharides-mediated increase in glucose-stimulated insulin secretion: involvement of the GLP-1 pathway. *Diabetes* 63, 471-482, doi:10.2337/db13-0903 (2014).

76 Raetz, C. R. & Whitfield, C. Lipopolysaccharide endotoxins. *Annu. Rev. Biochem.* 71, 635-700, doi:10.1146/annurev.biochem.71.110601.135414 (2002).

77 Beutler, B. & Rietschel, E. T. Innate immune sensing and its roots: the story of endotoxin. *Nat. Rev. Immunol.* 3, 169-176, doi:10.1038/nri1004 (2003).

78 Kulp, A. & Kuehn, M. J. Biological functions and biogenesis of secreted bacterial outer membrane vesicles. *Annu. Rev. Microbiol.* 64, 163-184, doi:10.1146/annurev.micro.091208.073413 (2010).

79 Schumann, R. R. *et al.* Structure and function of lipopolysaccharide binding protein. *Science* 249, 1429-1431 (1990).

80 Schroder, N. W. *et al.* Lipopolysaccharide binding protein binds to triacylated and diacylated lipopeptides and mediates innate immune responses. *J. Immunol.* 173, 2683-2691 (2004).

81 Wright, S. D., Ramos, R. A., Tobias, P. S., Ulevitch, R. J. & Mathison, J. C. CD14, a receptor for complexes of lipopolysaccharide (LPS) and LPS binding protein. *Science* 249, 1431-1433 (1990).

82 Park, B. S. & Lee, J. O. Recognition of lipopolysaccharide pattern by TLR4 complexes. *Exp. Mol. Med.* 45, e66, doi:10.1038/emm.2013.97 (2013).

83 Park, B. S. *et al.* The structural basis of lipopolysaccharide recognition by the TLR4-MD-2 complex. *Nature* 458, 1191-1195, doi:10.1038/nature07830 (2009).

84 Triantafilou, M. & Triantafilou, K. Lipopolysaccharide recognition: CD14, TLRs and the LPS-activation cluster. *Trends Immunol.* 23, 301-304 (2002).

85 Thompson, P. A., Tobias, P. S., Viriyakosol, S., Kirkland, T. N. & Kitchens, R. L. Lipopolysaccharide (LPS)-binding protein inhibits responses to cell-bound LPS. *J. Biol. Chem.* 278, 28367-28371, doi:10.1074/jbc.M302921200 (2003).

86 Nunes-Alves, C. Inflammasomes: new LPS receptors discovered. *Nat. Rev. Immunol.* 14, 582, doi:10.1038/nri3736 (2014).

87 Peri, F. & Piazza, M. Therapeutic targeting of innate immunity with Toll-like receptor 4 (TLR4) antagonists. *Biotechnol Adv* 30, 251-260, doi:10.1016/j.biotechadv.2011.05.014 (2012).

88 Sommer, F. & Backhed, F. The gut microbiota--masters of host development and physiology. *Nat. Rev. Microbiol.* 11, 227-238, doi:10.1038/nrmicro2974 (2013).

89 Ge, Y., Ezzell, R. M. & Warren, H. S. Localization of endotoxin in the rat intestinal epithelium. *J. Infect. Dis.* 182, 873-881, doi:10.1086/315784 (2000).

90 Benoit, R. *et al.* Pure endotoxin does not pass across the intestinal epithelium in vitro. *Shock* 10, 43-48 (1998).

91 Hersoug, L. G., Moller, P. & Loft, S. Gut microbiota-derived lipopolysaccharide uptake and trafficking to adipose tissue: implications for inflammation and obesity. *Obes. Rev.* 17, 297-312, doi:10.1111/obr.12370 (2016).

92 Graham, C., Mullen, A. & Whelan, K. Obesity and the gastrointestinal microbiota: a review of associations and mechanisms. *Nutr. Rev.* 73, 376-385, doi:10.1093/nutrit/nuv004 (2015).

93 Winer, D. A., Luck, H., Tsai, S. & Winer, S. The Intestinal Immune System in Obesity and Insulin Resistance. *Cell Metab.* 23, 413-426, doi:10.1016/j.cmet.2016.01.003 (2016).

94 Blaut, M. Gut microbiota and energy balance: role in obesity. *Proc. Nutr. Soc.* 74, 227-234, doi:10.1017/S0029665114001700 (2015).

95 Vreugdenhil, A. C., Snoek, A. M., van 't Veer, C., Greve, J. W. & Buurman, W. A. LPS-binding protein circulates in association with apoB-containing lipoproteins and enhances endotoxin-LDL/VLDL interaction. *J. Clin. Invest.* 107, 225-234, doi:10.1172/jci10832 (2001).

96 Schwartz, Y. & Dushkin, M. I. Endotoxin-lipoprotein complex formation as a factor in atherogenesis: associations with hyperlipidemia and with lecithin:cholesterol acyltransferase activity. *Biochemistry (Mosc)* 67, 747-752 (2002).

97 Besseling, J., Kastelein, J. J., Defesche, J. C., Hutten, B. A. & Hovingh, G. K. Association between familial hypercholesterolemia and prevalence of type 2 diabetes mellitus. *JAMA.* 313, 1029-1036, doi:10.1001/jama.2015.1206 (2015).

98 Lee, R. C., Feinbaum, R. L. & Ambros, V. The C. elegans heterochronic gene lin-4 encodes small RNAs with antisense complementarity to lin-14. *Cell* 75, 843-854 (1993).

99 Ebert, M. S. & Sharp, P. A. Roles for MicroRNAs in conferring robustness to biological processes. *Cell* 149, 515-524, doi:10.1016/j.cell.2012.04.005 (2012).

100 Lagos-Quintana, M., Rauhut, R., Lendeckel, W. & Tuschl, T. Identification of novel genes coding for small expressed RNAs. *Science* 294, 853-858, doi:10.1126/science.1064921 (2001).

101 Voinnet, O. Origin, biogenesis, and activity of plant microRNAs. *Cell* 136, 669-687, doi:10.1016/j.cell.2009.01.046 (2009).

102 Androulidaki, A. *et al.* The kinase Akt1 controls macrophage response to lipopolysaccharide by regulating microRNAs. *Immunity* 31, 220-231, doi:10.1016/j.immuni.2009.06.024 (2009).

103 Nazari-Jahantigh, M. *et al.* MicroRNA-155 promotes atherosclerosis by repressing Bcl6 in macrophages. *J. Clin. Invest.* 122, 4190-4202, doi:10.1172/JCI61716 (2012).

104 Tian, F. J. *et al.* Elevated microRNA-155 promotes foam cell formation by targeting HBP1 in atherogenesis. *Cardiovasc Res* 103, 100-110, doi:10.1093/cvr/cvu070 (2014).

105 Wei, Y. & Schober, A. MicroRNA regulation of macrophages in human pathologies. *Cell. Mol. Life. Sci*, doi:10.1007/s00018-016-2254-6 (2016).

106 Elton, T. S., Selemon, H., Elton, S. M. & Parinandi, N. L. Regulation of the MIR155 host gene in physiological and pathological processes. *Gene* 532, 1-12, doi:10.1016/j.gene.2012.12.009 (2013).

107 Tam, W. Identification and characterization of human BIC, a gene on chromosome 21 that encodes a noncoding RNA. *Gene* 274, 157-167, doi:S0378111901006126 [pii] (2001).

108 Eis, P. S. *et al.* Accumulation of miR-155 and BIC RNA in human B cell lymphomas. *Proc. Natl. Acad. Sci. U.S.A.* 102, 3627-3632, doi:10.1073/pnas.0500613102 (2005).

109 Ha, M. & Kim, V. N. Regulation of microRNA biogenesis. *Nat Rev Mol Cell Biol* 15, 509-524, doi:10.1038/nrm3838 (2014).

110 Han, J. *et al.* Molecular basis for the recognition of primary microRNAs by the Drosha-DGCR8 complex. *Cell* 125, 887-901, doi:10.1016/j.cell.2006.03.043 (2006).

111 Morlando, M. *et al.* Primary microRNA transcripts are processed co-transcriptionally. *Nat. Struct. Mol. Biol.* 15, 902-909 (2008).

112 Lee, Y. *et al.* The nuclear RNase III Drosha initiates microRNA processing. *Nature* 425, 415-419, doi:10.1038/nature01957 (2003).

113 Okada, C. *et al.* A high-resolution structure of the pre-microRNA nuclear export machinery. *Science* 326, 1275-1279, doi:10.1126/science.1178705 (2009).

114 Pasquinelli, A. E. MicroRNAs and their targets: recognition, regulation and an emerging reciprocal relationship. *Nature Rev. Genet.* 13, 271-282, doi:10.1038/nrg3162 (2012).

115 Foulkes, W. D., Priest, J. R. & Duchaine, T. F. DICER1: mutations, microRNAs and mechanisms. *Nature reviews. Cancer* 14, 662-672, doi:10.1038/nrc3802 (2014).

116 Kwak, P. B. & Tomari, Y. The N domain of Argonaute drives duplex unwinding during RISC assembly. *Nat. Struct. Mol. Biol.* 19, 145-151, doi:10.1038/nsmb.2232 (2012).

117 Zhou, H. *et al.* miR-155 and its star-form partner miR-155* cooperatively regulate type I interferon production by human plasmacytoid dendritic cells. *Blood* 116, 5885-5894, doi:10.1182/blood-2010-04-280156 (2010).

118 Filipowicz, W., Bhattacharyya, S. N. & Sonenberg, N. Mechanisms of post-transcriptional regulation by microRNAs: are the answers in sight? *Nat. Rev. Genet.* 9, 102-114, doi:10.1038/nrg2290 (2008).

119 Griffiths-Jones, S. The microRNA Registry. *Nuclei.c Acids Res.* 32, D109-111, doi:10.1093/nar/gkh023 (2004).

120 Friedman, R. C., Farh, K. K., Burge, C. B. & Bartel, D. P. Most mammalian mRNAs are conserved targets of microRNAs. *Genome Res.* 19, 92-105, doi:10.1101/gr.082701.108 (2009).

121 O'Connell, R. M., Taganov, K. D., Boldin, M. P., Cheng, G. & Baltimore, D. MicroRNA-155 is induced during the macrophage inflammatory response. *Proc. Natl. Acad. Sci. U.S.A.*. 104, 1604-1609 (2007).

122 Dueck, A., Eichner, A., Sixt, M. & Meister, G. A miR-155-dependent microRNA hierarchy in dendritic cell maturation and macrophage activation. *FEBS. Lett.* 588, 632-640, doi:http://dx.doi.org/10.1016/j.febslet.2014.01.009 (2014).

123 O'Connell, R. M., Chaudhuri, A. A., Rao, D. S. & Baltimore, D. Inositol phosphatase SHIP1 is a primary target of miR-155. *Proc. Natl. Acad. Sci. U.S.A.* 106, 7113-7118, doi:10.1073/pnas.0902636106 (2009).

124 Ruggiero, T. *et al.* LPS induces KH-type splicing regulatory protein-dependent processing of microRNA-155 precursors in macrophages. *The FASEB Journal* 23, 2898-2908, doi:10.1096/fj.09-131342 (2009).

125 Huang, R. S., Hu, G. Q., Lin, B., Lin, Z. Y. & Sun, C. C. MicroRNA-155 silencing enhances inflammatory response and lipid uptake in oxidized low-density lipoprotein-stimulated human THP-1 macrophages. *J. Investig. Med.* 58, 961-967, doi:10.231/JIM.0b013e3181ff46d7 (2010).

126 Wei, Y. *et al.* Regulation of Csf1r and Bcl6 in macrophages mediates the stage-specific effects of microRNA-155 on atherosclerosis. *Arterioscler. Thromb. Vasc. Biol.* 35, 796-803, doi:10.1161/ATVBAHA.114.304723 (2015).

127 Schober, A. & Weber, C. Mechanisms of MicroRNAs in Atherosclerosis. *Annu. Rev. Pathol.* 11, 583-616, doi:10.1146/annurev-pathol-012615-044135 (2016).

128 Wei, Y. & Schober, A. MicroRNA regulation of macrophages in human pathologies. *Cellular and molecular life sciences : CMLS.* 73, 3473-3495, doi:10.1007/s00018-016-2254-6 (2016).

129 Du, F. *et al.* MicroRNA-155 deficiency results in decreased macrophage inflammation and attenuated atherogenesis in apolipoprotein E-deficient mice. *Arterioscler Thromb Vasc Biol* 34, 759-767, doi:10.1161/atvbaha.113.302701 (2014).

130 Liu, S., Yang, Y. & Wu, J. TNFalpha-induced up-regulation of miR-155 inhibits adipogenesis by down-regulating early adipogenic transcription factors. *Biochem Biophys Res Commun* 414, 618-624, doi:10.1016/j.bbrc.2011.09.131 (2011).

131 Gaudet, A. D. *et al.* miR-155 Deletion in Female Mice Prevents Diet-Induced Obesity. *Sci. Rep.* 6, 22862, doi:10.1038/srep22862 (2016).

132 Chen, Y. *et al.* miR-155 regulates differentiation of brown and beige adipocytes via a bistable circuit. *Nat. Commun.* 4, 1769, doi:10.1038/ncomms2742 (2013).

133 Kloting, N. *et al.* MicroRNA expression in human omental and subcutaneous adipose tissue. *PloS ONE* 4, e4699, doi:10.1371/journal.pone.0004699 (2009).

134 Amano, S. U. *et al.* Local proliferation of macrophages contributes to obesity-associated adipose tissue inflammation. *Cell Metab.* 19, 162-171, doi:10.1016/j.cmet.2013.11.017 (2014).

135 Vreugdenhil, A. C., Snoek, A. M., van 't Veer, C., Greve, J. W. & Buurman, W. A. LPS-binding protein circulates in association with apoB-containing lipoproteins and enhances endotoxin-LDL/VLDL interaction. *J. Clin. Invest.* 107, 225-234, doi:10.1172/jci10832 (2001).

136 Chen, H. C. & Farese, R. V., Jr. Determination of adipocyte size by computer image analysis. *J Lipid Res* 43, 986-989 (2002).

137 Bucolo, G. & David, H. Quantitative determination of serum triglycerides by the use of enzymes. *Clin. Chem.* 19, 476-482 (1973).

138 Carter, J. D., Dula, S. B., Corbin, K. L., Wu, R. & Nunemaker, C. S. A practical guide to rodent islet isolation and assessment. *Biological procedures online* 11, 3-31, doi:10.1007/s12575-009-9021-0 (2009).

139 Li, D. S., Yuan, Y. H., Tu, H. J., Liang, Q. L. & Dai, L. J. A protocol for islet isolation from mouse pancreas. *Nat Protoc* 4, 1649-1652, doi:10.1038/nprot.2009.150 (2009).

140 Nuovo, G. J. *et al.* A methodology for the combined in situ analyses of the precursor and mature forms of microRNAs and correlation with their putative targets. *Nat. Protoc.* 4, 107-115 (2009).

141 Emmert-Buck, M. R. *et al.* Laser capture microdissection. *Science* 274, 998-1001 (1996).

142 Espina, V. *et al.* Laser-capture microdissection. *Nat. Protoc.* 1, 586-603, doi:10.1038/nprot.2006.85 (2006).

143 Miyazaki, J. *et al.* Establishment of a pancreatic beta cell line that retains glucose-inducible insulin secretion: special reference to expression of glucose transporter isoforms. *Endocrinology* 127, 126-132, doi:10.1210/endo-127-1-126 (1990).

144 Nakashima, K. *et al.* MIN6 is not a pure beta cell line but a mixed cell line with other pancreatic endocrine hormones. *Endocr. J.* 56, 45-53 (2009).

145 Ishihara, H. *et al.* Pancreatic beta cell line MIN6 exhibits characteristics of glucose metabolism and glucose-stimulated insulin secretion similar to those of normal islets. *Diabetologia* 36, 1139-1145 (1993).

146 Lowry, O. H., Rosebrough, N. J., Farr, A. L. & Randall, R. J. Protein measurement with the Folin phenol reagent. *J. Biol. Chem.* 193, 265-275 (1951).

147 Kramer, A., Green, J., Pollard, J., Jr. & Tugendreich, S. Causal analysis approaches in Ingenuity Pathway Analysis. *Bioinformatics (Oxford, England)* 30, 523-530, doi:10.1093/bioinformatics/btt703 (2014).

148 Cambronne, X. A., Shen, R., Auer, P. L. & Goodman, R. H. Capturing microRNA targets using an RNA-induced silencing complex (RISC)-trap approach. *Proc. Natl. Acad. Sci. U.S.A.* 109, 20473-20478, doi:10.1073/pnas.1218887109 (2012).

149 Wingender, E., Dietze, P., Karas, H. & Knuppel, R. TRANSFAC: a database on transcription factors and their DNA binding sites. *Nucleic Acids Res.* 24, 238-241 (1996).

150 Matys, V. *et al.* TRANSFAC: transcriptional regulation, from patterns to profiles. *Nucleic Acids Res.* 31, 374-378 (2003).

151 Nelson, M. & McClelland, M. Use of DNA methyltransferase/endonuclease enzyme combinations for megabase mapping of chromosomes. *Methods Enzymol.* 216, 279-303 (1992).

152 Wei, Y. *et al.* The microRNA-342-5p fosters inflammatory macrophage activation through an Akt1- and microRNA-155-dependent pathway during atherosclerosis. *Circulation* 127, 1609-1619, doi:10.1161/CIRCULATIONAHA.112.000736 (2013).

153 Weisberg, S. P. *et al.* Obesity is associated with macrophage accumulation in adipose tissue. *J. Clin. Invest.* 112, 1796-1808, doi:10.1172/JCI19246 (2003).

154 O'Connell, R. M. *et al.* MicroRNA-155 promotes autoimmune inflammation by enhancing inflammatory T cell development. *Immunity* 33, 607-619, doi:10.1016/j.immuni.2010.09.009 (2010).

155 Rodriguez, A. *et al.* Requirement of bic/microRNA-155 for normal immune function. *Science* 316, 608-611 (2007).

156 Rane, S. G. *et al.* Loss of Cdk4 expression causes insulin-deficient diabetes and Cdk4 activation results in beta-islet cell hyperplasia. *Nat Genet* 22, 44-52, doi:10.1038/8751 (1999).

157 Robitaille, K. *et al.* High-throughput Functional Genomics Identifies Regulators of Primary Human Beta Cell Proliferation. *J. Biol. Chem.* 291, 4614-4625, doi:10.1074/jbc.M115.683912 (2016).

158 Wang, L. *et al.* Deletion of Pten in pancreatic beta-cells protects against deficient beta-cell mass and function in mouse models of type 2 diabetes. *Diabetes* 59, 3117-3126, doi:10.2337/db09-1805 (2010).

159 Ammala, C., Ashcroft, F. M. & Rorsman, P. Calcium-independent potentiation of insulin release by cyclic AMP in single beta-cells. *Nature* 363, 356-358, doi:10.1038/363356a0 (1993).

160 Unger, R. H. Diabetic hyperglycemia: link to impaired glucose transport in pancreatic beta cells. *Science* 251, 1200-1205 (1991).

161 Heinrich, P. C., Behrmann, I., Muller-Newen, G., Schaper, F. & Graeve, L. Interleukin-6-type cytokine signalling through the gp130/Jak/STAT pathway. *Biochem J.* 334 (Pt 2), 297-314 (1998).

162 Murray, P. J. The JAK-STAT signaling pathway: input and output integration. *J. Immunol.* 178, 2623-2629 (2007).

163 Campbell, I. L., Cutri, A., Wilson, A. & Harrison, L. C. Evidence for IL-6 production by and effects on the pancreatic beta-cell. *J. Immunol.* 143, 1188-1191 (1989).

164 Ellingsgaard, H. *et al.* Interleukin-6 regulates pancreatic alpha-cell mass expansion. *Proc. Natl. Acad. Sci. U.S.A.* 105, 13163-13168, doi:10.1073/pnas.0801059105 (2008).

165 Ellingsgaard, H. *et al.* Interleukin-6 enhances insulin secretion by increasing glucagon-like peptide-1 secretion from L cells and alpha cells. *Nat. Med.* 17, 1481-U1500, doi:DOI 10.1038/nm.2513 (2011).

166 Kurowska-Stolarska, M. *et al.* MicroRNA-155 as a proinflammatory regulator in clinical and experimental arthritis. *Proc. Natl. Acad. Sci. U.S.A.* 108, 11193-11198, doi:10.1073/pnas.1019536108 (2011).

167 Murugaiyan, G., Beynon, V., Mittal, A., Joller, N. & Weiner, H. L. Silencing microRNA-155 ameliorates experimental autoimmune encephalomyelitis. *J. Immunol.* 187, 2213-2221, doi:10.4049/jimmunol.1003952 (2011).

168 Oertli, M. *et al.* MicroRNA-155 is essential for the T cell-mediated control of Helicobacter pylori infection and for the induction of chronic Gastritis and Colitis. *J. Immunol.* 187, 3578-3586, doi:10.4049/jimmunol.1101772 (2011).

169 Agarwal, V., Bell, G. W., Nam, J. W. & Bartel, D. P. Predicting effective microRNA target sites in mammalian mRNAs. *eLife* 4, doi:10.7554/eLife.05005 (2015).

170 Nishimura, W. *et al.* A switch from MafB to MafA expression accompanies differentiation to pancreatic beta-cells. *Dev. Biol.* 293, 526-539, doi:10.1016/j.ydbio.2006.02.028 (2006).

171 Artner, I. *et al.* MafB - An activator of the glucagon gene expressed in developing islet alpha- and beta-cells. *Diabetes* 55, 297-304, doi:DOI 10.2337/diabetes.55.02.06.db05-0946 (2006).

172 Gao, T. *et al.* Pdx1 maintains beta cell identity and function by repressing an alpha cell program. *Cell Metab.* 19, 259-271, doi:10.1016/j.cmet.2013.12.002 (2014).

173 Zhang, Y. *et al.* LNA-mediated anti-miR-155 silencing in low-grade B-cell lymphomas. *Blood* 120, 1678-1686, doi:10.1182/blood-2012-02-410647 (2012).

174 Belgardt, B. F. *et al.* The microRNA-200 family regulates pancreatic beta cell survival in type 2 diabetes. *Nat. Med.* 21, 619-627, doi:10.1038/nm.3862 (2015).

175 van de Bunt, M. *et al.* The miRNA profile of human pancreatic islets and beta-cells and relationship to type 2 diabetes pathogenesis. *PloS ONE* 8, e55272, doi:10.1371/journal.pone.0055272 (2013).

176 Jablonski, K. A., Gaudet, A. D., Amici, S. A., Popovich, P. G. & Guerau-de-Arellano, M. Control of the Inflammatory Macrophage Transcriptional Signature by miR-155. *PloS ONE* 11, e0159724, doi:10.1371/journal.pone.0159724 (2016).

177 Saltiel, A. R. & Kahn, C. R. Insulin signalling and the regulation of glucose and lipid metabolism. *Nature* 414, 799-806, doi:10.1038/414799a (2001).

178 Jiang, G. & Zhang, B. B. Glucagon and regulation of glucose metabolism. *Am J Physiol Endocrinol Metab* 284, E671-678, doi:10.1152/ajpendo.00492.2002 (2003).

179 Rorsman, P. & Braun, M. Regulation of insulin secretion in human pancreatic islets. *Annu Rev Physiol* 75, 155-179, doi:10.1146/annurev-physiol-030212-183754 (2013).

180 Henquin, J. C. & Rahier, J. Pancreatic alpha cell mass in European subjects with type 2 diabetes. *Diabetologia* 54, 1720-1725, doi:10.1007/s00125-011-2118-4 (2011).

181 Quesada, I., Tuduri, E., Ripoll, C. & Nadal, A. Physiology of the pancreatic alpha-cell and glucagon secretion: role in glucose homeostasis and diabetes. *J. Endocrinol.* 199, 5-19, doi:10.1677/JOE-08-0290 (2008).

182 Lee, Y. H., Wang, M. Y., Yu, X. X. & Unger, R. H. Glucagon is the key factor in the development of diabetes. *Diabetologia* 59, 1372-1375, doi:10.1007/s00125-016-3965-9 (2016).

183 Mosser, R. E. *et al.* High-fat diet-induced beta-cell proliferation occurs prior to insulin resistance in C57Bl/6J male mice. *Am. J. Physiol. Endocrinol. Metab.* 308, E573-582, doi:10.1152/ajpendo.00460.2014 (2015).

184 Kanno, A. *et al.* Compensatory hyperinsulinemia in high-fat diet-induced obese mice is associated with enhanced insulin translation in islets. *Biochem. Biophys. Res. Commun.* 458, 681-686, doi:10.1016/j.bbrc.2015.02.024 (2015).

185 Kilimnik, G., Kim, A., Steiner, D. F., Friedman, T. C. & Hara, M. Intraislet production of GLP-1 by activation of prohormone convertase 1/3 in pancreatic alpha-cells in mouse models of beta-cell regeneration. *Islets* 2, 149-155 (2010).

186 Lim, G. E. *et al.* Insulin regulates glucagon-like peptide-1 secretion from the enteroendocrine L cell. *Endocrinology* 150, 580-591, doi:10.1210/en.2008-0726 (2009).

187 Van Lenten, B. J., Fogelman, A. M., Haberland, M. E. & Edwards, P. A. The role of lipoproteins and receptor-mediated endocytosis in the transport of bacterial lipopolysaccharide. *Proc. Natl. Acad. Sci. U.S.A.* 83, 2704-2708 (1986).

188 Weinstock, C. *et al.* Low density lipoproteins inhibit endotoxin activation of monocytes. *Arterioscler. Thromb.* 12, 341-347 (1992).

189 Victorov, A. V. *et al.* Composition and structure of lipopolysaccharide-human plasma low density lipoprotein complex. Analytical ultracentrifugation, 31P-NMR, ESR and fluorescence spectroscopy studies. *Biochim. Biophys. Acta.* 984, 119-127 (1989).

190 Topchiy, E. *et al.* Lipopolysaccharide Is Cleared from the Circulation by Hepatocytes via the Low Density Lipoprotein Receptor. *PloS ONE* 11, e0155030, doi:10.1371/journal.pone.0155030 (2016).

191 Vreugdenhil, A. C. *et al.* Lipopolysaccharide (LPS)-binding protein mediates LPS detoxification by chylomicrons. *J. Immunol.* 170, 1399-1405 (2003).

192 Marchetti, P. *et al.* A local glucagon-like peptide 1 (GLP-1) system in human pancreatic islets. *Diabetologia* 55, 3262-3272, doi:10.1007/s00125-012-2716-9 (2012).

193 Heller, R. S. & Aponte, G. W. Intra-islet regulation of hormone secretion by glucagon-like peptide-1-(7--36) amide. *Am. J. Physiol.* 269, G852-860 (1995).

194 Cardozo, A. K., Kruhoffer, M., Leeman, R., Orntoft, T. & Eizirik, D. L. Identification of novel cytokine-induced genes in pancreatic beta-cells by high-density oligonucleotide arrays. *Diabetes* 50, 909-920 (2001).

195 Choi, S. E. *et al.* IL-6 protects pancreatic islet beta cells from pro-inflammatory cytokines-induced cell death and functional impairment in vitro and in vivo. *Transpl. Immunol.* 13, 43-53, doi:10.1016/j.trim.2004.04.001 (2004).

196 Artner, I., Hang, Y., Guo, M., Gu, G. & Stein, R. MafA is a dedicated activator of the insulin gene in vivo. *J. Endocrinol.* 198, 271-279, doi:10.1677/joe-08-0063 (2008).

197 Artner, I. *et al.* MafB: an activator of the glucagon gene expressed in developing islet alpha- and beta-cells. *Diabetes* 55, 297-304 (2006).

198 Artner, I. *et al.* MafA and MafB regulate genes critical to beta-cells in a unique temporal manner. *Diabetes* 59, 2530-2539, doi:10.2337/db10-0190 (2010).

199 Gao, T. *et al.* Pdx1 maintains beta cell identity and function by repressing an alpha cell program. *Cell Metab.* 19, 259-271, doi:10.1016/j.cmet.2013.12.002 (2014).

200 Planque, N. *et al.* Interaction of Maf transcription factors with Pax-6 results in synergistic activation of the glucagon promoter. *J. Biol. Chem.* 276, 35751-35760, doi:10.1074/jbc.M104523200 (2001).

201 Lu, J. *et al.* Reexpression of oncoprotein MafB in proliferative beta-cells and Men1 insulinomas in mouse. *Oncogene* 31, 3647-3654, doi:10.1038/onc.2011.538 (2012).

202 Spijker, H. S. *et al.* Conversion of mature human beta-cells into glucagon-producing alpha-cells. *Diabetes* 62, 2471-2480, doi:10.2337/db12-1001 (2013).

203 Spijker, H. S. *et al.* Loss of beta-Cell Identity Occurs in Type 2 Diabetes and Is Associated With Islet Amyloid Deposits. *Diabetes* 64, 2928-2938, doi:10.2337/db14-1752 (2015).

204 Kurokawa, H. *et al.* Structural basis of alternative DNA recognition by Maf transcription factors. *Mol. Cell Biol.* 29, 6232-6244, doi:10.1128/MCB.00708-09 (2009).

205 Sieweke, M. H., Tekotte, H., Frampton, J. & Graf, T. MafB is an interaction partner and repressor of Ets-1 that inhibits erythroid differentiation. *Cell* 85, 49-60 (1996).

206 Kim, H. & Seed, B. The transcription factor MafB antagonizes antiviral responses by blocking recruitment of coactivators to the transcription factor IRF3. *Nat. Immunol.* 11, 743-750, doi:10.1038/ni.1897 (2010).

207 Kim, K. *et al.* MafB negatively regulates RANKL-mediated osteoclast differentiation. *Blood* 109, 3253-3259, doi:10.1182/blood-2006-09-048249 (2007).

208 Lumeng, C. N. & Saltiel, A. R. Inflammatory links between obesity and metabolic disease. *J. Clin. Invest.* 121, 2111-2117, doi:10.1172/JCI57132 (2011).

209 Berg, A. H. & Scherer, P. E. Adipose tissue, inflammation, and cardiovascular disease. *Circ. Res.* 96, 939-949, doi:10.1161/01.RES.0000163635.62927.34 (2005).

210 Virtue, A. *et al.* MicroRNA-155 deficiency leads to decreased atherosclerosis, increased white adipose tissue obesity, and non-alcoholic fatty liver disease: A novel mouse model of obesity paradox. *J. Biol. Chem.* 292, 1267-1287, doi:10.1074/jbc.M116.739839 (2017).

211 Pi-Sunyer, X. *et al.* A randomized, controlled trial of 3.0 mg of Liraglutide in weight management. *N. Engl. J. Med.* 373, 11-22, doi:10.1056/NEJMoa1411892 (2015).

212 Lee, Y. S. *et al.* Glucagon-like peptide-1 inhibits adipose tissue macrophage infiltration and inflammation in an obese mouse model of diabetes. *Diabetologia* 55, 2456-2468, doi:10.1007/s00125-012-2592-3 (2012).

213 Ranganath, L. R. *et al.* Attenuated GLP-1 secretion in obesity: cause or consequence? *Gut* 38, 916-919 (1996).

214 Naslund, E. *et al.* Distal small bowel hormones: correlation with fasting antroduodenal motility and gastric emptying. *Dig Dis Sci* 43, 945-952 (1998).

215 Herzberg-Schafer, S., Heni, M., Stefan, N., Haring, H. U. & Fritsche, A. Impairment of GLP1-induced insulin secretion: role of genetic background, insulin resistance and hyperglycaemia. *Diabetes Obes. Metab.* 14 Suppl 3, 85-90, doi:10.1111/j.1463-1326.2012.01648.x (2012).

216 Madsbad, S. The role of glucagon-like peptide-1 impairment in obesity and potential therapeutic implications. *Diabetes Obes. Metab.* 16, 9-21, doi:10.1111/dom.12119 (2014).

217 Flint, A., Raben, A., Astrup, A. & Holst, J. J. Glucagon-like peptide 1 promotes satiety and suppresses energy intake in humans. *J. Clin. Invest.* 101, 515-520, doi:10.1172/jci990 (1998).

218 Gutzwiller, J. P. *et al.* Glucagon-like peptide-1 promotes satiety and reduces food intake in patients with diabetes mellitus type 2. *Am. J. Physiol.* 276, R1541-1544 (1999).

219 Verdich, C. *et al.* A meta-analysis of the effect of glucagon-like peptide-1 (7-36) amide on ad libitum energy intake in humans. *J. Clin. Endocrinol. Metab.* 86, 4382-4389, doi:10.1210/jcem.86.9.7877 (2001).

220 Taher, J. *et al.* GLP-1 receptor agonism ameliorates hepatic VLDL overproduction and de novo lipogenesis in insulin resistance. *Mol. Metab.* 3, 823-833, doi:10.1016/j.molmet.2014.09.005 (2014).

221 Arakawa, M. *et al.* Inhibition of monocyte adhesion to endothelial cells and attenuation of atherosclerotic lesion by a glucagon-like peptide-1 receptor agonist, exendin-4. *Diabetes* 59, 1030-1037, doi:10.2337/db09-1694 (2010).

222 Shah, Z. *et al.* Long-term dipeptidyl-peptidase 4 inhibition reduces atherosclerosis and inflammation via effects on monocyte recruitment and chemotaxis. *Circulation* 124, 2338-2349, doi:10.1161/CIRCULATIONAHA.111.041418 (2011).

223 Plutzky, J. The incretin axis in cardiovascular disease. *Circulation* 124, 2285-2289, doi:10.1161/CIRCULATIONAHA.111.064139 (2011).

224 Bullock, B. P., Heller, R. S. & Habener, J. F. Tissue distribution of messenger ribonucleic acid encoding the rat glucagon-like peptide-1 receptor. *Endocrinology* 137, 2968-2978, doi:10.1210/endo.137.7.8770921 (1996).

225 Liang, C. P., Han, S., Li, G., Tabas, I. & Tall, A. R. Impaired MEK signaling and SERCA expression promote ER stress and apoptosis in insulin-resistant macrophages and are reversed by exenatide treatment. *Diabetes* 61, 2609-2620, doi:10.2337/db11-1415 (2012).

226 Rader, D. J., Cohen, J. & Hobbs, H. H. Monogenic hypercholesterolemia: new insights in pathogenesis and treatment. *J. Clin. Invest.* 111, 1795-1803, doi:10.1172/JCI18925 (2003).

227 Singh, S. & Bittner, V. Familial hypercholesterolemia--epidemiology, diagnosis, and screening. *Curr. Atheroscler. Rep.* 17, 482, doi:10.1007/s11883-014-0482-5 (2015).

8 ACKNOWLEDGEMENTS

I would like to thank all the people who contributed in a certain way to the work described in this dissertation. First and foremost, I offer my sincerest gratitude to my supervisor Prof. Dr. med Andreas Schober. He has been supportive since the day I start my PhD with his patience and knowledge while giving me the room to work in my own way. Andreas has not only guided me academically, but also encouraged me emotionally through the rough road to finish this thesis. Thanks to him I had the opportunity to work in his laboratory and on this fantastic project. I have been always feeling comfortable working with Andreas, and I could not wish for a better supervisor.

It was a great pleasure to work with a cheerful and friendly group of colleagues, and I would like to thank them for their help. During my past few years, I have been advised and aided intensively by Dr. Yuanyuan Wei, an experienced and enthusiastic researcher in the role of miRNAs, whose supervision, contributions, and suggestions during my training and research work have enabled me produce this work. I would also like to acknowledge Dr. Ela Karshovska, Dr. Lucia Natarelli and Dr. Malihe Nazar-Jahantigh who have also contributed significantly to my work and training. I want to thank my fellow PhD students as well; Dr. Petra Hartman, a sincere friend who shared the same lab with me for more than three years, gave me great help in work and daily life. Dr. Richard Blay and Farima Zahedi who helped, encouraged and contributed in various ways to this project. I also acknowledge the support and contributions of our technicians; Kathrin Hyell, Claudia Geißler, Judith Campos and Lourdes Luiz-Heinrich, who spent much time and effort in various experiments. Additionally, I will like thank the China Scholarship Council (CSC) for the funding during my Doctoral studies.

Finally, I want to say thank you to my husband, Zhen Li, for her constant love and support. Thank you for listening to me when I grumble, comforting me when I feel disappointed, encouraging me when I lose faith, and accompanying me when I am alone. It would not be possible for me to finish writing this thesis without your support. I feel lucky to have you as my significant other. You are not just my companion, you are my inspiration.

Affidavit

Zhu Mengyu

Surname, first name

Hermann-Lingg-Straße 18

Street

80336 München

Zip code, town

Deutschland

Country

I hereby declare, that the submitted thesis entitled

Hyperlipidemia-induced microRNA-155-5p improves β-cell function by targeting *Mafb*

is my own work. I have only used the sources indicated and have not made unauthorised use of services of a third party. Where the work of others has been quoted or reproduced, the source is always given.

I further declare that the submitted thesis or parts thereof have not been presented as part of an examination degree to any other university.

Place, date

Signature doctoral candidate